

Technische Universität München
Lehrstuhl für Aerodynamik und Strömungsmechanik

Mesoscopic simulation of DNA using Smoothed Dissipative Particle Dynamics

Sergey Litvinov

Vollständiger Abdruck der von der Fakultät für Maschinenwesen der Technischen Universität München zur Erlangung des akademischen Grades eines

Doktor-Ingenieurs

genehmigten Dissertation.

Vorsitzender: Univ.-Prof. Dr.-Ing. Andreas Kremling

Prüfer der Dissertation: 1. Univ.-Prof. Dr.-Ing. Nikolaus A. Adams

2. Univ.-Prof. Dr. rer. nat. habil. Andreas Bausch

Die Dissertation wurde am 19.12.2013 bei der Technischen Universität München eingereicht und durch die Fakultät für Maschinenwesen am 09.04.2014 angenommen.

Contents

1	Summary	7
2	Introduction	9
2.1	Properties of isolated DNA and DNA in the flow	9
2.2	Mesoscale simulations of DNA	17
2.2.1	Numerical methods for mesoscale simulation	17
2.2.2	Smoothed Dissipative Particle Dynamics (SDPD)	18
2.2.3	Development of the SDPD method	21
2.2.4	Mesoscale simulation of DNA with the SDPD method	25
3	Self-Diffusion of SDPD particles	27
4	A Splitting scheme for SDPD	29
5	Wall-Bounded SDPD simulation	31
6	Free polymer simulation	33
7	Tethered polymer in shear flow	35
8	Papers	37
8.1	Paper I	37
8.2	Paper II	42
8.3	Paper III	51
8.4	Paper IV	57

8.5 Paper V 70

List of Figures

2.1	DNA pulled by a magnetic bead, experience friction from the solvent. Depending on the velocity the DNA is in different regimes [99]	11
2.2	Behavior of the DNA chain in shear flow can follow different scenarios: as the chain can relax to a coil, the chain can tumble end-over-end (the scheme is from Smith et al. [79])	15
2.3	The DNA in elongational flow can have different conformations depending on the initial conditions. From top to bottom: dumbbell, linked, half dumbbell, and folded [65].	16
2.4	Radial distribution function for the SDPD particles, inter-particle distance is 0.83.	20

1 Summary

In this work it is shown that the Smoothed Dissipative Particle Dynamics (SDPD) can correctly represent the static and dynamic behavior of DNA chains in flow [Litvinov et. al, Phys. Rev. E **77**, 66703 (2008)]. As an application, the dynamics of the wall-tethered DNA in shear flow is considered. Specifically, the cyclic motion of the tethered DNA was investigated [Litvinov et. al, Journal of Physics: Condensed Matter **23**, 184118 (2011)]. SDPD was introduced in [Español and Revenga, Phys. Rev. E **67**, 026705 (2003)] and can be considered as a generalization of the Smoothed Particle Hydrodynamics (SPH) method for mesoscale. In SDPD, a discretization element (particle) represents a packet of fluid whose specific size determines the level of thermal fluctuations in the hydrodynamic variables. Unlike other mesoscale particle-based methods SDPD has an explicit equation of state and speed of sound. In the SDPD method the viscosity is an explicit input parameter. It is shown that the self-diffusion coefficient of the SDPD particles follows a simple relation similar to the Stokes-Einstein relation [Litvinov et. al, J. Chem. Phys. **130**, 021101 (2009)]. This finding allows for “a priori” characterization of the fluid in simulations. A new integration scheme for SDPD aiming at highly dissipative cases typical for microfluidic applications is proposed [Litvinov et. al, J. Comp. Phys. **229**, 5457 – 5464 (2010)]. An “amorphous” wall boundary condition model is used to avoid an artificial particle layering. This boundary condition is used for tethered DNA simulations [Litvinov et. al, Physical Review E **82**, 066704 (2010)].

2 Introduction

Deoxyribonucleic acid (DNA) – as carrier of the genetic information – is one of the most investigated and best understood biomolecules. At the same time, it is the molecule which is most applied in bio- and nano-technology. This is mainly caused by the fact that a variety of methods have been developed over the last decades, which allow both synthesis and characterization of the molecule with exceptional high precision. The size, homogeneity and unbranched structure also make the DNA an ideal “model polymer” to aid theoretical polymer science [62].

2.1 Properties of isolated DNA and DNA in the flow

Historically the first experimental methods to study the dynamics of DNA were based on bulk or ensemble measurements: in those methods the average behavior of many molecules is measured and information on the single molecule configuration can be deduced [6]. The most widely used group of the bulk methods is based on light scattering spectroscopy. They can provide information on the molecular weight and the size of the DNA coils. More sophisticated experiments estimate the persistence length, elasticity, diffusion coefficient, torsional rigidity. Despite many successes the bulk methods have several limitations: the intermediate configuration of the DNA cannot be studied, heterogeneity of the solutions limits the accuracy of the methods, and the link between properties of the individual molecule and the measured quantities involves many assumptions, which are difficult to test directly. In recent years single-molecule techniques have emerged as a main tool to investigate mechanical properties of DNA [65]. Remarkably, most of the findings obtained with the bulk methods were confirmed.

Several types of the DNA molecules are used in experiments: DNA of T1, T2, T7, λ - phages, DNA of E. coil [76]. The DNA is a linear chain with flexibility which depends on the ionic

Force	Description
Viscous drag	frictional force from flowing solvent
Entropic elasticity	this force is generated when the polymer is out of the equilibrium coiled configuration
Brownian forces	caused by thermal “kicks” from solvent molecules
Hydrodynamic interaction (HI)	one segment of the chain affects another one due to disturbances of the flow
Excluded-volume (EV) interactions	repulsive force between segments
Internal viscosity (IV)	intrachain friction
Self-entanglement (SE)	intrachain entanglements

Table 2.1: Forces acting in single DNA [37]

strength of the solution (higher strength makes the molecule more flexible with a limiting persistence length of 50 nm), the length of the molecule is usually much longer than the persistence length. Very recently Brockman et al. developed a method to synthesize and directly observe single-stranded DNA which allows decreasing the persistence length below 50 nm [5, 51]. Larson [37] gives a list of the phenomena that are important for single chain dynamics (See Table 2.1), we use this list to structure the experimental data and models of the DNA.

Viscous drag is the frictional force that the chain experiences from the flowing solvent. In early work Wirtz [99] tethered the DNA to a small magnetic bead and pulled it by a calibrated force. As a result the first direct measurements of the DNA friction coefficient were obtained. With increasing velocity of the bead several regimes can be observed: (a) linear, (b) nonlinear intermediate regime (the chain adopts a trumpet shape) (c) nonlinear intermediate regime (the trumpet disappears), see Figure 2.1. Thomen et al. [92] measured the rotational drag on the doubled-stranded DNA and found that the value is 10 times higher than the one expected for a straight rigid rod. Note that for typical experimental conditions the viscous drag is dominating the inertia effects of the segments of the DNA and thus many models do not include inertia.

Probably the most simple polymer model which can be applied to the DNA was introduced by Kuhn [36]: the chain is modeled by beads connected by the spring forces, and the viscous force acts only on the beads. This model is called the dumbbell model and is surprisingly successful in predicting the steady-state stresses and birefringence in dilute polymer solutions.

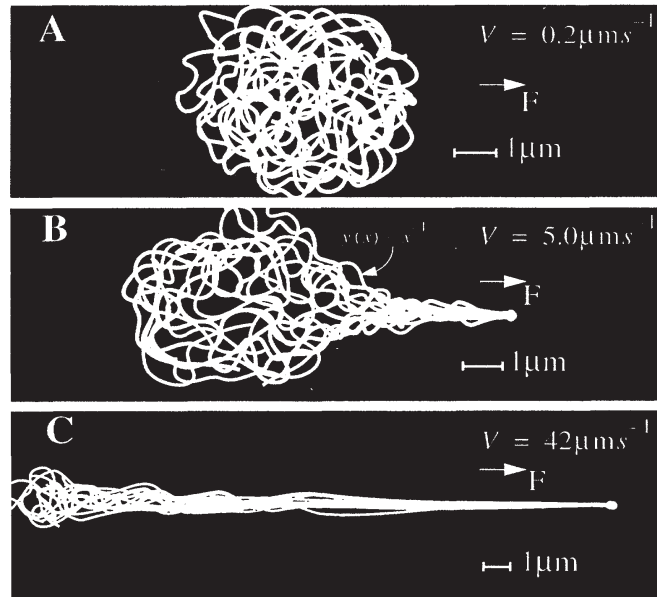


Figure 2.1: DNA pulled by a magnetic bead, experience friction from the solvent. Depending on the velocity the DNA is in different regimes [99]

For the DNA tethered at one end the dumbbell model correctly predicts the fractional extension as a function of velocity for uniform flow.

Brownian forces are caused by thermal “kicks” from the solvent molecules. In molecular visualization experiments Brownian motions of the segments of the DNA are apparent even in very strong flows. This force causes the trajectory of the molecule to be non-deterministic and it has the consequences for modeling. First, if the molecule is close to the equilibrium it allows applying tools of statistical mechanics even to a single molecule. Second, for non-equilibrium situations the Brownian forces make modeling very difficult.

The Brownian forces are responsible for the relaxation of the DNA: because of the thermal “kicks” the DNA “forgets” its initial configuration. The timescale on that it happens is characterized by “the longest relaxation time”. In experiments “the longest relaxation time” is determined by the following procedure. The molecule is stretched and then allowed to relax freely. The extension of the DNA is recorded as a function of time $x(t)$, and the fitting of a last part of the $x^2(t)$ curve by an exponential function $c_1 e^{-t/\tau} + c_2$ gives “the longest relaxation time” (τ) [65, 80, 76].

Entropic elasticity is important if the chain is out of the equilibrium. Smith et al [80]. found that the following expression can fit experimental measurements of the force (F) versus the extension (x) for λ -phage DNA:

$$\frac{FP}{kT} = \frac{1}{4} (1 - x/L)^{-2} - \frac{1}{4} + x/L. \quad (2.1)$$

P is the persistence length, k is the Boltzmann constant, T is the temperature, and L is the contour length. In the limit of small extension the law becomes Hookean.

Hydrodynamic interactions (HI) arise when disturbances of flow by one segment of the chain are felt by another segment. In contrast to *the viscous drag* and *the entropic elasticity* HI cannot be measured directly. However presence or absence of HI significantly affects the dynamics of the chain. Then HI are present the drag depends on the conformation of the chain. A simple model of a polymer with HI was named after Zimm [103]. It is a linear mean-field model: each segment of the chain interacts with an average conformation of its neighbors. The Zimm model predicts the scaling of the relaxation time of the polymer with chain length, this prediction was confirmed by experimental data [63].

Although the Zimm model was successful in explaining results of the earlier experiments many groups were trying to understand HI in more detail. One attempt was reported by Quake, Babcock and Chu [70], they measured the fluctuation of the DNA held in a partially extended state and found that its motion can be described by the normal modes, and the spectrum of relaxation times shows a power-law distribution with the exponent predicted by the Zimm model. In general this experiment does not refute the Zimm model but its ability to detect deviations from the Zimm model is relatively weak because in extended state inter-segment HIs are more difficult to measure [7]. Shusterman et al. [78] labeled DNA fragments at single points and

measured the monomer mean-square displacement. For a flexible single-stranded DNA the results are consistent with the Zimm model.

More recent works report deviations from the Zimm model. Cohen and Moerner [7] collected data on free-shape fluctuations of the DNA by using an anti-Brownian trap and reported signs of nonlinear hydrodynamics: they performed a principal component analysis of the density fluctuations of the chain projection and observed a correlation between modes which is not expected for the Zimm model. McHale and Mabuchi [53] used feedback tracking microscopy and FCS (fluorescence correlation spectroscopy) and reported results which are suggesting strong HI which are, however, not consistent with the Zimm model. Hinczewski and Netz [24] proposed a more refined treatment of hydrodynamic interaction which nevertheless is free of fitting parameters to describe end-monomer dynamics in FCS experiments [67]. The topic of HI interactions in DNA remains controversial and the capacity of FCS to provide information on intermolecular motion has been questioned [12].

The Excluded volume (EV) interaction is the repulsive force between different segments of the chain. The effect of EV increases with the expansion of the chain. For longer or extended chains EV are less important than for shorter and coiled chains. A direct consequence of the EV is a change of the scaling of the polymer radius of gyration with the number of beads. For ideal chains $R_g \propto N^{1/2}$, and, if EV interaction is important, the chain follows the Flory scaling law: $R_g \propto N^{0.6}$. More refined theories and simulations give a slightly different scaling $R_g \propto N^{0.588}$ [30, 69] which also extends to the dynamic quantities such as the diffusion coefficient ($D \propto N^{0.588}$). With increasing N the crossover from ideal to real behavior is expected, but a direct observation of such a crossover was possible only very recently for Poly(Ethylene Glycol) [9]. Data for the distribution of charged segments of the one-end tethered DNA shows the scaling $R_g \propto 0.57 \pm 0.05$ [39].

Several experimental works suggest that the DNA experiences strong EV interactions. Smith and co-authors [82] measured diffusion coefficients (D) for the DNA molecules from 2 to 140 μm in length. They found that $D \propto L^{-\mu}$ with $\mu = 0.611 \pm 0.016$. Robertson et al. [74] confirm this observation and give an estimate for the scaling exponent as 0.571 ± 0.014 . Atomic force microscopy provides a distribution of the position of one end of the long DNA with the other end attached to a non-adsorbing surface. This distribution reveals an estimate of the scaling

exponent as 0.589 ± 0.006 . For short DNA molecules a behavior typical for rigid rods was observed, although possible cross-over was not resolved [95]. Small-angle x-ray scattering of single-stranded DNA gives a value for the static exponent which is in the range of 0.55 to 0.7 depending on the salt concentration used. Note that this method does not involve labeling of the molecule which can potentially modify the mechanical properties of the DNA. However, recently the results of scanning fluorescence correlation spectroscopy (SFCS) of fluorescently labeled DNA molecules were obtained which challenge the assumptions of strong EV interactions in DNA [57]. The best power law fit of the gyration radii in these experiments gives $R_g \propto L^{0.52 \pm 0.02}$ with a length of the molecules spanning over two decades. DNA brushes on biochips do not show a collective stretch despite significant chain overlap, which is consistent with the weak excluded volume interactions [4].

Internal viscosity (IV), is a friction between segments of the chain [29]. IV can be caused by many mechanisms which can be separated into solvent-mediated (“wet”) with the magnitude proportional to the solvent viscosity and solvent-independent (“dry”). Direct experimental evidence for importance of IV in the DNA is difficult to get but postulating IV in the dumbbell model leads to a better fit of the experimental data for DNA in shear flow, especially for at higher Weissenberg numbers [101]. Note that for proteins IV was quantified [83] by considering different viscosities of the solvent and assuming that the limit of vanishing solvent viscosity corresponds to the case with only internal viscosity.

Self-entanglement is defined as “intrachain entanglements, in which an isolated polymer forms a knot” [37]. There are several ways to form a “knot” with a DNA molecule: using optical tweezers [3], using gel [96], or by collision of the DNA with defect [54]. Recently the compression of the DNA by an electrical field was used as a reliable way to induce “knotting” [89].

All forces in the Table 2.1 are involved when the DNA interacts with flow. Recently, Mai et. al. [49] reviewed microfluidic systems used in studies of DNA-flow interactions including channel-based flows, cross slots, arrays, and nanoscale confinements. The local flow field in a laminar flow can be represented as a combination of simple shear and elongational flows. This renders the investigations of the DNA in those two flows the most important from a fundamental point of view. Simple shear is relatively easy to generate and control in experiments,

several researchers visualized the DNA in simple shear in flow plane [79, 38] and in the flow gradient plane [75, 90]. It was revealed that the DNA dynamics is complex: the chain can be stretched, it can relax to a coil, it can undergo tumbling motions where the head of the chain overtakes the tail (see Figure (2.2)).

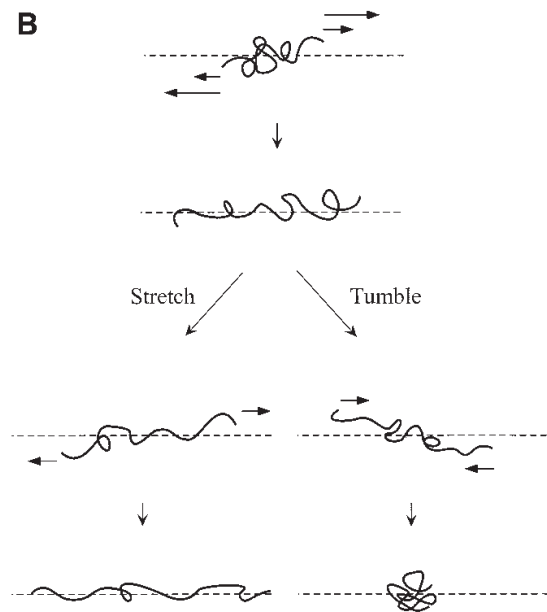


Figure 2.2: Behavior of the DNA chain in shear flow can follow different scenarios: as the chain can relax to a coil, the chain can tumble end-over-end (the scheme is from Smith et al. [79])

Perkins, Smith, and Chu [64] used a micro-channel with cross slot geometry to generate elongational flow and reported variation in the onset of stretching for different initial configurations of the molecules (chains with a dumbbell shape stretched more rapidly than folded ones). In their latter work [81] the effect of a sudden elongational flow on relaxed molecules was studied. This experiment allowed monitoring the evaluation of the chain configuration without initial perturbations. Again different dynamic scenarios were observed for the chains.

De Gennes used the expression “molecular individualism” to describe the sensitivity of the chain dynamics to the initial conditions [20]. Randall et al. [71] put “molecular individualism” in broader perspective: “molecular individualism is an example of the general phenomenon of transient chaos, which causes a complex system’s dynamics to be unpredictable even though the system eventually achieves a stable fixed point at long time.”. In Figure 2.3 we show images of the DNA stretched in elongational flow where four different conformations are observed [65]. In more recent experiments of Teixeira et al. it was found that exposure of the DNA molecular to identical flow histories [91] can lead to very different molecular conformations.

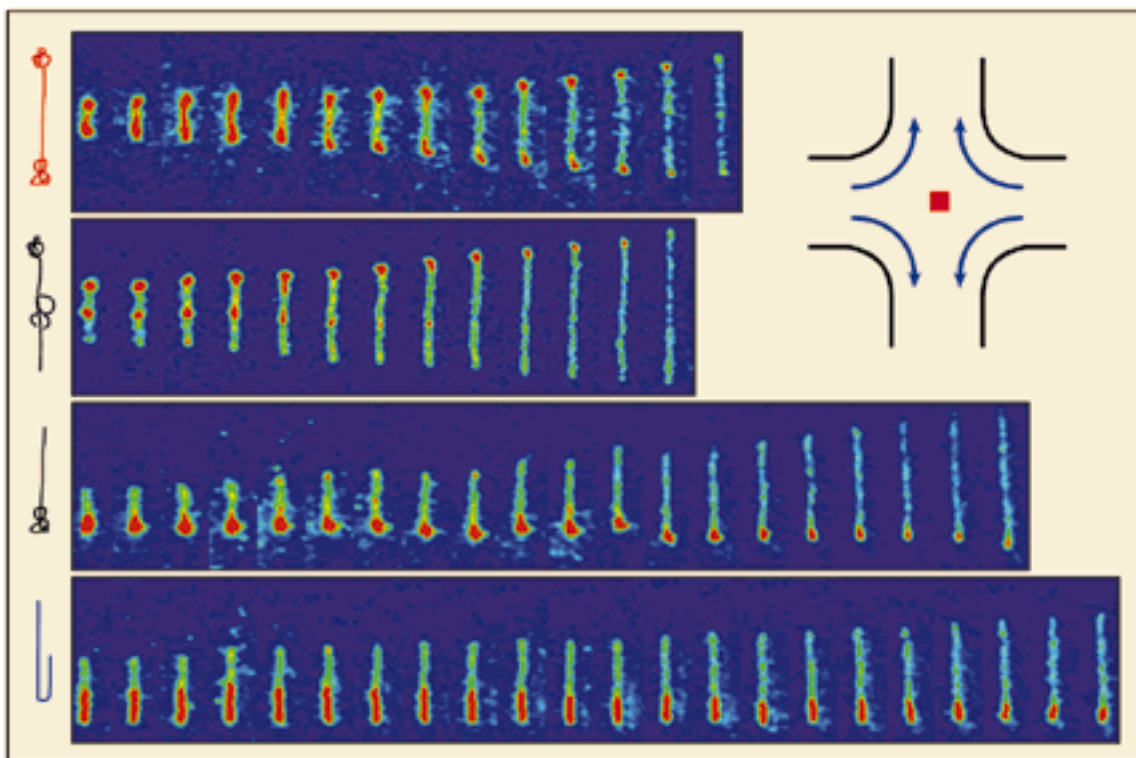


Figure 2.3: The DNA in elongational flow can have different conformations depending on the initial conditions. From top to bottom: dumbbell, linked, half dumbbell, and folded [65].

The interaction of the DNA with flows is a suitable case for validation of long standing hypothesis of polymer physics. Most microfluidic applications, however, involves more complex flow structures and the DNA can interact with continuing walls. It is possible to construct a

channel with typical dimensions on the order of, or even smaller than, the typical size of a DNA coil. The DNA experiences the presence of a wall by two effects: exclusion of chain configuration and hydrodynamic interactions with the surface [76]. For example in Poiseuille flow in the channel the DNA tends to migrate toward the center. Explanations of this phenomenon involve hydrodynamic interactions of wall and the DNA. There are various devices used to study the single DNA dynamics (curved channels, cross slots, and micro-fabricated obstacles and structures), we refer the reader to recent reviews [49, 51] for details. In this work we focus on one case of DNA-wall interaction: the tethered DNA in shear flow. In the following section we focus our attention on simulations of DNA dynamics.

2.2 Mesoscale simulations of DNA

In contrast to simple models a straightforward simulation approach is to build up a detailed model with atomistic phenomena taken into account. Although atomistic modeling was done by many authors it faces a challenge. The computational capacity required to perform a full atomistic simulation is very high. Methods based on mesoscopic theories, which connect the microscopic and macroscopic descriptions of the systems, are a promising alternative. By applying mesoscopic methods one expects to capture only essential microscopic parameters and relationships and to omit details which are not important for the phenomena under investigation [35].

2.2.1 Numerical methods for mesoscale simulation

The most popular approach in more complex situations is Brownian Dynamics (BD) [60]. Extended versions of the Brownian Dynamics technique, have been recently shown to produce accurate results for DNA dynamics in microfluidics at devices [31], but require a complicated modeling of hydrodynamic interactions (in particular when coupled with the no-slip boundary conditions at walls) mediated by a modified Rotne-Prager-Yamakawa (RPY) tensor. To remedy these problems, various researchers have focused in the past on other methods which use numerically effective coarse-grained models retaining the relevant hydrodynamic modes. Examples are Multi-Particle Collisions Dynamics (MPCD) [72], Lattice Boltzmann methods

(LBM) [1] and Dissipative Particle Dynamics (DPD). In particular, DPD is a mesoscopic methodology which has attracted increasing attention in the past years. DPD was originally proposed by Hoogerbrugge [25] and successively modified by Warren and Español in order to satisfy thermodynamic consistency [15]. The method has been shown to capture the relevant thermodynamics and hydrodynamic effects occurring in mesoscopic systems [84, 32, 87, 34], and it has been applied in the past years to a wide range of physical situations [17, 16]. Despite its great success, however, a number of conceptual shortcomings has been pointed out which affects the performance and accuracy of the technique. In particular they deal with (i) non-arbitrary choice of the fluid equation of state, (ii) no direct connection to the transport coefficients and (iii) unclear definition of the physical particle scales.

All problems mentioned above can be avoided by resorting to a further improved DPD version: the Smoothed Dissipative Particle Dynamics (SDPD) [13]. The main objective of this work is to apply the SDPD method to polymer simulations. But on the way to achieve this we address the following modeling problems: we derive an analytical expression for the self-diffusion coefficient of the SDPD particles, we show how the time stepping scheme can be improved to efficiently handle highly viscous flows, we show how a wall-boundary can be modeled in SDPD without finite size artifacts.

2.2.2 Smoothed Dissipative Particle Dynamics (SDPD)

SDPD is based on a second-order discretization of the Navier-Stokes equations. Transport coefficients are input parameters and do not need to be measured and adjusted via Green-Kubo relations as in MD, or extracted via kinetic theory as in conventional DPD. In addition, hydrodynamic behavior is obtained at length scales on the same order as the particle dimension, and no coarse-graining assumption is needed.

SDPD can be also viewed as an extension of a macroscopic method, namely Smoothed Particle Hydrodynamic (SPH) [55]. The SPH method is a fully Lagrangian, grid free method in which a smoothing kernel is introduced to approximate functions and their spatial derivatives originating from the interactions with neighboring particles. The SPH algorithm itself is similar to that of MD but uses additional thermodynamic variables which are obtained by a coarse

graining procedure from the underlying microscopic (molecular) physics. Since its introduction in [48] and [21], SPH has been applied to a wide range of macroscopic flow problems [55]. Español [13] proposed a way to include thermal fluctuations in a physically consistent way, by which the fluctuation magnitude increases naturally while the physical scale of the problem decreases to the mesoscopic scale. This combination constitutes the core of the SDPD method.

In the following paragraphs we briefly summarize the equations solved with the SDPD method. The density of the fluid is given by

$$\rho_i = m_i \sum_j W_{ij}. \quad (2.2)$$

The momentum equations are discretized as

$$\begin{aligned} \frac{d\mathbf{v}_i}{dt} = & -\frac{1}{m_j} \sum_j \left(\frac{p_i}{\sigma_i^2} + \frac{p_j}{\sigma_j^2} \right) \frac{\partial W_{ij}}{\partial r_{ij}} \mathbf{e}_{ij} \\ & + \frac{\eta}{m_i} \sum_j \left(\frac{1}{\sigma_i^2} + \frac{1}{\sigma_j^2} \right) \frac{\mathbf{v}_{ij}}{r_{ij}} \frac{\partial W_{ij}}{\partial r_{ij}}, \end{aligned} \quad (2.3)$$

where m_i is the mass of a particle, W_{ij} is a kernel function, σ_i is the inverse of a particle volume, \mathbf{e}_{ij} and r_{ij} are the normalized vector and distance from particle i to particle j , respectively. $\mathbf{v}_{ij} = \mathbf{v}_i - \mathbf{v}_j$ is a difference between velocities of interacting particles. Density (ρ) and pressure (p) are related by the equation of state

$$p = p_0 \left(\frac{\rho}{\rho_0} \right)^\gamma + b, \quad (2.4)$$

where p_0 , ρ_0 , b and γ are parameters which may be chosen based on a scale analysis so that the density variation is less than a given magnitude. For $\gamma = 7$ penetration of particles is precluded.

Eq. (2.2) and (2.2) represents the deterministic part of the particle dynamics [13, 27]. Using the GENERIC formalism (General Equation for Non-Equilibrium Reversible-Irreversible Coupling) [14] thermal fluctuations can be taken into account directly in (2.3) by introducing the random term

$$d\tilde{\mathbf{P}}_i = \sum_j B_{ij} d\overline{\overline{\mathcal{W}}}_{ij} \mathbf{e}_{ij}, \quad (2.5)$$

where $d\tilde{\mathbf{P}}_i$ is a change of the particle momentum due to random fluctuations, $d\overline{\overline{\mathcal{W}}}_{ij}$ is the traceless symmetric part of an independent increment of a Wiener process and B_{ij} is defined as

$$B_{ij} = \left[-4k_B T \eta \left(\frac{1}{\sigma_i^2} + \frac{1}{\sigma_j^2} \right) \frac{1}{r_{ij}} \frac{\partial W}{\partial r_{ij}} \right]^{1/2}. \quad (2.6)$$

Some properties of this particular set of discrete equations are:

- the total mass and the total momentum are exactly conserved,
- the linear momentum is locally conserved due to the anti-symmetric form of the particle pair force,
- the total energy is conserved and the total entropy is a monotonically increasing function of time [14],
- the conservation properties prevent particle penetration, and the radial distribution function (RDF) of the solvent particles exhibits a shape typical for liquids (See Figure 2.4).

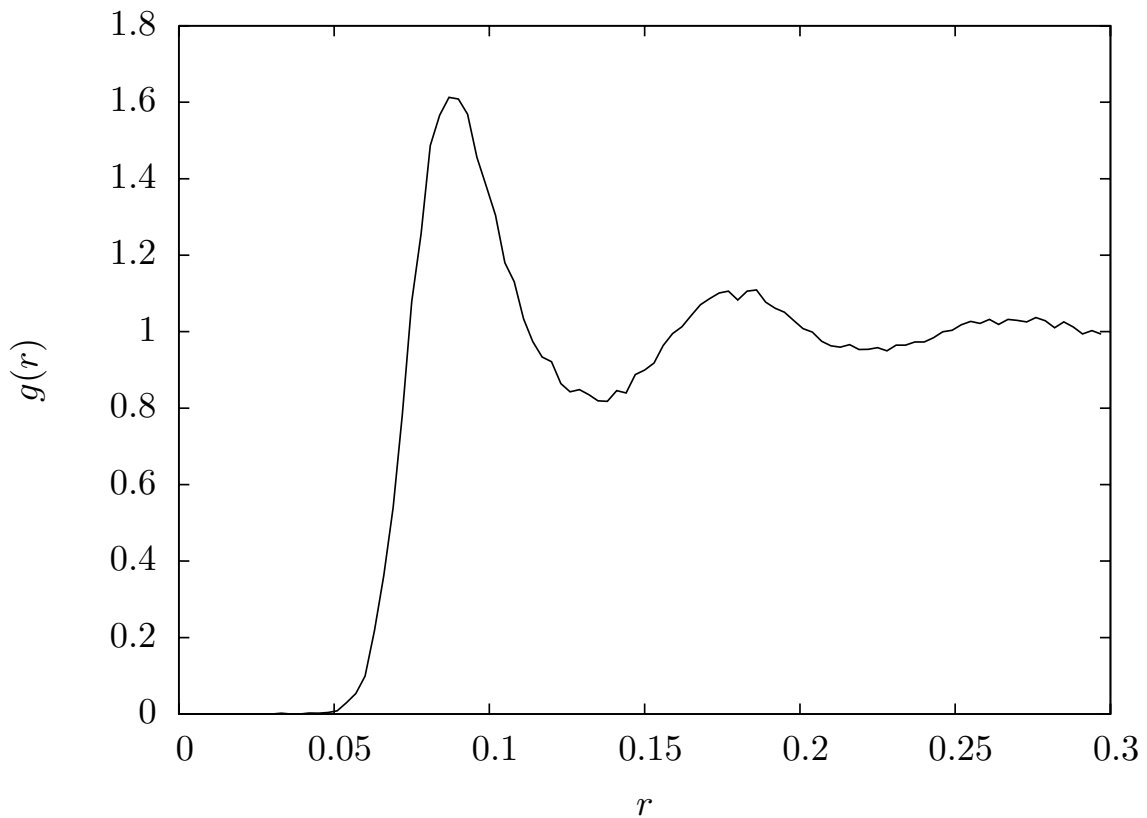


Figure 2.4: Radial distribution function for the SDPD particles, inter-particle distance is 0.83.

2.2.3 Development of the SDPD method

An important requirement for a mesoscopic method is the correct representation of transport properties. We review results on transport coefficients for two methods related to SDPD: DPD and MPCD. Already in earlier works on DPD [52, 22] an explicit prediction for the viscosity and the self-diffusion coefficient in terms of the model parameters were given. However, the validity of these analytical expressions is restricted to the ideal-gas equation of state and to the limit of small time steps. Furthermore, as found in [86], this prediction fails to reproduce the diffusion coefficient for the widely used velocity-Verlet integration scheme.

For MPCD two distinct regimes are identified, the gas-like dynamics regime and the collective regime with fluid-like dynamics. Molecular-chaos assumption gives an analytical expression which is in a good agreement with simulation data in the particle regime, but deviates in the collective regime. The predictions based on Stokes hydrodynamics and the Smoluchowski equation agree with simulations in the collective regime [73]. In [94] unbiased values for the transport coefficients were obtained for the MPCD, corrections to the self-diffusion coefficient to the molecular chaos approximation were proposed and analyzed. Noguchi et al. [59] have studied the viscosity and self-diffusion coefficient of MPCD and DPD. For both methods they consider cases with and without angular momentum conservation, results were derived for the ideal-gas equation of state and a finite-time step.

For the transport properties of SDPD viscosity is an input parameter. However, the self-diffusion coefficient D of fluid particle cannot be specified *a priori* and therefore it needs to be estimated. An accurate expression for D in terms of the model parameters is crucial for the determination of the Schmidt number Sc of the model liquid. For instance, the value of Sc affects strongly the non-equilibrium properties of suspended polymer molecules [86]. In the section 3 of this work a simple analytical expression for the diffusion coefficient of SDPD particle is introduced.

However, although the transport properties of the liquid can be controlled, many technical difficulties remain on the way to perform simulations with realistic physical parameters. One group of problems is related to the separation of timescales for simulation methods with explicit time stepping. When SDPD is used to simulate low-Reynolds-number and mesoscopic liquid

flows the time-step size limit for stable time integration is usually determined by viscous effects as such flows are highly dissipative. Specifically, this issue is referred to as “the Schmidt number problem” in DPD [88, 87] and also applies to SDPD. The Schmidt number is defined as the ratio of momentum diffusion (viscosity) and mass diffusion

$$\text{Sc} = \frac{\mu}{D\rho}, \quad (2.7)$$

where μ is dynamic viscosity, ρ is density and D is the diffusion coefficient. Typical Sc achieved by SDPD and DPD simulations are on the order $O(1)$, which is similar to that of a gas rather than a liquid with $\text{Sc} \sim O(10^3)$.

With respect to the meaning of the Schmidt number in simulations there is no consensus in the literature. Peters [66] suggested that the diffusion coefficient D appearing in the definition of Sc refers to the molecular diffusivity and therefore is an ill-defined quantity for coarse-grained systems. Simulations of Jiang et al. [32] show that the hydrodynamic interaction between polymer beads is developed under typical conditions of a DPD simulation ($\text{Sc} = 1$). However, it has been pointed out by Groot and Warren [22] that in order to achieve a realistic liquid behavior it is essential to recover the correct magnitude of Sc in DPD simulations. Furthermore, it was observed by Symeonidis et al. [88, 86] that an agreement between simulations and experiments with respect to the non-equilibrium properties of a DNA molecule in shear flow requires Sc numbers with a magnitude of that for a liquid.

A straightforward way to increase the Schmidt number is to increase the dissipative force. However, if the DPD particle velocity is updated explicitly, as in the traditional velocity-Verlet method [22], the time integration requires a very small, computationally inefficient time-step size to achieve correct equilibrium properties. Moreover for polymer simulations higher viscosity leads to higher value of relaxation time which requires even longer simulations to get enough statistically uncorrelated samples of polymer configuration. To cope with this difficulty, Pagonabarraga et al. [61] have proposed an iterative method where the particle velocity is updated implicitly. However, it is found that such a method is not very practical due to large computational cost. To achieve a higher Schmidt number Fan et al. [17] used a “generalized” weighing function for conservative and random forces

$$\omega^D(r_{ij}) = (\omega^R(r_{ij}))^2 = (1 - r_{ij}/r_c)^s, \quad (2.8)$$

a parameter $s < 2$ ($s = 2$ gives traditional DPD). A Schmidt number on the order of 10^3 was achieved. This approach was used also by other authors [19, 18]. Another method was introduced by Mai-Duy et al. [50]. They considered a DPD simulation with the mass of the particles approaching zero, correspondingly $Re \rightarrow 0$ and $Sc \rightarrow \infty$. In this case the system of equation becomes singular, but it can be stabilized by introducing a small artificial mass. Two methods are presented to solve this system: direct matrix inversion and iterative. The last approach is conceptually similar to the splitting scheme described below.

A splitting scheme for DPD was proposed by Shardlow [77]. While updating the contribution of the conservative force explicitly, this method updates the contributions of the dissipative and random forces in pairwise fashion. By this procedure the original DPD formulation of dissipative and random forces is preserved. Nikunen et al. [58] showed that the accuracy and performance of the Shardlow scheme is superior to that of several other schemes commonly used in DPD. However the kinetic temperature is still significantly overestimated when a large time-step size is used. It is interesting to note that in an earlier work of Monaghan [56] a splitting scheme similar to that of Shardlow [77] was described for handling the drag force on dust particles for modeling dust-gas flow with an SPH method. To recover very large drag coefficients pairwise interactions are computed by sweeping over all the dust-gas particle pairs several times. Although this method originally has been developed for a drag-force model an extension to general viscous flows is straightforward.

In [40] the Shardlow-splitting algorithm was developed for various conditions in DPD (constant-enthalpy, constant-energy). Moreover, the authors extended the method to systems of non-equal mass particles. For constant-energy DPD Shardlow scheme allows for a time step 10^3 larger, while the computational cost of one step is twice that of the standard velocity-Verlet algorithm. Howard and co-authors [26] used an operator splitting approach to simulate the Rouse model of polymer dynamics in flow. It was found that the splitting method has second-order weak convergence and is unconditionally stable. In section 4 a similar implicit time integration scheme for SDPD is proposed.

Another issue limiting the scope of application of mesoscopic particle methods is *layering* of the fluid particles near solid wall. Layering of liquids near a solid surface is a well known phenomenon in nanofluids and it has been intensively studied experimentally and numerically [33].

The effect is associated to large fluctuations arising in the molecular number density which are ultimately due to a structure induced in the liquid by the presence of the solid wall. The strong inhomogeneities of nanofluids caused by layering effects produce phenomena that are not observed in the continuum, as for example depletion layers, modified transport coefficients (viscosity, diffusivity coefficients) and slip flow. It has often been shown that the amount of layering observed in molecular dynamics (MD) simulations of confined fluids depends strongly on the type of wall as well as on the wall-liquid microscopic interaction parameters, and decreases rapidly as the distance from the surface exceeds typically a few molecule sizes [93]. At larger distances the number density becomes almost constant and the fluid behaves like a continuum. Although these phenomena are to be expected on the molecular level, they are artificial on larger scales [97].

The soft potential used in DPD does not prevent particle penetration into the solid wall. Hence, some effort must be made to enforce the boundary conditions. Approaches based on increased density of wall particles or increased interaction strength between fluid and wall particles have been proposed in the past, leading, however, to depletion of the particles and layering effects [68]. As suggested above, although the presence of wall-induced layering is physically reasonable on the length scale of an atom, it should not occur at the typical scales of DPD particles which are orders of magnitude larger.

Layering is also seen with the SPH method. However, particle layering does not produce inaccurate results since the macroscopic mass fluid density is kept constant and flow properties (e.g. velocity, pressure fields) are concerned. There are several physical situations in which, rather than the local hydrodynamic properties, the exact Lagrangian dynamics of a single fluid particle is the central focus of the investigation and study of a single polymer dynamic is an example of such situation. In such a case the artificial ordering exhibited by coarse-grained particle methods introduces spurious effects which must be avoided. Some attempts to remedy these problems involve, for example, reflection of the particles at the wall [98], adaptive models for wall-particle interactions [2, 68], an extension of the phase-field approach to DPD [100] and the multi-body DPD method [85]. In [18] the authors considered several types of boundary conditions combined with a bounce-back reflection rule and found that boundary conditions based on the frozen wall particles after a pre-processing stage were able to eliminate the number

density fluctuations in the near-wall region. Duong-Hong and co-authors [11] implemented a two-layer frozen-particle structure as a boundary condition and reported a reduction of number density fluctuations. Nevertheless, a bounce-back of the penetrating particles was still required. In [23] the solid wall in many-body DPD was represented by the amorphous particles when each particle is attached to a site by a harmonic spring. Additionally, a repulsive force is used on the liquid particles which penetrate into the wall. The method allows reducing particle layering and artifacts in the temperature field.

In section 5 we present a method to solve the wall penetration and particle layering problems in SDPD. To illustrate the proposed method we performed a simulation of the tethered DNA in flow. Note that no anomalous polymer densities close to the wall were reported in the recent direct observation of a single DNA [47, 46].

2.2.4 Mesoscale simulation of DNA with the SDPD method

A polymer chain in SDPD can be represented as several SDPD particles connected by a spring force. The quantitative validation of this model is a major part of this work and is presented below. Here we discuss qualitatively how the forces from table 2.1 are represented in such a model. *Viscous drag* is included by equation (2.3): a polymer bead interacts with solvent particles by the viscous force. *Entropic elasticity* is represented by the spring force between beads and represents a coarse-grained model of chemical bonds in the chain. *Brownian forces* are introduced by equation (2.6) in a thermodynamically consistent way. Excluded-volume interactions are represented by pressure forces, which are stronger than conservative forces in DPD and preclude particle penetrations. SDPD naturally includes *internal viscosity*. In the model considered below the viscous interaction between bead-bead pair is the same as for bead-solvent and solvent-solvent pairs, but it can easily be changed. If the typical extension of the spring is of about the interparticle distance chain crossing is almost impossible and chain *self-entanglement* can be modeled.

In the final part of the work we present applications. In section 6 we show that the method can correctly represent the statistics and the dynamic behavior of the chain. Also the effect of geometrical confinement is investigated. In section 7 a more complex case is considered: the

dynamics of the tethered DNA in shear flow. This case strongly relies on the wall model and polymer-wall interactions. Specifically, we study the so called cyclic motion of the tethered DNA. Doyle et al. [10] proposed that the tethered DNA changes between stretched and coiled configurations by repetitive recirculating motion (the cyclic motion). This motion can be described as follows. Typically, the chain is coiled and stays close to the wall until thermal fluctuations drive it away from the surface into the region of stronger flow. Subsequently, it stretches and its free end rotates back to the wall, and the chain recoils. An important question is whether this motion is representative behavior of the tethered DNA, such as the tumbling behavior of the free DNA in simple shear flow. In some earlier works periodic motion with a characteristic period of the order of magnitude larger than the relaxation time was reported [75, 8]. But more recent studies do not confirm the existence of periodic motions [47, 102]. Note the last two works used improved experimental and simulation techniques. Lueth et al. [47] for the first time visualized tethered DNA in flow gradient direction and Zhang et al. [102] showed the consistency of the simulation results between different simulation methods: Brownian Dynamics, Lattice Boltzmann, and direct Monte Carlo method.

For the tethered DNA our SDPD simulations show good agreement with experimental data for the static parameters of the DNA (the extension, the distance from the wall, the beads distribution), dynamic parameters (relaxation time) are consistent with molecular dynamics and Brownian dynamics simulations. The cyclic motion is studied by analyzing the power spectrum density, cross-power spectrum density, and cross-correlation function data, and it was found that the cyclic motion is more likely an isolated event and not a representative behavior of the tethered DNA in shear flow.

3 Self-Diffusion of SDPD particles

In paper I [42] an analytical expression for the self-diffusion coefficient D in an SDPD liquid was developed. The accuracy and the robustness of this prediction over a wide range of the model parameters were tested numerically. The method allows for a systematic control of the self-diffusion coefficient and the Schmidt number of the simulated liquid without the need to perform preliminary computations.

In the introduction a brief review of existing methods to study transport properties of liquids with a focus on the DPD is given. It is pointed out that for DPD the prediction of self-diffusion and viscosity is still an open question. In the following the Smoothed Dissipative Particle Dynamics method is introduced.

In the next part of the paper an analytical expression for diffusion coefficient following approach of Groot and Warren [22] is derived. Equation (10) of the paper is a Stokes-Einstein-type relation which links diffusion coefficient, temperature, viscosity, and resolution parameter of SDPD. It is a main result of the paper. Several simulations were performed to verify Equation (10) and it was found that it gives a correct prediction of the diffusion coefficients up to Schmidt number about 10^6 . Typical liquids have Schmidt number of 10^3 or larger. It was checked that solid-like structures do not occur in the simulation by inspecting the radial distribution function. No indications of any secondary peaks produced by partially crystallized structures were found.

I derived Equation (10), performed simulations, and prepared the journal publication.

4 A Splitting scheme for SDPD

In paper II [44] an implicit numerical scheme for SDPD to increase the time-step size was proposed. Simulations using the new method show close agreement with explicit-scheme results for Couette and Poiseuille flow. The results of benchmarks for temperature control are also presented. The radial distribution function of the mesoscopic model liquid is examined and found to be in agreement with experimental results.

In the introduction a brief review the SDPD method is given, and it was show that SDPD suffers from the same disadvantages as DPD. One of such disadvantages is *the Schmidt number problem.*, the difficulty to achieve realistic Schmidt number in simulations due to time step constraints.

In the method section the SDPD method is introduced and the time step constraints arising from the Courant-Friedrichs-Lewy condition and a time step constraint own to viscosity diffusion are discussed. The last condition is dominant for microscopic simulations. A novel implicit integration method which can be viewed as a combination of the Shardlow [77] and Monaghan [56] schemes applied to SDPD is presented. The performance of the method for conditions typical for microfluidic simulations is studied, and in particular the previously mentioned Schmidt number problem [86] is addressed. This new method is a main result of the paper.

The key idea of the method is to split the integration process in such a way that the conservative forces are calculated separately from the dissipative and random force. For the conservative terms the traditional explicit or semi-implicit techniques for SPH can be used. The random and the viscous forces (fluctuation-dissipation part) are updated in a pairwise fashion of the particles at a given time. The structure of the resulting pair interaction is very simple, and it is possible to obtain an implicit method that conserves momentum.

In the next sections several numerical validations of the method are given and show that for typical microfluidic conditions the method gives an acceptable overall accuracy for simulations performed without thermal fluctuations, and allows the very large Schmidt number when thermal fluctuations are included. Simulations of the polymer chain in shear and Poiseuille flow are performed to show how the methods can be used in the situation when the Schmidt number has a critical effect on the results.

I developed the method, wrote the necessary computer code, performed simulations and analyzed the results, and prepared the journal publication.

5 Wall-Bounded SDPD simulation

Paper III [43] is concerned with artifacts owing to the coarse-graining procedure for particle based methods. One of such artifacts is particle ordering in the near-wall region. In simulations of a polymer tethered at the wall undergoing shear flow this artifact is very pronounced: the polymer sticks to the wall and exhibits over-extension for higher shear rates. It is reported that a version of DPD with a so-called solidification boundary formulation and conservative-force interactions based on the equation of state allows for reducing the number density fluctuations in the near-wall region. The numerical model considered in this paper can be seen as a variant of SDPD [28].

In the introduction the literature on the wall layering problem and previously proposed remedies are reviewed. The remedies include: reflection of the particles at the wall, adaptive models for wall-particle interactions, an extension of the phase-field approach to DPD, the multi-body DPD method. A method is developed that replaces the classical expression for the conservative force by a new one involving an equation of state and “freezes” the boundary particles after they achieve thermal equilibrium, producing an amorphous solid structure. In contrast to existing methods this approach can be used for unsteady problems and arbitrarily shaped boundaries.

In the methods section the governing equations and the model of the polymer chain are presented. Details of the amorphous wall model are also given.

In the following section simulations of the 3D channel periodic in y and z directions and wall in x direction are reported. It is concluded that the amorphous wall does not induce any significantly ordered structure in the liquid close to the surface. The simulations section is concerned with tethered polymers. The amorphous wall eliminates the polymer-sticking effect and does not result in polymer over-stretching. The average polymer extension as a function of Weissenberg number agrees with experiments better than in the case of cubic-lattice wall.

I proposed the amorphous-wall approach. It was the most successful of many attempts we performed with co-authors to combat polymer sticking. I performed the simulation and analyzed the results, and prepared the journal publication.

6 Free polymer simulation

In paper IV [41], the Smoothed Dissipative Particle Dynamics method for mesoscopic flows is extended for a polymer molecule suspended in a Newtonian liquid. The method is used to study the configurational behavior of the polymer chain in bulk and confined geometries. In the unbounded case, exact static and dynamic scaling relations have been found according to the Zimm theory. The effect of confined geometries on the conformational properties of the polymer molecules has been analyzed showing results in agreement with previous numerical experiments.

In the introduction a review of numerical methods for simulation of polymer chains is provided. In the method section the equations for the SDPD solvent and a model of the solid wall are presented. The mechanical model of the polymer chain is a linear chain of polymer beads, each bead representing a mixture of polymer monomers together with solvent molecules. Hydrodynamic interactions between polymer beads occur via viscous and pressure terms between SDPD particles. Excluded-volume effects are directly taken into account through the pressure terms, there is no need to introduce short-range Lennard-Jones forces between beads. The model of the polymer chain is an original contribution of this paper.

In the following sections the conformational properties of the polymer molecule are investigated. First, the SDPD method is applied to the study of a polymer molecule in an infinite solvent medium under zero-flow condition. The theoretically predicted universal scaling laws for several polymer properties are tested numerically. The static and dynamic behavior of the conformational polymer properties as well as the structure factor have been intensely studied using a variety of methods and are compared here with the present results. Second, the effect of geometric confinement is investigated. It is generally known that the confinement alters the behavior of a polymer molecule which in a micro-channel extends along the channel axis to

a substantial fraction of its contour length. Scaling laws for the dependence of the polymer stretch upon the channel width have been proposed theoretically and validated numerically in a number of situations. The two-dimensional static properties of a polymer molecule confined in a micro-channel are investigated and the results are compared with previous theoretical and numerical work.

I wrote the necessary computer code, contributed to the method development, performed the simulations and analyzed the results, wrote manuscript of the journal publication.

7 Tethered polymer in shear flow

In V [45] an application of the SDPD method to the simulation of tethered DNA dynamics in shear flow is presented. The observed properties are in general agreement with previous experimental, numerical and theoretical work. The cyclic motion phenomenon is studied by power spectrum density and cross-correlation function analysis, which suggest that there is only a very weak coherent motion of the tethered DNA for characteristic timescales larger than the relaxation time. Cyclic motion is more likely an isolated event than a typical mode of DNA motion.

In the introduction an overview of the work on tethered polymers in shear flow is given. The method section outlines the SDPD method, the model for the polymer chain, and the amorphous wall model. Validation of the setup is done for a case without flow: the distribution of the polymer bead density and the distribution of the last bead are compared with theoretical predictions.

The results section is a central part of the paper. The two-dimensional bead distribution, the polymer extension, the normalized standard deviation of the extension are reported. Note that in experiments the last quantity has a characteristic maximum which was reproduced in our simulations. Furthermore, dynamical quantities of the polymer chain are reported: the mean-square displacement of chain center of mass and the extension relaxation time.

The discussion session is mainly concerned with the possible cyclic motion of the chain. It is defined as repeating changes between stretched and coiled configurations by a recirculating motion. This motion can be described as follows. Typically, the chain is coiled and stays close to the wall until thermal fluctuations drive it away from the surface into the region of stronger flow. Subsequently, it stretches and its free end rotates back to the wall and the chain recoils. As a first step to investigate the cyclic motion animated simulation data are visually

examined. Although one can find examples of cyclic events these events appear to be isolated and not representative since most of the time the DNA does not exhibit any repeating motion patterns. The cross-power spectrum density (CPSD) and the power spectrum density (PSD) of the autocorrelation function (ACF) are examined for indications of cyclic motion, and it is concluded that there is no evidence of the cyclic motion.

I wrote the necessary computer code, performed the simulations, post-processed the data and wrote the journal publication.

8 Papers

8.1 Paper I

Self-diffusion coefficient in smoothed dissipative particle dynamicsSergey Litvinov,¹ Marco Ellero,^{1,2,a)} Xiangyu Hu,¹ and Nikolaus A. Adams¹¹*Lehrstuhl für Aerodynamik, Technische Universität München, 85747 Garching, Germany*²*Departamento de Física Fundamental, UNED, Apartado 60141, 28080 Madrid, Spain*

(Received 25 September 2008; accepted 5 December 2008; published online 13 January 2009)

Smoothed dissipative particle dynamics (SDPD) is a novel coarse grained method for the numerical simulation of complex fluids. It has considerable advantages over more traditional particle-based methods. In this paper we analyze the self-diffusion coefficient D of a SDPD solvent by using the strategy proposed by Groot and Warren [J. Chem. Phys. **107**, 4423 (1997)]. An analytical expression for D in terms of the model parameters is developed and verified by numerical simulations. © 2009 American Institute of Physics. [DOI: 10.1063/1.3058437]

Soft matter systems, such as polymer suspensions, polymer melts, colloids, or emulsions, are an extremely active area of research for both academic and industrial purposes. The interest in dealing with increasingly complex problems in the micro- and macroscale has provided a strong stimulus for the development of a wide class of numerical methods specifically designed to model complex mesoscopic flow physics. A straightforward computational tool to study the transport properties of liquids is molecular dynamics (MD).¹ The obvious disadvantage of an atomistic representation of the liquid is the overwhelming computational cost for practically relevant length and time scales of macroscopic experiments. For simple configurations extensive studies by MD of transport properties have been performed, e.g., a self-diffusion coefficient has been extracted with high accuracy.² The large scale separation between atomistic and typical lengths occurring in soft matter systems has triggered the development of a new class of so-called mesoscopic methods allowing for simulations on much larger length and time scales than MD. Lattice gas automata,³ lattice Boltzmann methods,^{4,5} and multiparticle collision dynamics⁶ represent some popular examples. Among them, dissipative particle dynamics (DPD) (Ref. 7) is receiving considerable attention. A DPD fluid is represented as a collection of particles, which interact through conservative, dissipative, and stochastic forces. Stochastic forces take into account the thermal fluctuations, which describe diffusive processes at the mesoscopic scales. The correct hydrodynamics is recovered at larger scales due to the fact that linear and angular momenta are locally conserved by the particle interactions. Equilibrium and transport properties of DPD systems have been extensively studied in literature.^{8–10} Following the introduction of the method in Ref. 7, the basis of its statistical mechanics was established in Ref. 11.

A critical issue in DPD is the determination of the transport coefficients of the simulated liquid. In Refs. 12 and 13 explicit predictions for the viscosity and the self-diffusion coefficient in terms of the model parameters were given. However, the validity of these analytical expressions is re-

stricted to the ideal-gas equation of state and to the limit of small time step. Furthermore, as found in Ref. 14, the prediction failed to reproduce correctly the diffusion coefficient for the widely used velocity-Verlet integration scheme. In a recent work Noguchi and Gompper¹⁵ studied the time step dependence of the viscosity and diffusion coefficient. However, how to predict self-diffusion accurately in DPD is still an open question.

A few years ago a generalization of the smoothed particle hydrodynamics methods (SPH) (Ref. 16) for flow problems occurring at mesoscopic scales was introduced as smoothed dissipative particle dynamics (SDPD).¹⁷ Despite a resemblance with DPD, it has been shown that the new method possesses several improved features: (i) SDPD is based on a second-order discretization of the Navier–Stokes equations such that the transport coefficients (i.e., viscosity, thermal conductivity, etc.) are input parameters; (ii) hydrodynamic behavior is obtained at length scales of the same order of particle dimension and no coarse-graining assumption is needed; (iii) arbitrary expressions for the equation of state can be adopted and they are not restricted to the specific form used in DPD;¹³ and (iv) the fluid particles have a specified physical length and the thermal fluctuations scale correctly with this size.¹⁸

Concerning the transport properties of SDPD, viscosity is an input parameter; therefore no kinetic theory or preliminary computations are necessary to evaluate viscosity. However, the self-diffusion coefficient D of a fluid particle cannot be specified *a priori* and therefore needs to be estimated. It should be noted that an accurate expression for D in terms of the model parameters is crucial for the determination of the Schmidt number Sc of the model liquid. For instance, the value of Sc affects strongly the nonequilibrium properties of suspended polymer molecules.¹⁴

The objective of this Communication is the following: first, we will develop an analytical expression for the self-diffusion coefficient D in a SDPD liquid and, second, we will check numerically the accuracy and the robustness of this prediction over a wide range of the model parameters. The result allows for a systematic control of the self-diffusion coefficient and the Schmidt number of the simu-

^{a)}Electronic mail: marco.ellero@ aer.mw.tum.de.

lated liquid without the need to perform preliminary computations.

In the following we briefly review the main SDPD equations. The discretized isothermal Navier–Stokes equations (continuity and momentum) for a set of Lagrangian particles have been given, for example, in Refs. 16 and 19 and they read

$$\rho_i = m_i \sum_j W_{ij}, \quad (1)$$

$$\begin{aligned} \frac{d\mathbf{v}_i}{dt} = & -\frac{1}{m_j} \sum_j \left(\frac{p_i}{\sigma_i^2} + \frac{p_j}{\sigma_j^2} \right) \frac{\partial W_{ij}}{\partial r_{ij}} \mathbf{e}_{ij} \\ & + \frac{\mu}{m_i} \sum_j \left(\frac{1}{\sigma_i^2} + \frac{1}{\sigma_j^2} \right) \frac{\mathbf{v}_{ij}}{r_{ij}} \frac{\partial W_{ij}}{\partial r_{ij}}, \end{aligned} \quad (2)$$

where μ is the dynamic viscosity, m_i is the mass of a particle, W_{ij} is a kernel function, $\sigma_i = \sum_j W_{ij}$ is the inverse of the particle volume, and \mathbf{e}_{ij} and r_{ij} are the normalized vector and distance from particle i to particle j , respectively. ρ and p are related by the equation of state: In this work $p = p_0(\rho/\rho_0)^\gamma + b$ is adopted, where p_0 , ρ_0 , b , and γ are model parameters, which may be chosen such that the local mass density variation is smaller than a given magnitude. Equations (1) and (2) represent the deterministic part of the particle dynamics. By using the general equation for non-equilibrium reversible-irreversible coupling formalism,^{20,21} thermal fluctuations can be directly introduced in Eqs. (1) and (2) by adding the following terms:¹⁷ $d\tilde{m}_i = 0$ and $d\tilde{\mathbf{P}}_i = \sum_j B_{ij} d\tilde{W}_{ij} \mathbf{e}_{ij}$, where $d\tilde{W}_{ij}$ is the traceless symmetric part of an independent increment of a Wiener process and B_{ij} is defined as

$$B_{ij} = \left[-4k_B T \mu \left(\frac{1}{\sigma_i^2} + \frac{1}{\sigma_j^2} \right) \frac{1}{r_{ij}} \frac{\partial W}{\partial r_{ij}} \right]^{1/2}. \quad (3)$$

This expression represents the SDPD fluctuation-dissipation theorem and guarantees that all the energy introduced by the stochastic kicks on the particles is entirely dissipated by the viscous terms in Eq. (2).¹⁷ Unlike DPD, the tensorial generalization of the Wiener process in $d\tilde{\mathbf{P}}_i$ allows for a rigorous identification of the irreversible part of the dynamics as a second-order accurate SPH discretization of the Navier–Stokes equations.

Let us present now a derivation of the self-diffusion coefficient for the SDPD fluid particles. The following notation for the particle accelerations will be used:

$$\frac{d\mathbf{v}_i}{dt} = \frac{1}{m_i} (\mathbf{F}_i^C + \mathbf{F}_i^D + \mathbf{F}_i^R), \quad d\mathbf{r}_i = \mathbf{v}_i dt, \quad (4)$$

where $\mathbf{F}_i^{(C,D,R)} = \sum_j \mathbf{F}_{ij}^{(C,D,R)}$ are the total conservative, dissipative, and random force acting on particle i expressed as a sum of contributions of interactions with all the particles.

According to the derivation given by Groot and Warren in Ref. 13, we neglect the conservative forces and assume that all the particles except particle i are at rest. Additionally, by assuming that the density is uniformly distributed, one can write the following:

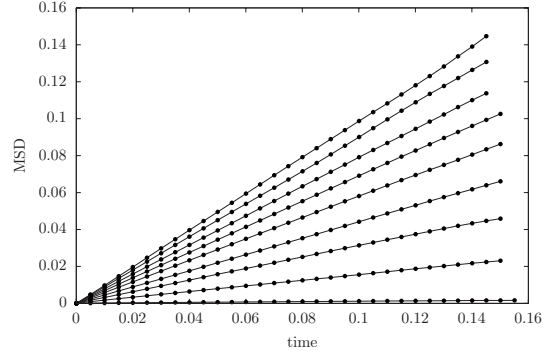


FIG. 1. Mean square displacement for different values of the viscosity: $\mu = 2200.2, 48.9, 24.7, 16.5, 12.4, 10.0, 8.3, 7.1$, and 6.2 (from top to bottom).

$$\frac{d\mathbf{v}_i}{dt} = \frac{1}{m_i} \sum_{i \neq j} \mathbf{F}_{ij}^D + \frac{1}{m_i} \sum_{i \neq j} \mathbf{F}_{ij}^R. \quad (5)$$

Using the fact that the dissipative part is linear in the velocity differences, one can rewrite the equation in a Langevin form as follows:

$$\frac{d\mathbf{v}_i}{dt} + \frac{\mathbf{v}_i}{\tau} = \frac{\mathbf{F}^R}{m_i}, \quad \frac{1}{\tau} = -\frac{2m\mu}{\rho^2} \sum_{i \neq j} \frac{1}{r_{ij}} \frac{\partial W_{ij}}{\partial r_{ij}}. \quad (6)$$

In SPH/SDPD the kernel typically takes the form¹⁶

$$W(\mathbf{r}_{ij}, h) = \frac{1}{h^3} f\left(\frac{|\mathbf{r}_{ij}|}{h}\right). \quad (7)$$

By replacing the summation in the viscous and random forces with an integration, we obtain

$$\frac{1}{\tau} = \frac{8\pi\mu}{\rho h^2} \int_0^{+\infty} f(s) ds. \quad (8)$$

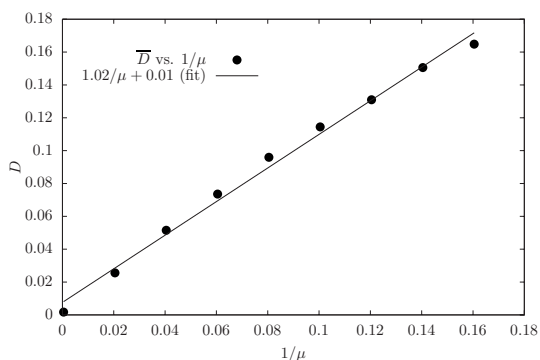
The solution of the Langevin equation (6) leads therefore to the following expression for the diffusion coefficient:

$$D = \frac{\tau k_B T}{3m} = \frac{\rho h^2 k_B T}{24\pi m \mu} \left(\int_0^{+\infty} f(s) ds \right)^{-1}. \quad (9)$$

Finally, for the quintic spline kernel²² used in this work, we obtain the following Stokes–Einstein-type relation:

$$D = \frac{\rho h^2 k_B T}{12m\mu}. \quad (10)$$

This represents the main result of this Communication. In order to verify numerically this expression, the following simulations are performed: A three-dimensional periodic box domain is considered. We take $k_B T = 1$, box size $L = 1.25$, mass density $\rho = 1$, number of particles $N = 15 \times 15 \times 15 = 3375$, and dynamic viscosity μ varying between 6 and 2200. As an initial condition a uniform distribution with the particles placed on a cubic lattice is taken. Particle mass is $m = \rho L^3 / N$, where $h = L/15$ is the kernel cutoff radius. With this choice of input parameters, Eq. (10) simplifies to $D\mu = 1$.

FIG. 2. Diffusion coefficient D plotted against the inverse viscosity $1/\mu$.

The system is advanced in time and the mean square particle displacement $\text{MSD} = \langle [\mathbf{r}(t) - \mathbf{r}(0)]^2 \rangle$ is calculated for different viscosities. The results are plotted in Fig. 1. We found that the domain size effects are negligible and do not affect the results.

The values of the diffusion coefficient for the different simulations performed are computed by fitting the MSD in the limiting linear regime and are plotted against the inverse viscosity in Fig. 2. The best linear approximation to the data is $\mu D = 1.02 \pm 0.03$, which is in good agreement with the prediction of Eq. (10) and confirms the validity of the approximation made by neglecting the conservative terms in Eq. (5). Simulations were repeated for temperatures $k_B T = 0.5, 2$ with the same results.

As mentioned above, an accurate analytical expression of D provides an easy way to control the Schmidt number. This is defined as $\text{Sc} = \nu/D$, where $\nu = \mu/\rho$ is the kinematic viscosity and gives an estimate of the time scale of momentum diffusion with respect to mass diffusion. In a liquid such as water Sc should be on the order of 10^3 or larger. With DPD, Sc does not always agree with the theoretical predictions¹⁴ so that for an unambiguous characterization of the diffusional properties of the solvent, extensive preliminary computations are needed. In the results reported here, very good agreement has been found between the diffusion coefficient evaluated from the simulations and the theoretical

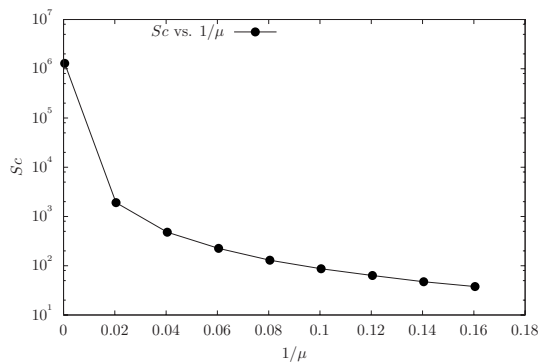
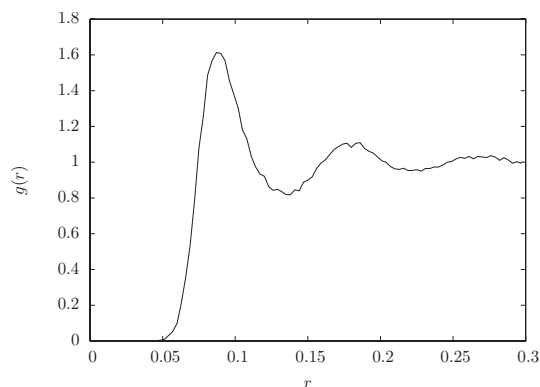


FIG. 3. Schmidt number plotted against inverse viscosity.

FIG. 4. Radial distribution function for $\mu=2200.2$.

predictions over a wide range of viscosities. Therefore one can specify *a priori* the simulated Schmidt number. Its values for the different viscosities considered are shown in Fig. 3 and indicate that, for the largest values of μ , $\text{Sc} \approx 10^6$ as encountered in real experiments. It should be pointed out that the Schmidt number defined in terms of Eq. (10) depends on the fluid particle size h , which is consistent with the physical view that large patches of fluid display less fluctuations than small ones and, consequently, different diffusion properties.¹⁸

As a last remark, we noticed that in Ref. 23 the authors were concerned about the existence of a solidlike structure in DPD simulations at high coarse-graining levels. When a solid structure develops the MSD, after an initial increase, it remains approximately constant, which could produce a misleading result of a very small self-diffusion coefficient and, consequently, large Sc . We have explicitly checked that this situation does not occur in our simulations: first, by looking at the MSD (always linearly increasing with time) and, second, by inspecting the radial distribution function $g(r)$. No indications of secondary peaks (typically indicating partially crystallized structures) were found, as can be seen from the plot in Fig. 4.

Financial support from the Deutsche Forschungsgemeinschaft (DFG) via Grant Nos. EL503/1-1 and AD186/8 is gratefully acknowledged. One of the authors (M.E.) would like to thank Pep Español for useful discussions and suggestions.

¹B. J. Alder and T. E. Wainwright, *J. Chem. Phys.* **31**, 459 (1959).

²K. Meier, A. Laesecke, and S. Kabelac, *J. Chem. Phys.* **121**, 9526 (2004).

³J. Hardy, O. de Pazzis, and Y. Pomeau, *Phys. Rev. A* **13**, 1949 (1976).

⁴G. R. McNamara and G. Zanetti, *Phys. Rev. Lett.* **61**, 2332 (1988).

⁵F. Higuera and J. Jimenez, *Europhys. Lett.* **9**, 663 (1989).

⁶A. Lamura, G. Gompper, T. Ihle, and D. Kroll, *Europhys. Lett.* **56**, 319 (2001).

⁷P. Hoogerbrugge and J. Koelman, *Europhys. Lett.* **19**, 155 (1992).

⁸P. Español, M. Serrano, and H. Öttinger, *Phys. Rev. Lett.* **83**, 4542 (1999).

⁹M. Ripoll, K. Mussawisade, R. Winkler, and G. Gompper, arXiv:cond-mat/0506484 (2005).

¹⁰A. Masters and P. Warren, *Europhys. Lett.* **48**, 1 (1999).

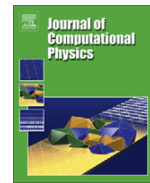
- ¹¹P. Español and P. Warren, *Europhys. Lett.* **30**, 191 (1995).
- ¹²C. A. Marsh, G. Backx, and M. H. Ernst, *Europhys. Lett.* **38**, 411 (1997).
- ¹³R. D. Groot and P. B. Warren, *J. Chem. Phys.* **107**, 4423 (1997).
- ¹⁴V. Symeonidis, G. Karniadakis, and B. Caswell, *J. Chem. Phys.* **125**, 184902 (2006).
- ¹⁵H. Noguchi and G. Gompper, *Europhys. Lett.* **79**, 36002 (2007).
- ¹⁶J. J. Monaghan, *Rep. Prog. Phys.* **68**, 1703 (2005).
- ¹⁷P. Español and M. Revenga, *Phys. Rev. E* **67**, 026705 (2003).
- ¹⁸A. Vázquez, M. Ellero, and P. Español, "Consistent scaling of thermal fluctuations in smoothed dissipative particle dynamics," *J. Chem. Phys.* (in press).
- ¹⁹X. Hu and N. Adams, *J. Comput. Phys.* **213**, 844 (2006).
- ²⁰M. Grmela and H. Öttinger, *Phys. Rev. E* **56**, 6620 (1997).
- ²¹H. Öttinger and M. Grmela, *Phys. Rev. E* **56**, 6633 (1997).
- ²²J. P. Morris, P. J. Fox, and Y. Zhu, *J. Comput. Phys.* **136**, 214 (1997).
- ²³I. Pivkin and G. Karniadakis, *J. Chem. Phys.* **124**, 184101 (2006).

8.2 Paper II



Contents lists available at ScienceDirect

Journal of Computational Physics

journal homepage: www.elsevier.com/locate/jcp

A splitting scheme for highly dissipative smoothed particle dynamics

S. Litvinov^a, M. Ellero^{a,b}, X.Y. Hu^{a,*}, N.A. Adams^a^a Lehrstuhl für Aerodynamik, Technische Universität München, 85748 Garching, Germany^b Departamento de Física Fundamental, UNED, Apartado 60141, 28080 Madrid, Spain

ARTICLE INFO

Article history:

Received 29 September 2009

Received in revised form 1 March 2010

Accepted 17 March 2010

Available online 30 March 2010

Keywords:

Smoothed particle hydrodynamics

Smoothed dissipative particle dynamics

Operator splitting

Schmidt number

ABSTRACT

Smoothed particle dynamics refers to Smoothed Particle Hydrodynamics (SPH) when simulating macroscopic flows and to Smoothed Dissipative Particle Dynamics (SDPD) when simulating mesoscopic flows. When the considered flow is highly dissipative, this otherwise very attractive method faces a serious time-step limitation. This difficulty, known in literature as Schmidt number problem for Dissipative Particle Dynamics (DPD), prevents the application of SDPD for important cases of liquid micro-flows. In this paper we propose a splitting scheme which allows to increase significantly the admissible time-step size for SPH and SDPD. Macroscopic and mesoscopic validation cases, and numerical simulations of polymer in shear flows suggest that this scheme is stable and accurate, and therefore efficient simulations at Schmidt numbers of order $O(10^6)$ are possible.

© 2010 Elsevier Inc. All rights reserved.

1. Introduction

Smoothed particle dynamics is a fully Lagrangian, grid free method, where a smoothing kernel is introduced to approximate functions and their spatial derivatives from data carried by neighboring particles. It is referred to as Smoothed Particle Hydrodynamics (SPH) when simulating macroscopic flows [1], and as Smoothed Dissipative Particle Dynamics (SDPD) when simulating mesoscopic flows [2,3]. SDPD also can be viewed as a modification of Dissipative Particle Dynamics (DPD), a popular mesoscopic particle-based method [4]. Compared to DPD, in SDPD transport coefficients can be prescribed as input parameters rather than being an indirect result of other model parameters. Thermal fluctuations can be introduced adaptively according to the size of the fluid particles.

When the smoothed particle dynamics method is used to simulate low-Reynolds-number and mesoscopic liquid flows, the time-step size limit for stable time integration is usually determined by the viscous effects as such flows are highly dissipative. Specifically, this issue is referred to as Schmidt number problem in DPD [5,6] and obviously also applies to SDPD. The Schmidt number is defined as the ratio of momentum diffusivity (viscosity) and mass diffusivity

$$Sc = \frac{\mu}{D\rho}, \quad (1)$$

where μ is dynamic viscosity, ρ is density and D is the diffusion coefficient. Typical Sc number achieved by SDPD and DPD simulations are of order $O(1)$, which is similar to that of a gas rather than a liquid with $Sc \sim O(10^3)$.

Peters [7] suggested that the diffusion coefficient D appearing in the definition of Sc refers to the molecular diffusivity and therefore is an ill-defined quantity for coarse-grained systems. Accordingly, one would not need to achieve realistically large Sc to capture correct hydrodynamic interactions [8–10]. However, it has been pointed out by Groot and Warren [11] that in order to achieve a realistic liquid behavior it is essential to recover the correct magnitude of Sc in DPD simulation. Furthermore, it was observed by Symeonidis et al. [5,12] that an agreement between simulations and experiments with

* Corresponding author.

E-mail address: Xiangyu.Hu@aer.mw.tum.de (X.Y. Hu).

respect to the non-equilibrium properties of a DNA molecule in a shear flow requires Sc numbers with a magnitude of that for a liquid.

For increasing Sc in DPD simulation one could generate a higher viscosity by increasing the stiffness of the conservative force or the number density of DPD particles, or the dissipative force. Since the represented length scale decreases with the increase of the former two quantities, these approaches contradict the intended coarse-graining property of the DPD method. Therefore, a common approach for increasing Sc is to increase the magnitude of the dissipative force. However, if the DPD particle velocity is updated explicitly, as in the traditional velocity-Verlet method [11], the time integration requires a very small, computationally inefficient time-step size to achieve correct equilibrium properties. To cope with this difficulty, Pagonabarraga et al. [13] have proposed an iterative method where the particle velocity is updated implicitly. However, it is found that such a method is not very practical due to large computational cost. Lowe [14] developed an alternative DPD method where the dissipative and random forces of the traditional DPD method are replaced by a pairwise momentum-conservative Andersen thermostat, which relates the resulting viscosity to a prescribed random relaxation parameter. Due to the Andersen thermostat the method recovers the correct kinetic temperature independently of the time-step size and can be used for simulating a DPD fluid with high Sc . One issue of this method is that the deterministic dissipative term in DPD is replaced by a stochastic term which may lead to strong spatial-temporal fluctuations of the dissipation rate when the time-step size is large.

More recently, a splitting scheme for DPD was proposed by Shardlow [15]. While updating the contribution of the conservative force explicitly, similarly to that of Lowe's method, this method updates the contributions of the dissipative and random forces in pairwise fashion. By this procedure the original DPD formulation of dissipative and random forces is preserved. Nikunen et al. [16] showed that the accuracy and performance of Shardlow's scheme is superior to that of several other schemes commonly used in DPD. However, compared to that of Lowe's method, the kinetic temperature is still significantly overestimated when a large time-step size is used. It is interesting to note that in an earlier work of Monaghan [17] a splitting scheme similar to that of Shardlow [15] was described for handling the drag force on dust particles when modeling dust-gas flow with an SPH method. To recover very large drag coefficients the pairwise interactions are computed by sweeping over all the dust-gas particle pairs several times. Although this method originally has been developed for a drag-force model an extension to general viscous flows appears to be straightforward.

In this work we present a splitting scheme for the smoothed particle dynamic method which can be viewed as a combination and extension of Shardlow's and Monaghan's schemes. The scheme achieves significantly larger time-step sizes than is possible by the standard predictor-corrector and velocity-Verlet schemes, and can be applied for general macroscopic and mesoscopic viscous flows. To demonstrate the robustness and efficiency of the method, a number of validation tests and examples for macroscopic and microscopic flows are given.

2. SPH and SDPD

For SPH the temporal evolution of discrete-particle location and properties is given by

$$\frac{d\mathbf{r}_i}{dt} = \mathbf{v}_i, \quad (2a)$$

$$\rho_i = m_i \sum_j W_{ij} = m_i \sigma_i, \quad (2b)$$

$$\frac{d\mathbf{v}_i}{dt} = -\frac{1}{m_i} \sum_j \left(\frac{p_i}{\sigma_i^2} + \frac{p_j}{\sigma_j^2} \right) \frac{\partial W_{ij}}{\partial r_{ij}} \mathbf{e}_{ij} + \frac{\mu}{m_i} \sum_j \left(\frac{1}{\sigma_i^2} + \frac{1}{\sigma_j^2} \right) \frac{\mathbf{v}_{ij}}{r_{ij}} \frac{\partial W_{ij}}{\partial r_{ij}}, \quad (2c)$$

representing a Lagrangian discretization of the Navier–Stokes equations for isothermal, weakly compressible flow [3]. Here, \mathbf{e}_{ij} and r_{ij} are the normalized vector and distance from particle i to particle j , respectively. $\mathbf{r}_i, \mathbf{v}_i, m_i, \rho_i$ and p_i are position, velocity, mass, density and pressure of a particle i , respectively. σ_i is the inverse of particle volume, and $W_{ij} = W(r_{ij}, h)$ is a kernel function with smoothing length h . An isothermal equation of state is given as

$$p = p_0 \left(\frac{\rho}{\rho_0} \right)^\gamma + b, \quad (3)$$

where p_0, ρ_0, b and γ are parameters which may be chosen based on a scale analysis so that the density variation is less than a given value, usually 1% [18].

Within the SDPD formulation [2] Eq. (2) presents the deterministic part of the particle dynamics. Using the GENERIC formalism [19,20] thermal fluctuations can be taken into account by postulating the following expressions for mass and momentum fluctuations

$$d\tilde{m}_i = 0, \quad (4a)$$

$$d\tilde{\mathbf{P}}_i = \sum_j B_{ij} d\overline{\overline{W}}_{ij} \mathbf{e}_{ij}, \quad (4b)$$

where $d\overline{\overline{W}}_{ij}$ is the traceless symmetric part of a tensor of independent increments of a Wiener process, and B_{ij} is defined as

$$B_{ij} = \left[-4k_B T \mu \left(\frac{1}{\sigma_i^2} + \frac{1}{\sigma_j^2} \right) \frac{1}{r_{ij}} \frac{\partial W}{\partial r_{ij}} \right]^{1/2}, \quad (5)$$

where k_B is Boltzmann constant and T is a prescribed fluid temperature [3]. Note that the evolution equations for SPH and SDPD can be written in a generic form as

$$d\mathbf{v}_i = \frac{1}{m_i} \left(\mathbf{F}_i^C dt + \mathbf{F}_i^D dt + d\tilde{\mathbf{P}}_i \right), \quad (6a)$$

$$d\mathbf{r}_i = \mathbf{v}_i dt, \quad (6b)$$

where $\mathbf{F}_i^C = \sum_j \left(\frac{p_i}{\sigma_i^2} + \frac{p_j}{\sigma_j^2} \right) \frac{\partial W_{ij}}{\partial r_{ij}} \mathbf{e}_{ij}$ is the conservative force and the $\mathbf{F}_i^D = \sum_j \left(\frac{1}{\sigma_i^2} + \frac{1}{\sigma_j^2} \right) \frac{\mathbf{v}_{ij}}{r_{ij}} \frac{\partial W_{ij}}{\partial r_{ij}}$ is the dissipative force as given by the right hand side of Eq. (2c)

When Eq. (6) is integrated by standard explicit schemes, such as a predictor–corrector scheme for SPH or velocity-Verlet for SDPD, the time-step size is constrained by the Courant–Friedrichs–Lewy (CFL) condition

$$\Delta t \leq \Delta t_c = 0.25 \frac{h}{c}, \quad c = 10V_{max}, \quad (7)$$

where c is a chosen speed of sound, V_{max} is the maximum flow speed, and

$$\Delta t \leq \Delta t_\mu = 0.125 \frac{\rho h^2}{\mu}. \quad (8)$$

Since typical micro-fluidic problems are characterized by very small Reynolds numbers and dominated by viscous effects [18], it is desirable to relax the viscous time-step limit Δt_μ for numerical simulation.

3. Splitting scheme

The fundamental concept of the splitting approach is that the contribution of the conservative force is updated separately from that of the dissipative and the random forces (time-splitting). The latter are updated implicitly in a pairwise fashion (operator-splitting).

The splitting scheme can be described as follows. First, an intermediate velocity $\tilde{\mathbf{v}}_i$, due to dissipative and random forces, is obtained in a pairwise fashion by sweeping over all pairs of neighboring particles a certain number of times (N_s). For a specific particle pair their velocities are updated according to the following two-step procedure. The first step is explicit, and can be written as

$$\mathbf{v}'_i = \mathbf{v}_i + \frac{1}{2} \frac{1}{m_i} \mathbf{F}_{ij}^D \Delta t_{N_s} + \frac{1}{2} \frac{d\tilde{\mathbf{P}}_{ij}}{m_i}, \quad (9a)$$

$$\mathbf{v}'_j = \mathbf{v}_j - \frac{1}{2} \frac{1}{m_j} \mathbf{F}_{ij}^D \Delta t_{N_s} - \frac{1}{2} \frac{d\tilde{\mathbf{P}}_{ij}}{m_j}, \quad (9b)$$

where $\Delta t_{N_s} = \Delta t/N_s$ is the sub-time-step size, and $d\tilde{\mathbf{P}}_{ij}$ is the momentum fluctuation between the particle pair. The second step is implicit, and can be written as

$$\tilde{\mathbf{v}}_i = \mathbf{v}'_i + \frac{1}{2} \frac{1}{m_i} \tilde{\mathbf{F}}_{ij}^D \Delta t_{N_s} + \frac{1}{2} \frac{d\tilde{\mathbf{P}}_{ij}}{m_i}, \quad (10a)$$

$$\tilde{\mathbf{v}}_j = \mathbf{v}'_j - \frac{1}{2} \frac{1}{m_j} \tilde{\mathbf{F}}_{ij}^D \Delta t_{N_s} - \frac{1}{2} \frac{d\tilde{\mathbf{P}}_{ij}}{m_j}, \quad (10b)$$

where $\tilde{\mathbf{v}}_i, \tilde{\mathbf{v}}_j$ on both sides of Eq. (10) are updated simultaneously. Monaghan [17] used an updating similar to Eq. (10), where no thermal fluctuations are present and $\tilde{\mathbf{F}}_{ij}^D$ is given by a drag-force model rather than by an expression for a general viscous force such as used here, see Eq. (2). As there are only two unknowns for two equations the solution of Eq. (10) is straightforward and stable, independently of Δt_{N_s} . For $\mu \rightarrow \infty$ the resulting velocities at the end of a single pair-update are

$$\tilde{\mathbf{v}}_j = \tilde{\mathbf{v}}_i = \frac{m_i \mathbf{v}_i + m_j \mathbf{v}_j}{m_i + m_j}, \quad (11)$$

a property also obtained by Lowe [14] after relaxation and before thermalization.

Using $\tilde{\mathbf{v}}_i$, a half-time-step velocity is obtained from half of the conservative-force acceleration (first part of velocity-Verlet scheme)

$$\mathbf{v}_i^{n+1/2} = \tilde{\mathbf{v}}_i + \frac{1}{2} \frac{1}{m_i} \mathbf{F}_i^C \Delta t, \quad (12)$$

where Δt is time step, and \mathbf{F}_i^C is the total conservative force evaluated from the particle position \mathbf{r}_i^n . The new-time-step particle position is updated

$$\mathbf{r}_i^{n+1} = \mathbf{r}_i^n + \mathbf{v}_i^{n+1/2} \Delta t. \quad (13)$$

At last, the new-time-step velocity is obtained from

$$\mathbf{v}_i^{n+1} = \mathbf{v}_i^{n+1/2} + \frac{1}{2} \frac{1}{m_i} \mathbf{F}_i^{C,n+1} \Delta t, \quad (14)$$

where $\mathbf{F}_i^{C,n+1}$ is evaluated at the new-time-step particle position \mathbf{r}_i^{n+1} .

Eq. (10) is an operator-splitting approach similar to that of Shardlow [15] where the particle velocities are solved implicitly and locally in a pairwise fashion instead over the entire domain. An important difference is that here the pairwise updating of the particle velocities is performed in N_s sweeps for all particle pairs. For macroscopic flow simulations, optimum accuracy can be obtained by an adaptive sweeping scheme following Whitehouse et. al. [21]. For every time step consecutively $N_s = 2^m$ and $N_s = 2^{m+1}$ sweeps are performed, with m increasing until the relative error between the evaluated velocities is less than a specific dimensionless tolerance ε . The last calculated velocity is adopted and at the next time step the index m is decreased by one. It is found that a tolerance $\varepsilon = 5 \times 10^{-3}$ gives a good compromise between computational efficiency and accuracy. Note that the relaxed viscous stability on one hand allows for large time-step sizes, on the other hand may increase the temporal truncation error for large time-step sizes. For mesoscopic flow simulations, it is difficult to specify discrete tolerance ε a priori. For such cases our numerical experiments, as also will be shown in next sections, suggest that a fixed parameter $N_s = 5$ is sufficient to achieve Sc up to order $O(10^6)$.

4. Validation tests

The splitting scheme is tested by macroscopic Poiseuille and Couette flows and a mesoscopic temperature control test. For the macroscopic cases, the overall accuracy is measured by using an L_1 -norm error defined as

$$L_1 = \frac{\sum_{i=1}^N |U_i^{th} - U_i^{SPH}|}{\sum_{i=1}^N |U_i^{th}|}, \quad (15)$$

where U_i^{th} , U_i^{SPH} are the theoretical and the simulated velocity fields evaluated at the particle positions \mathbf{r}_i , and N is the total number of particles. For the mesoscopic case the accuracy of the splitting scheme is measured by the difference between the measured kinetic temperature of the SDPD particle and the input value. Another validation, which is considered as an important issue in DPD [22], is the qualitative comparison between the computed radial distribution functions (RDF) of the SDPD particles and that which is typically obtained for liquids.

4.1. Poiseuille flow

For the first macroscopic case we consider a Poiseuille flow between two walls at $y = 0$ and $y = L$. The flow is initially at rest and suddenly driven by a constant body force F parallel to the x -axis. Periodic boundary conditions are employed in the flow direction. The flow parameters are chosen as $F = 10^{-4}$, $L = 10^{-3}$, $\rho = 10^3$ and $\mu = 10^{-6}$, which gives a maximum velocity at steady state of $V_{max} = FL^2/\mu$. The Reynolds number is $Re = Lv_{max}/\eta = 1.25 \times 10^{-2}$, which is typical for micro-fluidic systems. A series of simulations are performed with increasing particle numbers $N_x = N_y = 10, 20, 40, 80$ (note that the particles initially are on a lattice), $\varepsilon = 5 \times 10^{-3}$ and time-step sizes ranging from $\Delta t = \Delta t_\mu = 7.8125 \times 10^{-5}$ to $16\Delta t_\mu$.

A comparison between the computed velocity profile with $N_y = 40$ and $\Delta t = 4\Delta t_\mu$ at time $t_m = 0.63$ and the theoretical solution is shown in Fig. 1(top). At this time the velocity profile is found to be very close to the steady state solution [18]. Fig. 2 (top) and Fig. 3(top) show the behavior of L_1 -errors with increasing space and time resolution, which suggest at least first-order convergence.

4.2. Couette flow

For the second macroscopic test case we consider a Couette flow between two walls at $y = 0$ and $y = L$, where one wall is at rest and the other is moving at constant speed V_0 . Periodic boundary conditions are employed in the flow direction. The flow parameters are chosen as $\mu = 10^{-6}$, $V_0 = 1.25 \times 10^{-5}$, $L = 10^{-3}$ and $\rho = 10^3$, which gives a Reynolds number of $Re = V_0 L/\mu = 1.25 \times 10^{-2}$ as in the first case. Similarly as in the first case, a series of simulations are performed with $N_x = N_y = 10, 20, 40, 80$, $\varepsilon = 5 \times 10^{-3}$ and time-step sizes ranging from $\Delta t = \Delta t_\mu = 7.8125 \times 10^{-5}$ to $16\Delta t_\mu$.

The comparison between SPH and the analytical solution of the velocity at time instant $t_m = 0.06$ is shown in Fig. 1 (bottom). The L_1 -norm errors at $t_m = 0.06$ are shown in Fig. 2 (bottom) and Fig. 3 (bottom). Again, first-order convergence is obtained.

4.3. Temperature control of SDPD fluid

A mesoscopic box of fluid is considered. The simulation parameters are $k_B T = 1$, box size is $L = 1.25$, density $\rho = 1$, number of particles $N = 15 \times 15 \times 15 = 3375$, which give the input average thermal velocity $v_{kin} = \sqrt{3k_B T/m}$, where m is mass of a

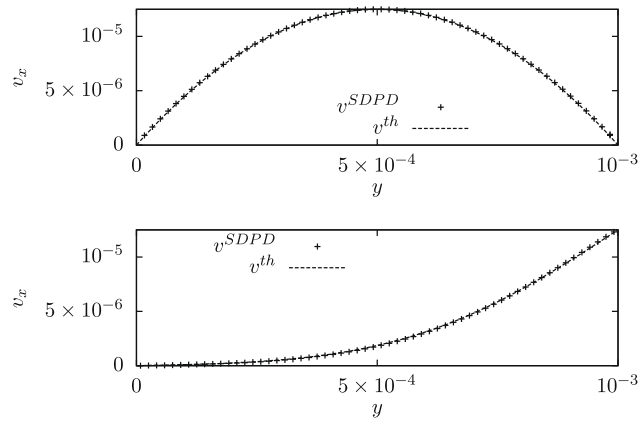


Fig. 1. Comparison of SPH and theoretical solutions for the Poiseuille flow (top) and the Couette flow (bottom) at time $t_m = 0.63$ and $t_m = 0.06$, respectively ($N_y = 40, \Delta t = 4\Delta t_\mu$).

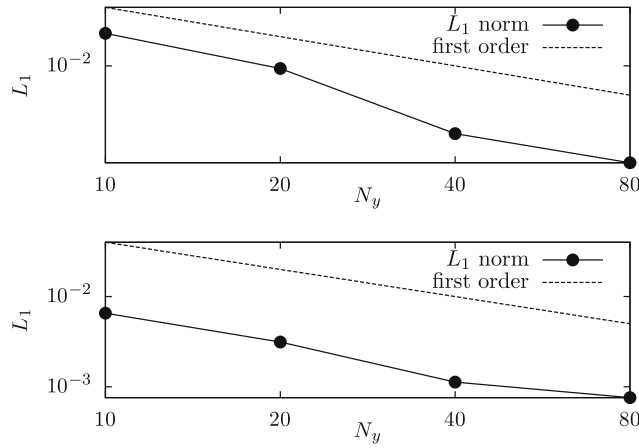


Fig. 2. Comparison of the L_1 -norm error for the Poiseuille flow (top) and Couette flow (bottom) as a function of N_y ($\Delta t = 4\Delta t_\mu$).

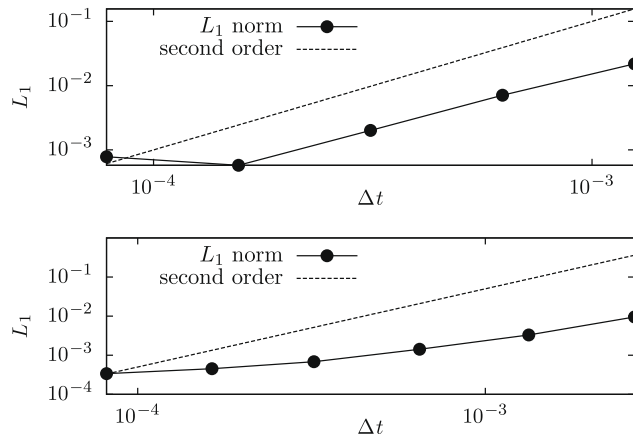


Fig. 3. Comparison of the L_1 -norm error for the Poiseuille flow (top) and Couette flow (bottom) as a function of Δt ($N_y = 40$).

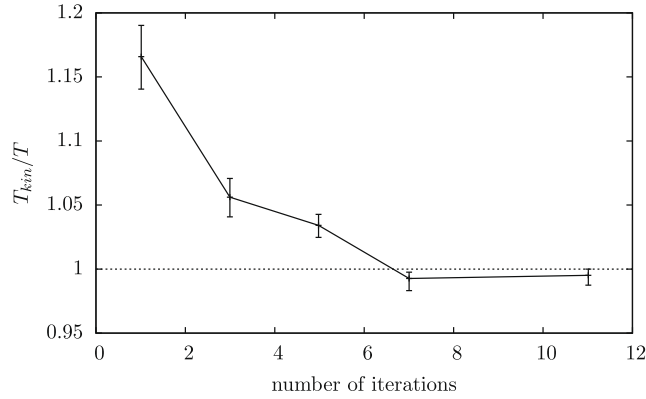


Fig. 4. Difference between the measured averaged kinetic temperature (solid line) and the input temperature (dash line) with increasing number of sweeps.

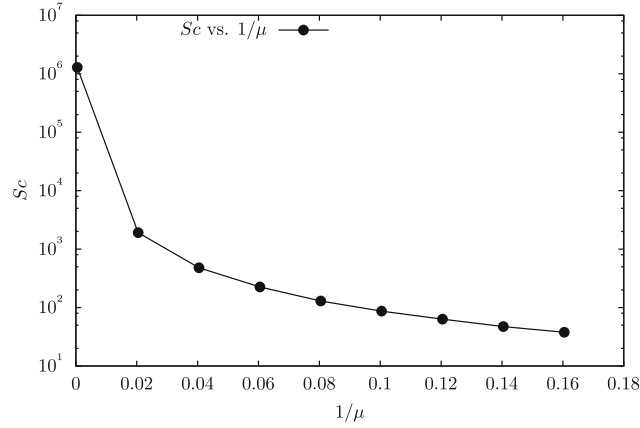


Fig. 5. Relation between the computed Schmidt number of the SDPD fluid and the inputted viscosity (the inversed values is shown on x axis).

particle. In order to study the potential of the splitting scheme a large range of viscosities, from $\mu = 6.25$ to 2.2×10^3 , has been used. The time step used is based on the CFL condition and kept constant for all simulations. To obtain Sc from Eq. (1), the self-diffusion coefficient is measured by fitting the mean-square displacement of the particles.

The relation of the number of sweeps N_s to the predicted kinetic temperature $T_{kin} = m v_{kin}^s / 3k_B$, where v_{kin}^s is the average thermal velocity of the particles, for the maximum input viscosity $\mu = 2.2 \times 10^3$ is shown in Fig. 4.

It is found that the measured kinetic temperature converges to the input value T_{th} with increasing N_s . Note that reasonably small errors below 5% are achieved with $N_s = 5$, where the total computational effort increases by less than 20%. Further numerical experiments show that even fewer N_s sweeps are required for accurate temperature control at smaller viscosities. The relation between Sc and the input viscosity is shown in Fig. 5, suggesting that a Sc of order $O(10^6)$ has been achieved.

The computed RDF of the SDPD particles is shown in Fig. 6, which is not affected by the implicit treatment of the viscous terms and preserves the shape typical for liquids.

5. Polymer in simple shear flow

In this case, the effect of Sc on a polymer chain in simple shear flow is studied. A mesoscopic box of fluid with a 5-bead free polymer in simple shear is considered similarly as in [12]. The polymer is modeled by a chain of double-linked beads [9] which have all properties of SDPD particles, and additionally are subjected to interaction forces with neighboring polymer beads according to the FENE potential

$$U_{FENE} = -\frac{1}{2} k R_0^2 \ln \left[1 - \left(\frac{r}{R_0} \right)^2 \right], \quad (16)$$

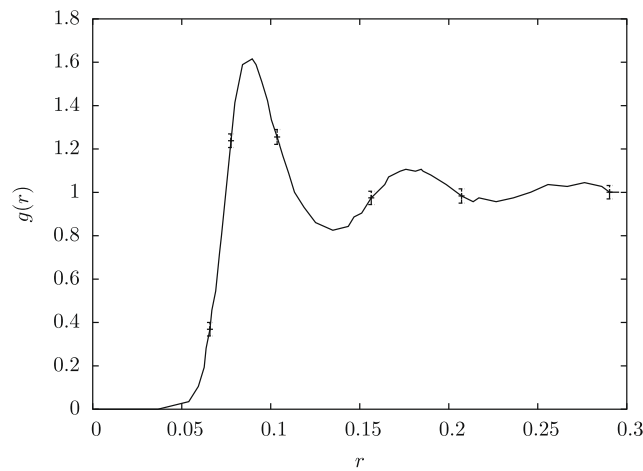


Fig. 6. Computed radial distribution function for the SDPD fluid with $\mu = 2.2 \times 10^3$ and Sc number of order $O(10^6)$.

Table 1

Gyration radius of a free polymer in static solution and in simple shear flow.

Sc	1.225×10^3	2.5×10^3	2.5×10^5	1.0×10^6
$\langle R_g \rangle$	0.0048	0.0052	0.0048	0.0048
$\langle R_g^{\text{flow}} \rangle$	0.0057	0.0058	0.0092	0.0120

where r is the distance between neighboring beads, R_0 is the maximum spring extension, and k is the spring constant. This model of polymer in suspension produces correct scaling laws for static and dynamic properties, see [9] for further details. Other simulation parameters are $k_B T = 1$, box size $L = 0.75$, mass density $\rho = 1$, shear rate $\dot{\gamma} = 0.5$ and number of particles $N = 15 \times 15 \times 15 = 3375$. Periodic boundary conditions are employed in the flow direction and the spanwise direction, and a Lees–Edwards boundary condition [23] is applied at the upper and lower boundaries.

Table 1 summarizes the relations between the values of Sc and gyration radius of a free polymer in static solution ($\langle R_g \rangle$) and in a simple shear flow ($\langle R_g^{\text{flow}} \rangle$).

It is found that the average size of the polymer in static fluid is nearly independent of Sc. However, when the polymer is in a shear flow, its gyration radius increases dramatically with Sc of the solvent, which is in good agreement with the results of [12].

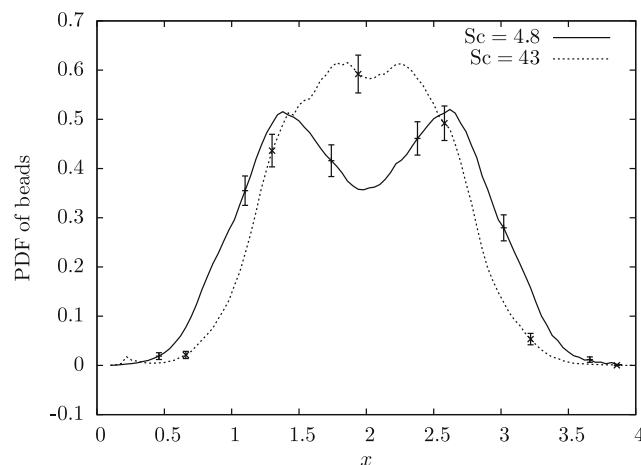


Fig. 7. Effect of Sc on the polymer density profile in Poiseuille flow, where $x = 0$ and 4 correspond the channel walls, for the cases Sc = 4.8 and 43, respectively.

6. Polymer in Poiseuille flow

The SDPD simulation of a polymer in a Poiseuille flow is set up in a box with dimensions $L_x \times L_y \times L_z$, where $L_y = 4.0$, $L_z = 8.0$, and $L_x = 4.0$ is the distance between the walls (at $y = 0$ and $y = L_y$). The flow is driven by a body force in the direction of the z axis. Periodic boundary conditions are employed in the flow direction and the spanwise direction. The number of particles is $N_x \times N_y \times N_z = 10 \times 10 \times 20$, and 20 of them were connected to form a polymer in dilute solution. To illustrate the effect on the distribution of the polymer beads in the channel two simulations are performed with Sc of 4.8 and 43, respectively. The spanwise distribution of polymer mass is shown in Fig. 7. It is found that the depletion region at the center of the channel is more pronounced with low Sc , and the polymer concentration tends to be higher in the center with smaller off-center peaks with high Sc . These results are in agreement with those in the recent study of Millan and Laradji [24], and suggest a strong influence of Sc on the polymer behavior in a shear flow.

7. Concluding remarks

We have developed a splitting scheme for highly dissipative smoothed particle dynamics. In the time-splitting part of the scheme, the contribution of the conservative force is updated separately from that of the dissipative and random forces. In the operator-splitting part of the scheme the particle velocities are updated by sweeping over all particle pairs within the domain in a pairwise fashion with an explicit/implicit two-step algorithm. The number of sweeps in the present scheme is adjusted adaptively to achieve higher accuracy. Numerical experiments show that the present scheme has a great potential in addressing realistic dissipative mesoscopic flow problems without significantly increasing the computational effort.

References

- [1] J.J. Monaghan, Smoothed particle hydrodynamics, *Rep. Prog. Phys.* 68 (8) (2005) 1703–1759.
- [2] P. Español, M. Revenga, Smoothed dissipative particle dynamics, *Phys. Rev. E* 67 (2) (2003) 26705.
- [3] X. Hu, N. Adams, A multi-phase SPH method for macroscopic and mesoscopic flows, *J. Comput. Phys.* 213 (2) (2006) 844–861.
- [4] P. Hoogerbrugge, J. Koelman, Simulating microscopic hydrodynamic phenomena with dissipative particle dynamics, *Europhys. Lett.* 19 (3) (1992) 155–160.
- [5] V. Symeonidis, G.E. Karniadakis, B. Caswell, Dissipative particle dynamics simulations of polymer chains: scaling laws and shearing response compared to DNA experiments, *Phys. Rev. Lett.* 95 (7) (2005) 76001.
- [6] V. Symeonidis, G.E. Karniadakis, A family of time-staggered schemes for integrating hybrid dpd models for polymers: algorithms and applications, *J. Comput. Phys.* 218 (1) (2006) 82–101.
- [7] E.A.J.F. Peters, Elimination of time step effects in DPD, *Europhys. Lett.* 66 (3) (2004) 311–317.
- [8] W.H. Jiang, J.H. Huang, Y.M. Wang, M. Laradji, Hydrodynamic interaction in polymer solutions simulated with dissipative particle dynamics, *J. Chem. Phys.* 126 (4) (2007) 44901.
- [9] S. Litvinov, M. Ellero, X. Hu, N. Adams, Smoothed dissipative particle dynamics model for polymer molecules in suspension, *Phys. Rev. E* 77 (6) (2008) 66703.
- [10] A. Vázquez-Quesada, M. Ellero, P. Español, Consistent scaling of thermal fluctuations in smoothed dissipative particle dynamics, *J. Chem. Phys.* 130 (2009) 034901.
- [11] R.D. Groot, P.B. Warren, Dissipative particle dynamics: bridging the gap between atomistic and mesoscopic simulation, *J. Chem. Phys.* 107 (11) (1997) 4423–4435.
- [12] V. Symeonidis, G. Karniadakis, B. Caswell, Schmidt number effects in dissipative particle dynamics simulation of polymers, *J. Chem. Phys.* 125 (2006) 184902.
- [13] I. Pagonabarraga, M. Hagen, D. Frenkel, Self-consistent dissipative particle dynamics algorithm, *Europhys. Lett.* 42 (4) (1998) 377–382.
- [14] C. Lowe, An alternative approach to dissipative particle dynamics, *Europhys. Lett.* 47 (1999) 145–151.
- [15] T. Shardlow, Splitting for dissipative particle dynamics, *SIAM J. Sci. Comput.* 24 (4) (2003) 1267–1282.
- [16] P. Nikunen, M. Karttunen, I. Vattulainen, How would you integrate the equations of motion in dissipative particle dynamics simulations?, *Comput. Phys. Commun.* 153 (3) (2003) 407–423.
- [17] J. Monaghan, Implicit SPH drag and dusty gas dynamics, *J. Comput. Phys.* 138 (2) (1997) 801–820.
- [18] J.P. Morris, P.J. Fox, Y. Zhu, Modeling low Reynolds number incompressible flows using sph, *J. Comput. Phys.* 136 (1) (1997) 214–226.
- [19] M. Grmela, H. Öttinger, Dynamics and thermodynamics of complex fluids. I: Development of a general formalism, *Phys. Rev. E* 56 (6) (1997) 6620–6632.
- [20] H. Öttinger, M. Grmela, Dynamics and thermodynamics of complex fluids. II: Illustrations of a general formalism, *Phys. Rev. E* 56 (6) (1997) 6633–6655.
- [21] S. Whitehouse, M. Bate, Smoothed particle hydrodynamics with radiative transfer in the flux-limited diffusion approximation, *Mon. Not. R. Astron. Soc.* 353 (4) (2004) 1078–1094.
- [22] F. Thalmann, J. Farago, Trotter derivation of algorithms for brownian and dissipative particle dynamics, *J. Chem. Phys.* 127 (12) (2007) 124109.
- [23] A. Lees, S. Edwards, The computer study of transport processes under extreme conditions, *J. Phys. C: Solid State Phys.* 5 (1972) 1921–1928.
- [24] J.A. Millan, M. Laradji, Cross-stream migration of driven polymer solutions in nanoscale channels: a numerical study with generalized dissipative particle dynamics, *Macromolecules* 42 (3) (2009) 803–810.

8.3 Paper III

Particle-layering effect in wall-bounded dissipative particle dynamics

Sergey Litvinov, Marco Ellero, Xiangyu Hu, and Nikolaus A. Adams

Lehrstuhl für Aerodynamik, Technische Universität München, 85747 Garching, Germany

(Received 18 June 2010; revised manuscript received 6 October 2010; published 10 December 2010)

Dissipative particle dynamics (DPD) is a mesoscopic simulation method that describes “clusters” of molecules as a single numerical particle. DPD is a very effective method but it introduces numerical artifacts through the coarse-graining procedure, such as particle ordering in the near-wall region. These artifacts can result in nonphysical phenomena during a simulation of a polymer tethered to the wall undergoing shear flow: polymer sticking and overextension for higher shear rates. In this paper we report that a version of DPD with a so-called solidification boundary formulation and conservative-force interactions based on the equation of state allows to reduce number density fluctuations in near-wall region significantly.

DOI: [10.1103/PhysRevE.82.066704](https://doi.org/10.1103/PhysRevE.82.066704)

PACS number(s): 47.11.-j, 83.10.Pp, 36.20.-r, 83.10.Rs

I. INTRODUCTION

Layering of liquids near a solid surface is a very well known phenomena in nanofluids and it has been intensively studied experimentally and numerically [1]. The effect is associated to large fluctuations arising in the molecular number density which are ultimately due to a structure induced in the liquid by the presence of the solid wall. The strong inhomogeneities of nanofluids caused by layering effects produce phenomena that are not observed in the continuum, as for example depletion layers, modified transport coefficients (e.g., viscosity) and slip flow [2,3]. It has been often shown that the amount of layering observed in molecular-dynamics simulations of confined fluids depends strongly on the type of wall as well as on the wall-liquid microscopic interaction parameters, and decreases rapidly as the distance from the surface exceeds typically a few molecule sizes [4]. At larger distances the number density becomes almost constant and the fluid behaves like a continuum. Although this phenomena is to be expected on the molecular level, it must be seen as an artifact on larger scales [5].

Recently, numerical methods operating on a coarse-grained level have been developed which try to achieve larger spatiotemporal scales by reducing the number of atomistic degrees of freedom. An important method in this class is dissipative particle dynamics (DPD). DPD is a relatively new mesoscopic method [6] that uses Lagrangian discretization elements (particles) to represent a cluster of molecules rather than individual fluid constituents, allowing for the simulation of complex systems at length and time scales inaccessible to molecular-dynamics (MD) methods. DPD captures important properties of the microscopic flow but it is known to produce numerical artifacts and anomalous behavior under specific situations. For example the implementation of no-slip boundary conditions in DPD remains a challenge. Unlike MD, the soft potential used in DPD does not prevent particle penetration into the solid boundaries, hence some effort must be made to enforce them correctly. Approaches based on increased density of wall particles or increased interaction strength between fluid and wall particles have been proposed in the past, leading, however, to depletion of particles and layering effects [7]. As suggested above, although the presence of wall-induced layering is physically reason-

able at atomistic distances from the solid wall, it should not occur at the typical scales of the DPD particles which are orders of magnitude larger.

It should be noted that layering is frequently observed for many particle-based techniques, such as for example the continuum smoothed particle hydrodynamics (SPH) method [8]. In this method, however, particle layering does not produce inaccurate results as long as the macroscopic mass fluid density is kept constant and the fluid flow properties (e.g., velocity, pressure fields) are concerned. In spite of this, there are several physical situations in which, rather than the local hydrodynamic properties, the exact Lagrangian dynamics of a single fluid particle is the central focus of the investigation. In such cases the artificial ordering exhibited by coarse-grained particle methods introduces spurious effects which must be avoided. Some attempts to remedy these problems involve, for example, reflection of particles near the wall [9], adaptive models for wall-particle interactions [7,10], extension of the phase-field approach to DPD [11] and the multi-body DPD method [12]. In [13] the authors considered several types of boundary conditions combined with a bounce-back reflection rule and found that boundary conditions based on frozen wall particles after a preprocessing stage were able to eliminate the number density fluctuations in the near-wall region. Duong-Hong and co-authors [14] implemented a two-layer frozen-particle structure as a boundary condition and reported a reduction of number density fluctuations. Nevertheless, a bounce-back of penetrating particles was still required.

The objective of this paper is to present a method to solve simultaneously the wall penetration and the unphysical particle-layering problems in coarse-grained DPD simulations. This is achieved by replacing the classical expression for the conservative force by a new one involving an equation of state (described in detail [15]). Additionally, instead of using frozen particles on a lattice to model a solid wall, boundary particles are solidified after achieving thermal equilibrium, producing a final amorphous solid structure. This last idea is not entirely new and has been employed in one of the original papers on DPD [6]. However, unlike previous approaches, the method presented in this work does ensure complete wall impermeability, removes unwanted layering effects, and can be used for unsteady problems and arbitrary-shape boundaries.

To illustrate the proposed method we consider the dynamics of a tethered DNA molecule under constant shear flow. The level of coarse graining for practical simulations of a DNA macromolecule by DPD [5,16,17] requires that the typical size of a DPD particle exceeds the thickness of the atomistic wall monolayer and therefore nanoscopic surface effects are not likely to be important. Moreover, no anomalous behavior for the monomer densities close to the wall has been reported in recent experimental observations of a single-molecule motion [18].

As a final remark, it should be noted that, recently, Delgado-Buscalioni and Coveney [19] reported overextension in MD and hybrid MD-continuum simulations of a tethered DNA molecule under large shear flow when compared with experiments. Near-wall layering of solvent particles was suggested as principal cause of the anomalous behavior. The results presented in this paper confirm this explanation.

II. METHOD

A. Fluid solvent modeling

We employ a modification of the DPD method involving an equation of state in the expression of the conservative forces, similarly to the one used in the smoothed dissipative particles dynamics (SDPD) method [15,20]. The equations of motion for a set of solvent particles characterized by positions/velocities $(\mathbf{r}_i, \mathbf{v}_i)$ can be written in a general form as

$$\begin{aligned} \frac{d\mathbf{r}_i}{dt} &= \mathbf{v}_i, \\ m_i \frac{d\mathbf{v}_i}{dt} &= \sum_j (F_{ij}^C + F_{ij}^D + F_{ij}^R) \mathbf{e}_{ij}, \end{aligned} \quad (1)$$

where m_i is mass of the particle, \mathbf{e}_{ij} the unit vector joining particle i and j and $F_{ij}^{(C,D,R)}$ are the conservative, dissipative, and random interactions between them, given by

$$\begin{aligned} F_{ij}^D &= \eta \xi \frac{A_{ij}}{r_{ij}} (\mathbf{e}_{ij} \cdot \mathbf{v}_{ij}), \\ F_{ij}^R &= (2k_B T \eta)^{1/2} \left(-\xi \frac{A_{ij}}{r_{ij}} \right)^{1/2} \zeta_{ij}, \\ F_{ij}^C &= \left(\frac{p_i m_i^2}{\rho_i^2} + \frac{p_j m_j^2}{\rho_j^2} \right) \frac{\partial W}{\partial r_{ij}}. \end{aligned} \quad (2)$$

Here, η denotes the fluid viscosity, T the temperature, k_B the Boltzmann constant, p_i the pressure for a given particle and $\mathbf{v}_{ij} = \mathbf{v}_i - \mathbf{v}_j$. $A_{ij} = (m_i^2 / \rho_i^2 + m_j^2 / \rho_j^2) \frac{\partial W}{\partial r_{ij}}$, ξ is calibration parameter and ζ_{ij} is a Gaussian variable with zero mean and a variance equal to Δt^{-1} where Δt is the time step [15]. A quintic spline kernel function $W(\mathbf{r}, h)$ is adopted [21], where $W_{ij} = W(\mathbf{r}_i - \mathbf{r}_j, h)$, h being the cutoff radius, and the mass density ρ_i is evaluated by the summation formula

$$\rho_i = m_i \sum_j W_{ij}. \quad (3)$$

Particle pressures are finally calculated from the following ideal gas equation of state:

$$p_i = c \rho_i, \quad (4)$$

where c is the artificial speed of sound which should be sufficiently large in order to keep relative mass density fluctuations below 3% [21].

It turns out that Eqs. (2) correspond to the typical choice adopted in SDPD and represent a Lagrangian discretization of the fluctuating hydrodynamics equations [20]. Note that, unlike standard DPD schemes, here the conservative terms appearing in Eq. (2) depend on the local particle density ρ_i and are truly multibody. By choosing the speed of sound properly, the pressure term reacts strongly to small variations in the density, by increasing the local particle repulsion in areas of large concentration and vice versa. This strategy, successfully employed also in SPH [8], prevents fluid particles to penetrate solid walls completely, without the need to introduce extra bounce-back rules.

B. Tethered polymer model

The model of the polymer consists of a linear chain of N_b DPD particles interacting by finitely extendable nonlinear elastic springs (FENE potential) [22]

$$U(r) = -\frac{HR_0^2}{2} \ln \left(1 - \frac{r^2}{R_0^2} \right). \quad (5)$$

In order to simulate a tethered polymer, the first bead of the chain is located at the wall surface and is not allowed to move.

C. Amorphous wall model

In this paper we consider two alternative ways to model solid walls, namely:

- (i) particles frozen on lattice positions within the solid region (denoted as “simple cubic”), and
- (ii) particles frozen after initial equilibration of the particle distribution (denoted as “random”).

In the latter case, a preliminary run is performed without flow where both, solid and fluid particles are allowed to move according to Eqs. (1). Spatial equilibration is monitored by looking at the evolution of standard order parameters indicating the melt of the initial lattice structure. When a melted state is achieved, solid particles are frozen in their current positions and the shear-flow simulation started.

The present procedure produces an amorphous solid structure with effective wall roughness of about half the average particle distance Δx , therefore below the relevant discretization length h . In other words: roughness introduced in this way does not correspond to a physically “resolved” wall-roughness (which could be reproduced only on scale of several DPD particles) but it is a numerical wall property which can be controlled in order to impose correct boundary conditions. In the next section the implementation of cubic and

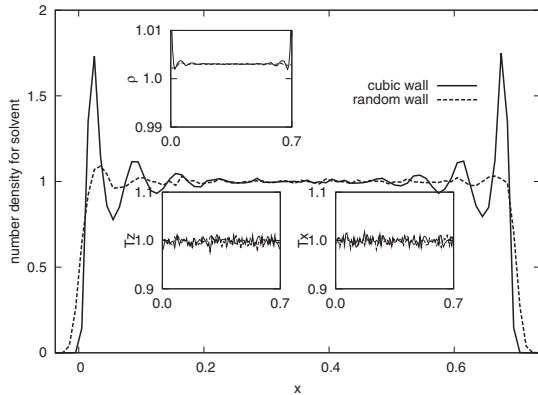


FIG. 1. Normalized density and temperature profiles in the normal directions to the flow (the size of histogram bead is 0.01). Temperature is not influenced by the wall for both models.

random wall models is investigated on the coarse-grained dynamics of a tethered polymer.

III. SIMULATIONS

We consider a three-dimensional (3D) channel geometry defined by a physical domain $L_x \times L_y \times L_z = 1 \times 1.75 \times 1$ corresponding to a total number of DPD fluid particles (excluding wall particles) equal to 14 000. Periodicity is applied in the y and z directions, while in the x directions wall boundary conditions are imposed. A Couette flow is applied by moving the wall opposite to the polymer tethered location ($x = L_x$) with constant velocity V in the y direction, and the flow gradient is in the x direction. In the following simulations the fluid mass density is set to 1.0, viscosity is 1.0, temperature is 0.3, wall velocity $V=20$ corresponding to a shear rate $\dot{\gamma}=20$, and sound speed $c=2000$. Average fluid particle spacing is $\Delta r=0.05$ and cutoff radius $h=3\Delta r=0.15$. The parameters of the FENE chain are $R_0=2\Delta r=0.1$ and $HR_0^2=15$. Simulations are performed for a chain with a number of beads $N_b=30$. A velocity-Verlet algorithm is used to integrate the equations of motion with dimensionless time step $\Delta t=6.25 \times 10^{-5}$ chosen according to the stability condition based on sound speed [21]. All the quantities mentioned above are dimensionless. We take the channel gap L_y as the unit of length, the fluid mass density ρ as unit of density and the thermal energy $k_B T$ as the unity of energy.

In order to extract averaged quantities, three sets of simulations are separately run for the “cubic” and “random” wall models for a duration of 10^6 time steps each: the first 10^5 time steps are not considered in the averages.

A. Near-wall layering

In the Fig. 1 averaged profiles for the mass density, particle number density, and temperature for the two wall models described above are shown. Note that, whereas the mass density ρ evaluated by Eq. (3) is almost constant and independent of the boundary conditions adopted (top inset), the

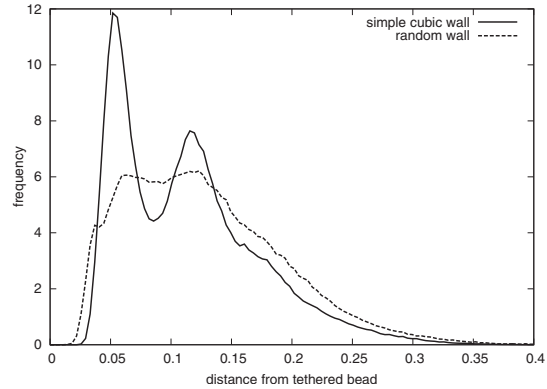


FIG. 2. Probability of finding a polymer bead in x coordinates (direction of the flow gradient). The first fixed bead is excluded from the histogram.

number density evaluated as histogram by counting the number of particles present in every bin and averaging in time, shows large fluctuations close to the wall surfaces. Although this local particle ordering has no practical effects when hydrodynamic properties of the fluid are concerned, strong artifacts can be expected for situations where the exact dynamics of a fluid particle is required, as for instance the polymer-bead motion near the wall. In this context, Fig. 1 shows that the choice of the “random” wall model (dotted line) is able to reduce strongly the layering effect. The amorphous wall does not induce any significantly ordered structure in the liquid adjacent to the surface as it is evident by the strongly reduced density peaks which show now maximal fluctuations smaller than 5% (note the first peak for the “cubic” wall model was exceeding the bulk value for more than 60%). As already mentioned, hydrodynamic quantities are not affected by this artificial layering. In the two bottom insets of Fig. 1 the temperature along the normal directions to the channel wall is shown to exhibit almost flat profiles and no visible effects of the particular choice of the boundary conditions are observed. This is different to the temperature profiles showed for example in [23] or [7] where deviations corresponding, respectively, to local cooling/heating effects close to walls were reported. This behavior might be related to the nature of the many-body conservative interactions considered here and it has been already observed in [24].

Let us focus now on the behavior of the polymer close to the wall surface. Figure 2 shows the density of polymer beads across the channel (the tethered bead is excluded from the statistics). For a simple “cubic” wall the effect of wall-induced ordering is very pronounced and persists up to distances $\approx 2\Delta x$, where Δx is the average interparticle spacing. The large peaks observed in the bead distribution are due to minimization of the polymer-bead/solvent-particle potential energy by alignment of bead positions with the most probable ordered solvent-particle locations near the walls [25]. At the nanoscopic level the local packing effect of fluid molecules is well understood and produces typical monolayers which extend up to few molecule distances away from the wall. In DPD, however, the typical bead-bead distance

adopted in the freely jointed FENE chain corresponds to the polymer persistence length which is unlikely to exceed the atomistic thickness of the fluid monolayers [17]. Therefore, the distorted bead distribution, although having a clear interpretation on atomistic scales, should not be present at the coarse-grained level of the DPD simulations. Figure 2 shows how the choice of a “random” wall by reducing strongly the near-wall fluid layering inhibits also the occurrence of artificial peaks in the polymer-beads distribution.

B. Polymer sticking

Another phenomenon related to the distorted near-wall bead distribution is apparent polymer sticking. As discussed above, the wall-induced layering effect of the fluid particles increases the residence probability of the polymer beads close to the wall. This effect has been observed already in [17] and is related to the first large peak in the bead probability distribution shown in Fig. 2. This results in an unrealistic enhanced near-wall residence time for the beads, which can exceed sometimes even the longest polymer relaxation time. As shown in Fig. 2, the use of the “random” wall removes almost completely the peaks and no polymer sticking phenomenon can be observed. This result agrees also with experiments on tethered DNA where no near-wall anomalous polymer behavior was reported [18,26].

C. Polymer overextension

In [25], overextensive behavior in the hybrid MD-continuum simulation of a tethered polymer under shear flow was reported in comparison with experimental data using tethered DNA. More recently, Delgado-Buscalioni and Covey suggested an atomistic effect mediated by the wall as possible cause of the altered dynamics [19]. In particular, the anomalous behavior was observed only in the large shear-rate regime when the polymer width in the wall-normal direction becomes comparable with the interaction length of the solvent molecules causing its complete sticking to the surface. Fluid layering was suggested as cause of the artificial wall-normal compression (sticking) and the wall-parallel overextension.

In Fig. 3 we have plotted the polymer mean fractional extension in the flow direction Y/L_p , where $Y = \langle \max(y_i) - \min(y_i) \rangle$ and $L_p = (N_p - 1)\Delta x$ is the polymer contour length. The Weissenberg number is evaluated as $Wi = \tau\dot{\gamma}$, where τ is the longest polymer relaxation time determined from a stretching-relaxation simulation. Data corresponding to individual stretched tethered DNA experiments under shear flow are also shown for comparison [18,26]. For $Wi < 40$ the polymer stretches strongly reaching an almost saturated level of extension with a weak Wi dependence. DPD results of the tethered polymer interacting with the “random” wall (*) show very good agreement with the experimental data up to $Wi \approx 140$. On the other hand, simulations with a “cubic” wall model overestimate the final fractional extension by more than 15%. Our results seem to confirm the arguments presented in [19], indeed as evident from Fig. 3, overextension is clearly associated to wall-induced ordering and polymer

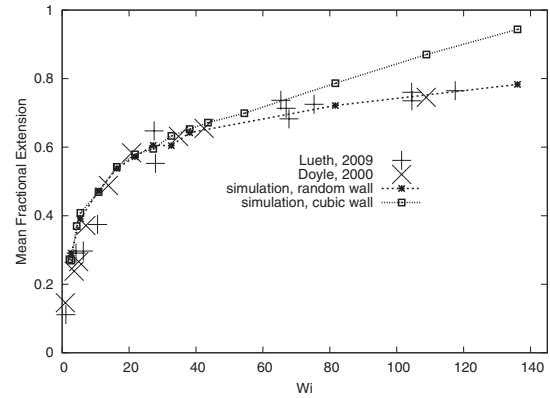


FIG. 3. The average polymer extension (Y) vs $Wi = \tau\dot{\gamma}$, where τ is the longest relaxation time. Experimental data are from [18,26].

sticking phenomena which are both absent when the “random” wall boundary conditions are used.

The previous problem is connected to the Wi dependence of the fractional extension at large shear rates. It is generally acknowledged that for low-to-moderate Weissenberg numbers the polymer-extension deficit defined as $\epsilon = 1 - Y/L_p$ should decrease as $\epsilon \sim Wi^{-1/3}$. This result is in agreement with the theoretical prediction for wormlike-chain (WLC) models and is confirmed also by numerical simulations [19] and experimental data [26]. Figure 4 shows the results of our simulations with “random” and “cubic” walls compared with Doyle’s experimental results. When random walls are used, no crossover behavior for ϵ is observed which follows the $-1/3$ scaling up to $Wi \approx 140$ in perfect agreement with the experiments. Moreover, the use of cubic wall model produces the expected polymer overextension reported in [19]. The results of our simulations thus confirm their hypothesis, suggesting that wall-induced layering effects can have a dramatic effect on the dynamics of a tethered polymer under shear. The use of the amorphous-wall model proposed in this

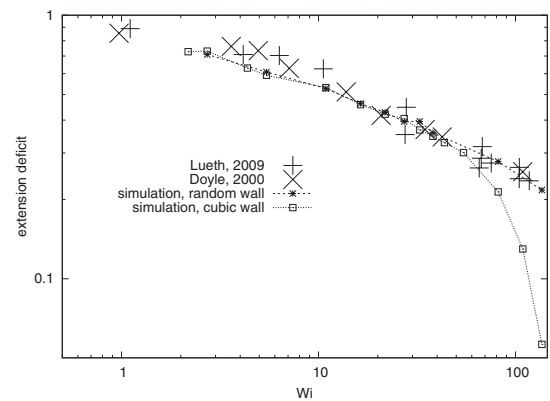


FIG. 4. The average polymer-extension deficit ($1 - Y/L_p$) vs Wi . Experimental data are from [18,26].

work allows to remove artificial ordering in the fluid adjacent a solid surface and to reproduce physically sensible data.

IV. CONCLUSIONS

In this paper, a strategy to solve simultaneously the wall penetration and the unphysical particle-layering problems in coarse-grained DPD simulations is presented. Amorphous wall models, which are known to suppress realistic near-wall fluid layering in molecular-dynamics simulation of nanoscale flows, are employed in a dissipative particle dynamics model

in order to remove the artificial coarse-grained layering and, simultaneously, enforce wall impermeability. The goal is achieved by replacing the classical expression for the two-body conservative force commonly used in DPD by a new one involving an effective multibody pressure term. The method is finally tested by studying the dynamics of a tethered DNA molecule under constant shear flow where no anomalous behavior for the monomer densities close to the wall have been reported in recent experimental observations [18]. Good quantitative results compared with experiments and previous numerical calculations are obtained.

-
- [1] G. Karniadakis, A. Beskok, and N. Aluru, *Microflows and Nanoflows* (Springer, New York, 2005).
- [2] Y. Zhu and S. Granick, *Phys. Rev. Lett.* **87**, 096104 (2001).
- [3] Y. Zhu and S. Granick, *Phys. Rev. Lett.* **88**, 106102 (2002).
- [4] P. A. Thompson and M. O. Robbins, *Phys. Rev. A* **41**, 6830 (1990).
- [5] C. M. Wijmans and B. Smit, *Macromolecules* **35**, 7138 (2002).
- [6] P. J. Hoogerbrugge and J. M. V. A. Koelman, *EPL* **19**, 155 (1992).
- [7] I. V. Pivkin and G. E. Karniadakis, *Phys. Rev. Lett.* **96**, 206001 (2006).
- [8] J. J. Monaghan, *Rep. Prog. Phys.* **68**, 1703 (2005).
- [9] S. M. Willemsen, H. C. J. Hoefsloot, and P. D. Iedema, *Int. J. Mod. Phys. C* **11**, 881 (2000).
- [10] A. M. Altenhoff, J. H. Walther, and P. Koumoutsakos, *J. Comput. Phys.* **225**, 1125 (2007).
- [11] Z. J. Xu and P. Meakin, *J. Chem. Phys.* **130**, 234103 (2009).
- [12] T. Steiner, C. Cupelli, R. Zengerle, and M. Santer, *Microfluid. Nanofluid.* **7**, 307 (2009).
- [13] D. A. Fedosov, I. V. Pivkin, and G. E. Karniadakis, *J. Comput. Phys.* **227**, 2540 (2008).
- [14] D. Duong-Hong, N. Phan-Thien, and X. J. Fan, *Comput. Mech.* **35**, 24 (2004).
- [15] X. Hu and N. Adams, *Phys. Fluids* **18**, 101702 (2006).
- [16] P. Malfreyt and D. Tildesley, *Langmuir* **16**, 4732 (2000).
- [17] Y. Gratton and G. W. Slater, *Eur. Phys. J. E* **17**, 455 (2005).
- [18] C. A. Lueth and E. S. G. Shaqfeh, *Macromolecules* **42**, 9170 (2009).
- [19] R. Delgado-Buscalioni and P. V. Coveney, *Physica A* **362**, 30 (2006).
- [20] P. Español and M. Revenga, *Phys. Rev. E* **67**, 026705 (2003).
- [21] J. Morris, P. Fox, and Y. Zhu, *J. Comput. Phys.* **136**, 214 (1997).
- [22] S. Litvinov, M. Ellero, X. Hu, and N. A. Adams, *Phys. Rev. E* **77**, 066703 (2008).
- [23] X. Fan, N. Phan-Thien, N. T. Yong, X. Wu, and D. Xu, *Phys. Fluids* **15**, 11 (2003).
- [24] B. Henrich, C. Cupelli, M. Moseler, and M. Santer, *EPL* **80**, 60004 (2007).
- [25] S. Barsky, R. Delgado-Buscalioni, and P. V. Coveney, *J. Chem. Phys.* **121**, 2403 (2004).
- [26] P. S. Doyle, B. Ladoux, and J. L. Viovy, *Phys. Rev. Lett.* **84**, 4769 (2000).

8.4 Paper IV

Smoothed dissipative particle dynamics model for polymer molecules in suspension

Sergey Litvinov,¹ Marco Ellero,^{1,2} Xiangyu Hu,¹ and Nikolaus A. Adams¹
¹*Lehrstuhl für Aerodynamik, Technische Universität München, 85747 Garching, Germany*
²*Departamento de Física Fundamental, UNED, Apartado 60141, 28080 Madrid, Spain*
 (Received 4 October 2007; published 5 June 2008)

We present a model for a polymer molecule in solution based on smoothed dissipative particle dynamics (SDPD) [Español and Revenga, *Phys. Rev. E* **67**, 026705 (2003)]. This method is a thermodynamically consistent version of smoothed particle hydrodynamics able to discretize the Navier-Stokes equations and, at the same time, to incorporate thermal fluctuations according to the fluctuation-dissipation theorem. Within the framework of the method developed for mesoscopic multiphase flows by Hu and Adams [*J. Comput. Phys.* **213**, 844 (2006)], we introduce additional finitely extendable nonlinear elastic interactions between particles that represent the beads of a polymer chain. In order to assess the accuracy of the technique, we analyze the static and dynamic conformational properties of the modeled polymer molecule in solution. Extensive tests of the method for the two-dimensional (2D) case are performed, showing good agreement with the analytical theory. Finally, the effect of confinement on the conformational properties of the polymer molecule is investigated by considering a 2D microchannel with gap H varying between 1 and 10 μm , of the same order as the polymer gyration radius. Several SDPD simulations are performed for different chain lengths corresponding to $N=20-100$ beads, giving a universal behavior of the gyration radius R_G and polymer stretch X as functions of the channel gap when normalized properly.

DOI: [10.1103/PhysRevE.77.066703](https://doi.org/10.1103/PhysRevE.77.066703)

PACS number(s): 47.11.St, 05.10.-a, 47.57.Ng

I. INTRODUCTION

The increasing technological need to create and manipulate structures on micrometer scales and smaller for the design of micro- and nanodevices has triggered the development of many numerical methods for simulating problems at mesoscales [1–3]. One specific area of investigation is microfluidics, which refers to the fluid dynamics occurring in devices or flow configurations with the smallest design length on the order of micrometers [4]. A typical application is, for example, the dynamics of a polymer molecule in a channel or other confined geometries such as micropumps, mixers, and sensors. For instance, the mechanical response of a tethered DNA molecule to hydrodynamic flow is currently under investigation by some groups and can be used for local sensing, leading to the concept of using an immobilized DNA molecule as a mechanical-fluidic sensor or for microfabricated metallic wires and networks [5–7]. The development of single-molecule concepts is of great importance for future applications in proteomics, genomics, and biomedical diagnostics, and it is therefore evident that the ability to improve the predictive computational tools at this spatiotemporal level would greatly improve the engineering tasks.

It is worth noting that the Navier-Stokes equations describing the dynamics of a Newtonian liquid at the macroscopic level still remain valid at the microfluidic scales, therefore providing a natural framework based on the continuum description. On the other hand, it is also clear that, whenever the physical dimensions of the considered objects (i.e., polymer molecules, colloidal particles) are in the sub-micrometer range, the surrounding fluid starts to be affected by the presence of its underlying molecular structure, and hydrodynamic variables will be influenced by thermodynamic fluctuations according to the Landau and Lifshitz

theory [8]. Standard macroscopic approaches, based, for example, on finite-volume or finite-element methods, are not suitable for this type of simulation. They neglect thermal fluctuations which, as mentioned above, are the most crucial ingredient of the mesoscopic dynamics. On the other hand, direct microscopic approaches, such as molecular dynamics, are able to resolve the smallest details of the molecular structures but they are computationally very expensive and are limited by the available computer resources. Nowadays, these approaches are restricted to computational domains of length of the order of nanometers which represent only the smallest scales (dimensions of one nanostructure) in the range covered by the considered system. Despite their high computational cost, molecular dynamics (MD) methods have been used frequently for studying the dynamics of polymer molecules in a solvent, described by Lennard-Jones interaction potentials, producing valuable results [9–11]. The advantage of these methods is that hydrodynamics emerges naturally from intermolecular interactions and does not need to be modeled.

Other methods based on Brownian dynamics techniques have been shown recently to produce accurate results for DNA dynamics in microfluidic devices [12] but require a complicated modeling of hydrodynamic interactions (in particular when coupled with the no-slip boundary conditions at the walls) mediated by a modified Rotne-Prager-Yamakawa tensor. To remedy these problems, various researchers have focused in the past on mesoscopic methods which employ numerically effective coarse-grained models retaining the relevant hydrodynamics modes. Examples are multiparticle collision dynamics [13], lattice Boltzmann methods (LBMs) [14], and dissipative particle dynamics (DPD). In particular, DPD is a mesoscopic methodology which has attracted increasing attention in recent years. DPD was originally proposed by Hoogerbrugge and Koelman in 1992 [15] and successively modified by Español and Warren in order to satisfy

thermodynamic consistency [16]. The method has been shown to capture the relevant thermodynamic and hydrodynamic effects occurring in mesoscopic systems [17–20], and it has been applied in recent years to a wide range of physical situations [21–23]. Despite its great success, a number of conceptual shortcomings have been recently pointed out which affect the performance and accuracy of the technique. In particular, they concern (i) the nonarbitrary choice of the fluid equation of state, (ii) no direct connection to the transport coefficients, (iii) the unclear definition of the physical particle scales, and (iv) particle penetration due to the employed soft two-body potentials [24]. These drawbacks prevent also an *a priori* control of the spatiotemporal scale in DPD and require a tuning of model parameters in order to compare the numerical results with experimental data. All these problems can be avoided by resorting to a further improved DPD version, smoothed dissipative particle dynamics (SDPD) [25].

SDPD represents a powerful generalization of the so-called smoothed particle hydrodynamics (SPH) method [26–28] for mesoscales. Being based on a second-order discretization of the Navier-Stokes (NS) equations, transport coefficients are input parameters and do not need to be measured by Green-Kubo relations as in MD or extracted via kinetic theory as in conventional DPD. In SDPD, the particles represent therefore physical fluid elements whose specific size determines the level of thermal fluctuations in the hydrodynamic variables. At the same time, since the method is based on a Lagrangian discretization of the NS equations, hydrodynamic behavior is obtained at the particle scale and no coarse-graining assumption is needed.

In this paper, we propose a SDPD model for the investigation of the static and dynamic behavior of a polymer molecule in unbounded and confined geometries. The polymer molecule is represented by a polymer chain constituted by beads interacting by finitely extendable nonlinear elastic (FENE) forces. In order to validate the model, the two-dimensional (2D) case of a polymer molecule in a bulk solvent fluid is considered first. Note that 2D polymer dynamics does not represent an oversimplified picture of reality, but rather reflects realistic situations often encountered in polymer technology, and has recently been the focus of several numerical and experimental investigations [29–34]. In many cases polymer dynamics occurs within a very thin layer with thickness considerably smaller than the gyration radius, and the motion can be considered as truly two dimensional. Practical examples are thin polymer films, polymers adsorbed to surfaces, or polymers confined between biological interfaces. For example, recently Maier and Rädler performed experiments with a single DNA molecule electrostatically confined to a surface of fluid lipid membranes [30]. The confinement was found not to inhibit the lateral mobility of the molecule, and results for the conformational statistics were in good agreement with theoretical predictions in 2D. From a numerical point of view, extensive Monte Carlo and molecular dynamics simulations have been performed in the past and have proven to be extremely useful in corroborating analytical theories or explaining anomalous scaling behavior in bulk and confined situations [9,11,32,35].

In this work, static and dynamic scaling exponents are extracted from the SDPD simulations showing excellent

agreement with the theoretical Zimm predictions and previous numerical results. As a further validation test, the case of a polymer molecule confined between two parallel walls is considered, that is, an infinite 2D microchannel. The influence that the channel gap H has on the polymer conformational properties is investigated. According to previous studies in the 3D case [12,20,36], it is found that, for lengths of the gap comparable to the molecule gyration radius (i.e., on the order of micrometers), strong anisotropic effects start to affect the polymer statistics, such as, e.g., the average gyration radius and polymer stretch. In addition, the power law behavior of the polymer stretch as function of the normalized channel width has also been verified numerically, giving an exponent in excellent agreement with the analytical results predicted from scaling arguments in 2D by de Gennes [37]. The results will be discussed in the final section.

II. THE SIMULATION METHOD

A. Macroscopic hydrodynamics

We consider the isothermal Navier-Stokes equations on a moving Lagrangian grid

$$\frac{d\rho}{dt} = -\rho \nabla \cdot \mathbf{v}, \quad (1)$$

$$\frac{d\mathbf{v}}{dt} = \mathbf{g} - \frac{1}{\rho} \nabla p + \mathbf{F}, \quad (2)$$

where ρ , \mathbf{v} , and \mathbf{g} are the material density, velocity, and body force, respectively. A simple equation of state is $p = -\kappa_T V$ where κ_T is the isothermal compressibility. It can be rewritten as

$$p = a^2 \rho. \quad (3)$$

When Eqs. (1) and (2) are used for modeling of low-Reynolds-number incompressible flows with the artificial-compressibility method, a is equal to the artificial speed of sound. An alternative equation of state for incompressible flows is

$$p = p_0 \left(\frac{\rho}{\rho_0} \right)^\gamma + b, \quad (4)$$

where p_0 , ρ_0 , γ , and a are parameters. The parameters in Eq. (3) and (4) may be chosen based on a scale analysis [26,38,39] so that the density variation is less than a given value. \mathbf{F} denotes the viscous force

$$\mathbf{F} = \frac{1}{\rho} \nabla \cdot \Pi^{(\nu)} \quad (5)$$

where the shear stress is $\Pi^{(\nu)} = \eta(\nabla \mathbf{v} + \nabla \mathbf{v}^T)$. If the bulk viscosity is assumed as $\zeta=0$, for incompressible flow the viscous force simplifies to

$$\mathbf{F} = \nu \nabla^2 \mathbf{v}, \quad (6)$$

where $\nu = \eta/\rho$ is the kinematic viscosity.

1. Density evolution equation

Let us introduce the particle number density d_i , which is defined by

$$d_i = \sum_j W_{ij}, \quad (7)$$

where $W_{ij} = W(r_{ij}, h) = W(\|\mathbf{r}_i - \mathbf{r}_j\|, h)$, and $W(r, h)$ is a generic shape function with compact support h which is radially symmetric and has the properties $\int W(\mathbf{r} - \mathbf{r}') d\mathbf{r}' = 1$ and $\lim_{h \rightarrow 0} W(\mathbf{r} - \mathbf{r}') = \delta(\mathbf{r} - \mathbf{r}')$ (in this work, a quintic spline function has been used). According to (7), d_i will have larger values in a dense particle region than in a dilute particle region. Equation (7) introduces also a straightforward definition of the volume of particle i , which is $\mathcal{V}_i = 1/d_i$. The average mass density of a particle is therefore defined as $\rho_i = m_i/\mathcal{V}_i$ where m_i is the mass of a particle. Other forms of evaluating the mass density are possible in SPH, which take into account a direct discretization of the continuity equation in (1). However, the direct particle summation adopted here and based on Eq. (7) has the advantage that the total mass is algebraically conserved.

2. Momentum equation

Concerning the momentum equation, it has been shown [25,40] that a possible SPH discretization of the *pressure force* appearing in (2) is

$$\frac{d\mathbf{v}_i^{(p)}}{dt} = -\frac{1}{m_i} \sum_j \left(\frac{p_i}{d_i^2} + \frac{p_j}{d_j^2} \right) \frac{\partial W}{\partial r_{ij}} \mathbf{e}_{ij}, \quad (8)$$

where $d\mathbf{v}_i^{(p)}/dt$ is the particle acceleration caused by pressure effects, p_i is the pressure associated with particle i [41], and \mathbf{e}_{ij} is the unit vector connecting particles i and j . It can be shown that this expression represents a second-order SPH discretization of the gradient of the scalar field p . Since this expression has an antisymmetric form with respect to exchange of i and j , global conservation of momentum is satisfied. Equation (8) is similar to the form preferred by Monaghan [26].

Concerning the *viscous force*, similarly to Flekkøy *et al.* [42], the interparticle-averaged shear stress is approximated as

$$\overline{\Pi}_{ij}^{(v)} = \frac{\eta}{r_{ij}} (\mathbf{e}_{ij} \mathbf{v}_{ij} + \mathbf{v}_{ij} \mathbf{e}_{ij}) \quad (9)$$

where $\mathbf{v}_{ij} = \mathbf{v}_i - \mathbf{v}_j$. Hence, the particle acceleration due to the shear force in conservative form is given by

$$\frac{d\mathbf{v}_i^{(v)}}{dt} = \frac{\eta}{m_i} \sum_j \left(\frac{1}{d_i^2} + \frac{1}{d_j^2} \right) \frac{1}{r_{ij}} \frac{\partial W}{\partial r_{ij}} (\mathbf{e}_{ij} \cdot \mathbf{v}_{ij} \mathbf{e}_{ij} + \mathbf{v}_{ij}). \quad (10)$$

Note that this expression does not strictly conserve angular momentum. Conservation of total angular momentum can be restored by adopting either suitable artificial viscosity models based on interparticle central forces [26] for which, though, there is no direct connection to the Navier-Stokes form of the stress tensor, or linearly consistent versions of SPH [43].

B. Mesoscopic hydrodynamics

The method outlined above is strictly analogous to the SPH technique widely used to describe macroscopic flow problems in a Lagrangian framework. In order to include mesoscopic effects, i.e., the presence of thermal fluctuations in the physical quantities, we follow the approach given by Español and Revenga, i.e., smoothed dissipative particle dynamics [25], which represents a powerful and elegant generalization of SPH at the mesoscopic scales. It should be noticed, that the method has been generalized for the study of viscoelastic liquids [44] and also, more recently, for mesoscopic multiphase flow problems [40].

Thermal fluctuations

In the current SPH method the irreversible part of the particle dynamics is

$$\begin{aligned} \dot{m}_i|_{\text{irr}} &= 0, \\ \dot{\mathbf{P}}_i|_{\text{irr}} &= \eta \sum_j \left(\frac{1}{d_i^2} + \frac{1}{d_j^2} \right) \frac{1}{r_{ij}} \frac{\partial W}{\partial r_{ij}} (\mathbf{e}_{ij} \cdot \mathbf{v}_{ij} \mathbf{e}_{ij} + \mathbf{v}_{ij}). \end{aligned} \quad (11)$$

According to the general equation for non-equilibrium reversible-irreversible coupling (GENERIC) formalism [45–47], the mass and the momentum fluctuations of particle i caused by thermal noise are postulated to be

$$\begin{aligned} d\tilde{m}_i &= 0, \\ d\tilde{\mathbf{P}}_i &= \sum_j B_{ij} d\tilde{\mathcal{W}}_{ij} \cdot \mathbf{e}_{ij}, \end{aligned} \quad (12)$$

where $d\tilde{\mathcal{W}}_{ij}$ is the traceless symmetric part of a matrix of independent increments of a Wiener process $d\mathcal{W}_{ij} = d\mathcal{W}_{ji}$, i.e., $d\tilde{\mathcal{W}}_{ij} = (d\mathcal{W}_{ij} + d\mathcal{W}_{ij}^T)/2 - \text{tr}[d\mathcal{W}_{ij}]\mathbf{I}/d$, and d is the spatial dimension. The isothermal deterministic irreversible equations are obtained as

$$\begin{aligned} \dot{m}_i|_{\text{irr}} &= 0, \\ \dot{\mathbf{P}}_i|_{\text{irr}} &= -\sum_j \frac{B_{ij}^2}{4k_B T} (\mathbf{e}_{ij} \cdot \mathbf{v}_{ij} \mathbf{e}_{ij} + \mathbf{v}_{ij}), \end{aligned} \quad (13)$$

in which k_B is the Boltzmann constant and T is the system temperature. Comparing Eq. (13) to (11) one obtains

$$B_{ij} = \left[-4k_B T \eta \left(\frac{1}{d_i^2} + \frac{1}{d_j^2} \right) \frac{1}{r_{ij}} \frac{\partial W}{\partial r_{ij}} \right]^{1/2}. \quad (14)$$

By postulating these magnitudes for the noise terms (12), the fluctuation-dissipation theorem dictates a form for the irreversible dynamics in (13) which is exactly analogous to the SDPD discretization of the Navier-Stokes dissipation given in Eq. (10).

Note also that the kernel function W needs to be a monotonically decreasing function of r for B_{ij} in (14) to be real valued.

In summary, the SDPD equations of motion for the fluid particles at the mesoscopic scales read

$$\frac{d\mathbf{r}_i}{dt} = \mathbf{v}_i,$$

$$\frac{d\mathbf{v}_i}{dt} = \frac{d\mathbf{v}_i^{(p)}}{dt} + \frac{d\mathbf{v}_i^{(v)}}{dt} + \frac{1}{m_i} d\tilde{\mathbf{P}}_i, \quad (15)$$

with $d\mathbf{v}_i^{(p)}/dt$, $d\mathbf{v}_i^{(v)}/dt$, and $d\tilde{\mathbf{P}}_i$ being given, respectively, in Eqs. (8), (10), and (12).

C. Solid wall modeling

In this work, we consider periodic boundary conditions to model a bulk fluid and solid boundary conditions for confined situations. In the latter case, the solid body region is filled with virtual particles [48]. Whenever the support of a fluid particle overlaps with the wall surface, a virtual particle is placed inside the solid body, mirrored at the surface. The virtual particles have the same volume (i.e., mass and density), pressure, and viscosity as their fluid counterparts but the velocity is given as $\mathbf{v}_{\text{virtual}} = 2\mathbf{v}_{\text{wall}} - \mathbf{v}_{\text{real}}$ for a no-slip velocity boundary condition or $\mathbf{v}_{\text{virtual}} = \mathbf{v}_{\text{real}}$ for a free-slip boundary condition. Currently, only straight channel walls are considered. For curved wall surfaces, the virtual particle approach may introduce considerable errors. To increase the accuracy near curved surfaces, Takeda *et al.* [49], Morris *et al.* [38], and more recently Ellero *et al.* [50] have introduced special wall particles which interact with the fluid particles in such a way that more general boundary conditions are represented accurately.

D. Mechanical modeling of the polymer chain

The model for the polymer molecule in suspension adopted in this work can be described in the following terms. The solvent liquid is represented by SDPD particles which represent physical elements of fluid containing potentially thousands of solvent (i.e., water) molecules and interacting hydrodynamically. Concerning the polymer model, we consider it as a linear chain of polymer beads, each bead being represented as a mixture of real polymer monomers together with solvent molecules. The numerical realization of this physical model is obtained by selecting a number of SDPD fluid particles and letting them interact, as well as hydrodynamically, also by additional finitely extendable nonlinear elastic springs

$$\mathbf{F}^{\text{FENE}}(\mathbf{r}_{ij}) = \frac{K\mathbf{r}_{ij}}{1 - (r/R_0)^2}, \quad (16)$$

where K is the spring constant, $r = \sqrt{\text{tr}(\mathbf{r}_{ij}\mathbf{r}_{ij})}$ is the bead-bead distance, and R_0 represents the maximum extensibility.

A typical configuration is sketched in Fig. 1. Light-blue particles represent the fluid while dark-blue particles are the beads forming the model polymer chain. All particles interact by the hydrodynamics forces given in Eq. (15). Polymer beads interact with each other additionally by the FENE forces which produce an elastic contribution due to the portion of real polymer monomers assumed to be contained in the bead.

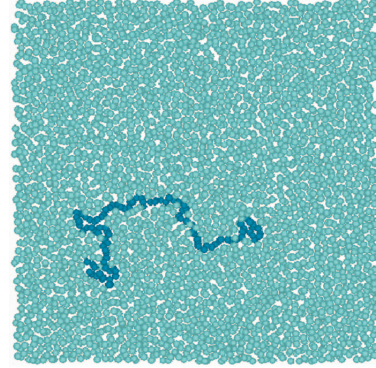


FIG. 1. (Color) Typical simulation configuration: light-blue particles represent solvent particles and dark-blue particles represent polymer beads. All particles interact by the hydrodynamic forces given in Eq. (15). Beads interact with each other additionally by FENE forces. In order to simulate bulk conditions, standard periodic boundary conditions are employed at the edges of the simulation box. For this case a total number of $N_p = 3600$ particles were considered. Among them, $N = 100$ particles were selected as beads defining the polymer chain.

According to the previous discussion, hydrodynamic interactions between polymer beads occur via *viscous* and *pressure* terms and are justified by the fact that within every bead there is a large amount of water molecules which produce hydrodynamic behavior on the same scale as the SDPD particle.

Note that excluded-volume effects are directly taken into account through the pressure terms appearing in the discretized hydrodynamic equations (8) which produce repulsive forces between approaching particles, and therefore there is no need to introduce short-range Lennard-Jones forces between beads. It should be noted also that, by considering a bead as a special case of a SDPD particle, we bypass the problem of modeling separately the *hydrodynamic coupling* of polymer beads and solvent particles which is taken into account through the SDPD friction forces in Eq. (10). Since these forces are written in antisymmetric form with respect to the particle indices, they conserve exactly the total linear momentum also during fluid-bead interactions. This represents a remarkable advantage compared to LB methods, where special models must be introduced for the fluid-bead interactions in order to conserve the total linear momentum of the system [14].

In summary, the momentum equation for the bead i reads

$$m_i \frac{d\mathbf{v}_i}{dt} = \mathbf{F}_i^{\text{hydro}} + \mathbf{F}_{i,i_1}^{\text{FENE}} + \mathbf{F}_{i,i_2}^{\text{FENE}}, \quad (17)$$

$\mathbf{F}_i^{\text{hydro}}$ being the total sum of the resulting SDPD forces acting on particle i given in Eq. (15), and i_1, i_2 the two next neighboring beads of bead i in the polymer chain.

A final remark on the structure of these equations is in order. As can be seen in Eq. (16), the additional bead-bead interaction, although entropic in origin, appears as a conse-

quence of the GENERIC framework in the model Eq. (17) as an ordinary interparticle force [51]. Therefore, there is no particular concern about the general structure of the modified SDPD model equations which is still consistent with the GENERIC model. In particular, the magnitudes of the stochastic terms are uniquely prescribed in terms of the dissipative forces between the particles, which in this model remain unaltered.

III. NUMERICAL SETUP

In this work, the statistical properties of a single polymer molecule immersed in a Newtonian liquid under good solvent conditions are investigated in an infinite domain and in a confined geometry. In the first case, the simulation domain is represented by a 2D square box of physical length $L = 10^{-5}$ m. A total number $N_p = 3600$ of SDPD particles is used. Among them, N particles representing polymer beads are selected and allowed to interact by the FENE forces. N ranges from 20 to 100. Concerning the input parameters entering the FENE model, we choose $K = 5.3 \text{ N m}^{-1}$ and $R_0 = 4\Delta r$, where $\Delta r = 1.66 \times 10^{-7}$ m is the initial particle spacing [52].

Fluid particles interact by the forces given in Eq. (15) with cutoff radius $h = 5.0 \times 10^{-7}$ m, and the kernel function used is a quintic spline kernel. This implies an average number of 20 neighboring SDPD particles entering the interpolation process.

Depending on the particular case, periodic or solid boundary conditions are used. In the latter case, solid walls are modeled by virtual particles as discussed in Sec. II. The method prevents particles penetrating the solid wall (impenetrability condition) and forces the tangential component of the fluid velocity to be exactly zero at the interface (no-slip condition) [40]. The previous conditions are crucial in taking into account hydrodynamic effects due to the confinement.

Concerning the solvent, we consider a Newtonian fluid characterized by a dynamic viscosity $\mu = 10^{-6} \text{ kg m}^{-1} \text{ s}^{-1}$ and $\rho = 10^3 \text{ kg m}^{-3}$, and the fluid temperature is set to $T = 300 \text{ K}$. According to these parameters, the solvent is ideally good and θ collapse never occurs. Concerning the numerical integration of the equations of motion for the particles, a second-order predictor-corrector scheme is used. To maintain numerical stability, a Courant-Friedrichs-Lewy time step restriction based upon artificial sound speed (isothermal compressibility), body force, and viscous dissipation [38,53,54] is employed. When thermal fluctuations are introduced in the mesoscopic simulation, the time steps are further decreased to recover the correct kinetic temperature. The artificial speed of sound of the solvent liquid keeps relative density fluctuations below 1% and models a quasi-incompressible fluid.

Statistical averages are computed by extracting independent polymer configurations. The production run is performed after an equilibration period (500–2000 time steps depending on the length of the polymer chain) in order to avoid spurious effects due to the initial nonrandom polymer configuration.

Finally, a remark on the numerical efficiency of the method is in order. The operation count of SDPD, as for

DPD or any other particle method, scales as $N_p \log N_p$ when proper linked-list cell algorithms are employed. However, the fact that the mass density ρ_i must be evaluated for every particle before calculating the interaction forces makes it potentially slightly slower. Nevertheless, the conceptual and technical advantages gained from the thermodynamical consistency of SDPD and its direct connection to the Navier-Stokes equations overwhelm the performance penalty.

IV. SIMULATION RESULTS

In this section, the conformational properties of the polymer molecule are investigated in a two-dimensional space. The objective is twofold: First, we apply the SDPD method to the study of a polymer molecule in an infinite solvent medium under zero-flow condition. In this case, the stochastic Wiener process entering Eq. (15) represents the only forcing term mimicking the presence of thermal fluctuations in the system. Under these conditions, the flow is isotropic, and theoretically predicted universal scaling laws for several polymer properties can be tested numerically. In particular, the static and dynamic behavior of the conformational polymer properties as well as the structure factor have been intensely studied using a variety of methods [9,10,14] and are compared here with the present results.

Second, the effect of geometrical confinement, in particular due to the presence of solid walls in microchannels, is investigated. This is an important validation test because it allows us to estimate the accuracy of SDPD in simulating real geometries encountered in microfluidic devices. It is generally known that confinement alters dramatically the behavior of a polymer molecule which in a microchannel, for example, will extend along the channel axis to a substantial fraction of its contour length. Scaling laws for the dependence of the polymer stretch upon the channel width have been proposed theoretically [37] and validated numerically in a number of 3D situations. As a further test for the SDPD method, the two-dimensional static properties of a polymer molecule confined in a microchannel are investigated and the results are compared with previous theoretical and numerical work [12,20,36].

A. Conformational properties of a polymer in a bulk medium

1. Chain statics

Conformational properties of a polymer chain, in particular deformation and orientation, can be analyzed by monitoring the evolution of several tensorial quantities such as, for instance the *gyration tensor*

$$\mathbf{G} \equiv \frac{1}{2N^2} \sum_{i,j} \langle \mathbf{r}_i \mathbf{r}_j \rangle, \quad (18)$$

or the *end-to-end tensor* defined as

$$\mathbf{R} \equiv \langle (\mathbf{r}_N - \mathbf{r}_1)(\mathbf{r}_N - \mathbf{r}_1) \rangle. \quad (19)$$

Here, $\mathbf{r}_{ij} = \mathbf{r}_j - \mathbf{r}_i$ with \mathbf{r}_i being the position of the i th bead in the chain. The indices i, j run from 1 to N , the total number of beads. Related quantities are the *radius of gyration* R_G

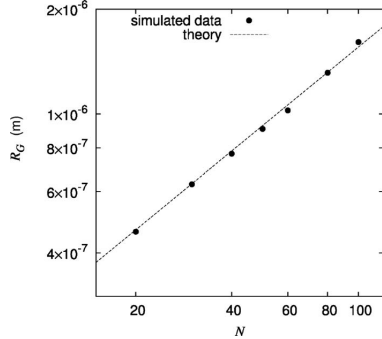


FIG. 2. Scaling of the radius of gyration R_G for several chain lengths corresponding to $N=20, 30, 40, 50, 60, 80, 100$ beads. The dotted line represents the best fit consistent with the theory ($R_G \propto N^\nu$) and gives a static exponent $\nu=0.76 \pm 0.012$.

$=\sqrt{\text{tr } \mathbf{G}}$ and the *end-to-end radius* $R_E = \sqrt{\text{tr } \mathbf{R}}$. The effect of the number of beads N on R_G and R_E is known to follow the analytical expressions

$$\begin{aligned} R_E &= a_E(N-1)^\nu, \\ R_G &= a_G[(N^2-1)/N]^\nu, \end{aligned} \quad (20)$$

where ν is called the *static factor exponent* and, from renormalization theory, it assumes the value $\nu \approx 0.588$ in three dimensions, with a_E and a_G being suitable constants. In the limiting case of $N \gg 1$, both quantities scale as $R_E \approx R_G \propto N^\nu$. Notice that this result is valid only in three dimensions. Because the goal of this work is to test the numerical scheme first in a 2D case, the static exponent ν extracted by our simulations should be compared with the analogous two-dimensional Flory formula, which gives a value 0.75 in good solvent conditions [37,55]. This value has been verified recently by several authors using molecular dynamics simulations [32–34].

In order to extract the exponent ν , SDPD simulations have been carried out with five different chain lengths characterized by $N=20, 40, 60, 80, 100$ beads. In all cases the time-averaged values of the gyration radius R_G have been evaluated from several independent steady-state polymer configurations. Figure 2 shows a log-log plot of the time-averaged R_G versus N . Error bars are within the symbol dimensions. The results can be fitted (dotted line in the figure) by a power law with exponent $\nu=0.76 \pm 0.012$, which is in good agreement with theoretical results and previous numerical investigations. It should be noticed that this way to evaluate ν is quite time consuming since simulations at large N are necessary in order to fit accurately the data in Fig. 2.

An alternative way to extract ν is, instead of using the scaling law (20), by employing the static structure factor defined as

$$S(\mathbf{k}) \equiv \frac{1}{N} \sum_{i,j} \langle \exp(-i\mathbf{k} \cdot \mathbf{r}_{ij}) \rangle. \quad (21)$$

In the limit of small wave vector $|\mathbf{k}|R_G \ll 1$, the structure factor can be approximated by $S(\mathbf{k}) \approx N(1 - \mathbf{k}^2 R_G/3)$, while

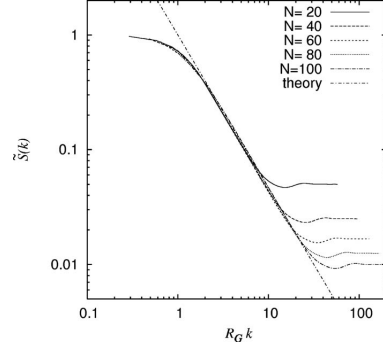


FIG. 3. Normalized equilibrium static structure factor $\tilde{S}(k) = S(k)/S(0)$ versus $R_G k$ corresponding to several chain lengths. All the curves collapse on a master line for $2 < R_G k < 8$ (scaling regime). In this region $\tilde{S}(k) \propto k^{-1/\nu}$ with $\nu=0.75$ (dotted line).

for $|\mathbf{k}|R_G \gg 1$ $S(\mathbf{k}) \approx 2N/k^2 R_G$ holds. The intermediate regime $|\mathbf{k}|R_G \sim 1$ contains information about the intramolecular spatial correlations. In the absence of external perturbation and close to equilibrium, $S(\mathbf{k})$ is isotropic and therefore depends only on the magnitude of the wave vector $k=|\mathbf{k}|$. $S(k)$ probes therefore different length scales even for a single polymer, and in the intermediate regime is shown to behave like

$$S(k) \propto k^{-1/\nu}. \quad (22)$$

Figure 3 shows a log-log plot of $S(k)$ vs $R_G k$. From this figure it is possible to see how curves evaluated from simulations with different chain lengths (N) collapse on a single curve for $2 < R_G k < 8$, the slope of the linear region being $-1/\nu$. The dotted line in the figure represents the theory with $\nu=0.75$ and shows very good agreement with the SDPD results.

This way provides a more efficient route to calculate the static exponent ν , since one single simulation with $N=20$ is sufficient for accurate estimates.

These two tests are commonly performed to validate the equilibrium conformational properties of a FENE polymer molecule. These scaling laws have been also verified by other techniques such as, for instance, DPD in three dimensions [17].

2. Chain dynamics

The dynamic conformational behavior of the polymer molecule represents another important feature that must be checked. The starting point is the *dynamical structure factor* defined as

$$S(\mathbf{k}, t) \equiv \frac{1}{N} \sum_{i,j} \langle \exp(-i\mathbf{k} \cdot [\mathbf{r}_i(t) - \mathbf{r}_j(0)]) \rangle. \quad (23)$$

Dynamic scaling arguments applied to the Zimm model in isotropic conditions predict a functional form of $S(k, t)$ of the type

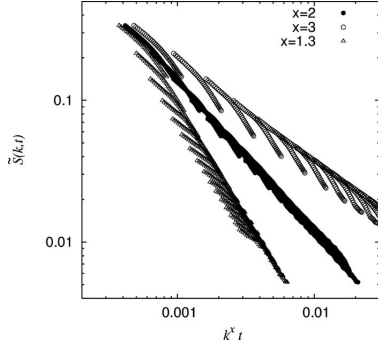


FIG. 4. Scaling plot of the normalized dynamic structure factor $\tilde{S}(k,t)=S(k,t)/S(k,0)$ for $N=20$ in log-log coordinates. The best collapse for $x=2$ is clearly visible. For different dynamic exponents ($x=1.3, 3$), the 2D data fail to collapse on a single curve. The range of k was consistent with the scaling regime $2 < R_G k < 8$.

$$S(k,t) = N(kR_G)^{-(1/\nu)} F[tD_G R_G^{-2}(kR_G)^x] \quad (24)$$

where $x=2+\nu_D/\nu$ (dynamical scaling exponent), D_G is the diffusion constant, and ν_D is the diffusion scaling exponent. Therefore, if we plot $S(k,t)/S(k,0)$ vs tk^x , in the scaling regime, a universal curve should be obtained for all the values of k and t . This is indeed predicted by the theory with a scaling exponent $x=3$ in 3D. Although the result has been verified in the three-dimensional case, anomalous scaling has been observed in the two-dimensional case, giving a value $x=2$. The goal here is to verify this result with the present SDPD model.

Figure 4 shows the dynamical structure factor data plotted versus $k^x t$ for three different values of the dynamic scaling exponent, that is, $x=1.3, 2, 3$. The figure suggests that in the appropriate scaling regime (that is, $2 < R_G k < 8$ from Fig. 2) the best collapse is obtained indeed for $x=2$ whereas, for $x=1.3$ and 3, the data indeed do not exhibit any collapse. This confirms the previous results indicating that anomalous scaling occurs in 2D polymer dynamics [32]. It should be noticed that, if we assume $D_G \propto N^{-\nu_D}$, this result implies that $\nu_D=0$ for the chain diffusion constant in 2D. Indeed, this has been recently verified given the logarithmic scaling of D_G with N [33,34].

3. Rouse mode analysis

As a further test of the polymer dynamics we calculate the internal modes of the chain. This can be done by evaluating the so-called Rouse coordinates \mathbf{R}_p defined as

$$\mathbf{R}_p = \frac{1}{N} \sum_{n=1}^N \cos\left(\frac{p\pi(n-\frac{1}{2})}{N}\right) \mathbf{r}_n, \quad (25)$$

where \mathbf{r}_n is the position of the bead n and $p=0, 1, 2, \dots, N$ are the normal modes of a polymer chain constituted of N beads. For example, \mathbf{R}_0 is the chain's center of mass, while \mathbf{R}_p for $p > 1$ represent high-order modes describing the internal motion of the polymer molecule.

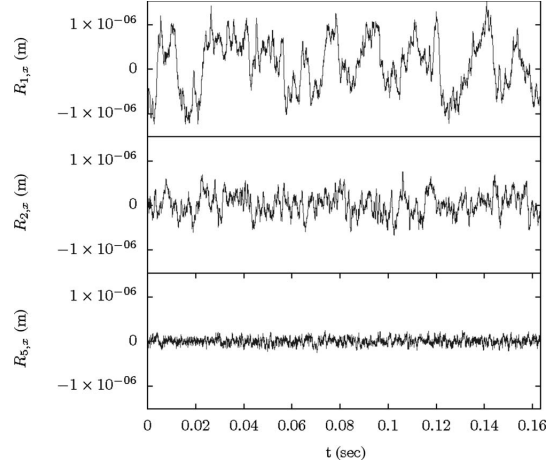


FIG. 5. Rouse coordinate histories for $R_{p,x}$ with $p=1, 2, 5$ and a chain length $N=80$. The magnitudes of fluctuations decrease with increasing p according to analytical theories.

In Fig. 5 the Rouse coordinate histories for the x direction are plotted for three different modes $p=1, 2, 5$ corresponding to a polymer chain with $N=80$ beads. Analogously to what was observed in [11], all these quantities fluctuate around zero with magnitudes decreasing for increasing values of p . In order to quantify the level of fluctuations we define the mean square Rouse coordinate as

$$\langle \mathbf{R}_p^2 \rangle = \frac{1}{2N^2} \sum_{n,m=1}^N \cos\left(\frac{p\pi(n-\frac{1}{2})}{N}\right) \cos\left(\frac{p\pi(m-\frac{1}{2})}{N}\right) \times \langle (\mathbf{r}_n - \mathbf{r}_m)^2 \rangle. \quad (26)$$

It has been recently shown that, for long chains, this quantity scales as $\sim p^{-(2\nu+1)}$, where ν is the static scaling exponent [11]. For the two-dimensional case, a scaling exponent $(2\nu+1) \approx 5/2$ should be observed. Figure 6 shows the mean square amplitude $\langle \mathbf{R}_p^2 \rangle$ for different chain lengths ($N=20, 40, 60, 80, 115$) versus the mode index p . The picture confirms the observation of Fig. 5 showing a monotonic decrease of $\langle \mathbf{R}_p^2 \rangle$ vs p . The solid line represents the best fit which, for $N=115$, gives a value of the slope equal to -2.61 ± 0.05 in reasonable agreement with the value -2.5 predicted by the theory for the two-dimensional case. This value was calculated by using the static scaling exponent $\nu=0.75$ obtained from the results in the previous section. In addition, an increasing trend of $\langle \mathbf{R}_p^2 \rangle$ vs N is also observed in Fig. 6 in agreement with the analytical results, which predict a dependence $\sim N^{2\nu}$ [11].

4. Diffusion coefficient

In this section we present results for the center-of-mass (c.m.) diffusion coefficient D of the polymer molecule. This is evaluated from the mean square displacement of the center of mass defined as

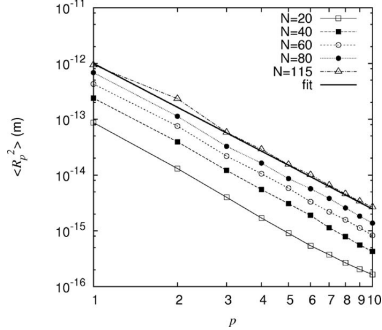


FIG. 6. Rouse mode mean square amplitudes $\langle R_p^2 \rangle$ vs mode p for different polymer chains corresponding to $N=20, 40, 60, 80, 115$ beads. The decrease of fluctuations with increasing value of p is clear. The solid curve represents the best fit of the data corresponding to $N=115$ and gives a slope equal to -2.61 ± 0.05 , in good agreement with the theory.

$$[\Delta \mathbf{R}_0(t)]^2 = \langle [\mathbf{R}_0(t + t_0) - \mathbf{R}_0(t_0)]^2 \rangle \quad (27)$$

where \mathbf{R}_0 is defined by (25). The single-chain diffusion coefficient is finally computed from the equation

$$[\Delta \mathbf{R}_0(t)]^2 = 4Dt \quad (28)$$

in the limit of large t , when the linear regime is reached.

Previous studies in the three-dimensional case indicate that strong box-size effects in the evaluation of D occur. These finite-size corrections are of the order of $1/L$; hence, in principle, it is easy to determine the diffusion coefficient in the thermodynamic limit ($L \rightarrow \infty$) by simply plotting D versus $1/L$ and extrapolating the value at the intercept of the y coordinate [18]. These results have been shown to produce a scaling relation, that is, $D_\infty(N)$ collapses on a master curve proportional to $N^{-\nu_D}$, $\nu_D=0.59$ being the dynamic scaling exponent.

The situation is more subtle in two dimensions due to the infinite range of the hydrodynamic interactions. Consistency with our evaluation of the dynamic scaling factor ($x=0$) would require $\nu_D=0$. In order to verify it, we plotted the data for D vs N logarithmically for different values of L and N , namely, $N=10, 20, 40$ and $L=0.75 \times 10^{-5}, 1.0 \times 10^{-5}, 1.25 \times 10^{-5}$, and no collapse was found. However, a decreasing scaling exponent (slope of the curves) was observed as the system size increased, analogously to previous findings [18]. In order to check quantitatively that $\nu_D=0$, Falck *et al.* [33], proposed an analytical formula for the 2D diffusion coefficient of a polymer molecule which reads

$$D = \frac{k_B T}{2\pi\mu} [-\ln(R_g/L) + \text{const} + O((R_g/L)^2)]. \quad (29)$$

Note that this expression explains also why it is impossible to extrapolate D in the thermodynamic limit, obtaining for $L \rightarrow \infty$ divergent values.

Following Falck *et al.* [33], in order to check the behavior of D vs N in the limit of large box sizes, we have inserted the values of the gyration radii R_g evaluated in Sec. IV into Eq.

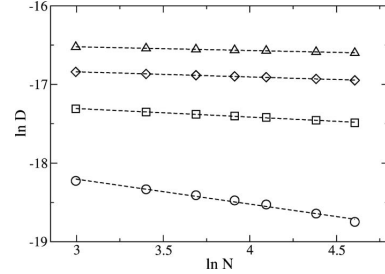


FIG. 7. Dependence of the diffusion coefficient D on N for different cutoff lengths L_{cut} in Eq. (29): (○) $L_{\text{cut}}=10^{-5}$ m, (□) $L_{\text{cut}}=10^{-3}$ m, (◇) $L_{\text{cut}}=10^{-1}$ m, and (△) $L_{\text{cut}}=10$ m.

(29) and evaluated the curves for several numbers of beads $N \in [20; 100]$ and for several cutoff lengths $L=L_{\text{cut}} \in [1.0 \times 10^{-5}; 10]$ m. Note that, because the thermodynamic limit is not defined, we select arbitrarily large but finite values L_{cut} in Eq. (29) and look at the trending behavior of $D(N)$. The results are shown in Fig. 7: as reported in [33], the slopes of the curves (ν_D) decrease monotonically from 0.32 (smallest cutoff) to 0.04 (largest cutoff), according with $x=0$ previously evaluated.

B. Effect of confinement on the polymer conformation

As already mentioned, confinement between two parallel walls significantly affects the polymer configuration statistics and induces anisotropic effects. The situation is the following. A polymer molecule is immersed in a Newtonian solvent modeled with SDPD particles. Periodic boundary conditions are applied at the edges of the box in the x direction while solid boundary conditions using virtual particles are applied at the top and at the bottom of the simulation box thereby confining the solvent between two impenetrable walls placed a distance H apart (channel width).

Kong *et al.* in 1994 [20] performed DPD simulations of this system and analyzed the components of the polymer gyration radius parallel and perpendicular to the confining walls. The results were clearly indicating anisotropic statistics and showed the collapse of the results for different chain lengths on a universal curve as a function of the normalized channel width.

The objective here is to validate our numerical model in the two-dimensional case analogous to that described above. The first issue is to show that a similar universal scaling can be obtained for different chain lengths and channel widths. We performed simulations with polymer molecules modeled with $N=20, 60$ beads and channel gaps H ranging from 1 to 10 μm . The length of the box in the periodic direction was chosen such that $L_x > 4R_G$. This choice ensures that statistical averages are independent of the box size in the periodic direction [36].

In order to observe an anisotropic effect it is convenient to decompose the gyration radius R_G into components parallel and perpendicular to the walls as follows:

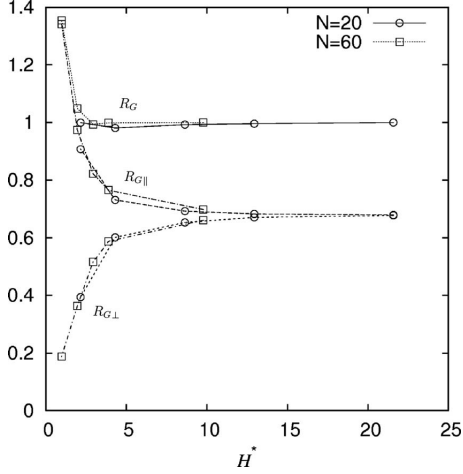


FIG. 8. Variation of the normalized gyration radius R_G^* together with its parallel ($R_{G||}^*$) and perpendicular ($R_{G\perp}^*$) components. The data correspond to different chain lengths ($N=20, 60$) and values of the normalized channel gap H^* ranging from 1 to 22. All the quantities have been made dimensionless by the gyration radius R_G^∞ of the corresponding polymer molecule without confinement.

$$R_{G||} = \frac{1}{2N^2} \sum_{ij} \langle x_{ij}^2 \rangle, \quad R_{G\perp} = \frac{1}{2N^2} \sum_{ij} \langle y_{ij}^2 \rangle, \quad (30)$$

where $x_{ij} = x_i - x_j$ and $y_{ij} = y_i - y_j$. Figure 8 shows these components together with the gyration radius R_G plotted for different values of the channel gap H . All the quantities have been made dimensionless by dividing them by the relative bulk free radii of gyration R_G^∞ corresponding to the respective chain length and given in Fig. 2; for example, $H^* = H/R_G^\infty$. The excellent collapse of the results for different chain lengths on a single curve indicates that universal scaling is obtained, analogously to previous works [36]. For large ratios H^* , the results are consistent with the bulk behavior and no anisotropies are observed. For values of H^* smaller than 14, slight departures in the results are visible, which become evident for $H^* < 10$, where $R_{G||}^*$ starts to differ remarkably from $R_{G\perp}^*$. For decreasing values of H^* , $R_{G\perp}^*$ tends to zero while $R_{G||}^*$ continues to increase toward larger values: for $H^* = 1$, $R_{G||}^* \approx 1.35$.

Unlike previous DPD simulations [20,36], in this work $R_{G||}^*$ is found to be strongly dependent on the confinement, which supports the common perception that the average polymer molecule orientation becomes increasingly aligned with the channel axis depending on the gap H^* . Diverging values of the parallel and perpendicular components of the gyration radius for a polymer molecule confined in a slit and in a cylinder have been documented by Cifra *et al.* [56] in qualitative agreement with our findings.

Another interesting feature is represented by the dependence of the global gyration radius R_G^* on the channel gap. Indeed, although deviations in $R_{G||}^*$ and $R_{G\perp}^*$ start to be visible already for $H^* \approx 10$, R_G^* remains nearly constant up to H^*

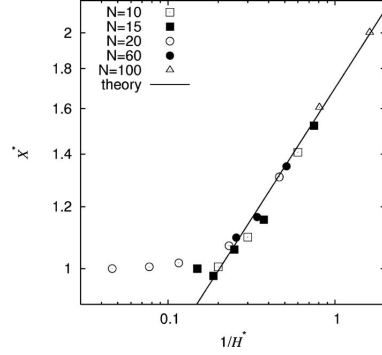


FIG. 9. Normalized polymer stretch X^* as a function of the inverse of the channel gap H^* for several chain lengths ($N=10, 15, 20, 60, 100$). Deviations from the bulk behavior appear at $1/H^* \approx 0.2$. For $1/H^* > 0.4$ universal scaling is realized, the slope of the fitted line being $z=1/3$ (theory).

≈ 3 . For $H^* < 3$, a sudden increase takes place due to the diverging values assumed by $R_{G||}^*$.

If we describe the conformational state of the polymer molecule in terms of an ellipsoid, then it is clear from Fig. 8 that different regimes can be observed. In almost unconfined conditions ($H^* > 12$), the principal axes of the ellipsoid are randomly distributed in space and this is reflected by the equal values assumed by $R_{G||}^*$ and $R_{G\perp}^*$; the presence of solid walls has no effect in this situation. A second regime can be characterized for values of the channel gap $3 < H^* < 12$ (slight confinement) where the ellipsoid tends to align itself on the channel axis preserving, however, its overall statistical length. In this regime, R_G^* remains constant and the polymer molecule does not undergo any net deformation. Finally, the sudden increase of R_G^* for $H^* < 3$ (strong confinement) reflects the overall stretching of the polymer chain induced by the presence of the parallel walls which try to squeeze it along the channel axis.

In [56] a similar behavior was reported; in that work Cifra noticed also the presence of a minimum in R_G^* located at $H^* \approx 2$, before the sharp increase happens. This is only slightly visible in Fig. 8 where R_G^* exhibits a smaller value compared to the bulk for $H^* \approx 3$ (see the third squared symbol from the left). Statistical errors in the results, however, do not allow for further comparisons. Longer simulations as well as more extensive parameter studies of H^* in this region would be necessary to confirm the analogy.

In order to compare these results quantitatively, we plotted in Fig. 9 the polymer stretch X as a function of the channel gap H . Instantaneous polymer stretch represents the maximum extension of the molecule along the channel direction and it is defined as

$$X(t) = \max_{i=1, \dots, N} [x_i(t)] - \min_{i=1, \dots, N} [x_i(t)]. \quad (31)$$

In Fig. 9, the corresponding dimensionless quantities $X^* = X/X^\infty$ and $H^* = H/R_G^\infty$ are plotted, X^∞ being the equilibrium polymer stretch in an unconfined domain and $X = \langle X(t) \rangle$. Ana-

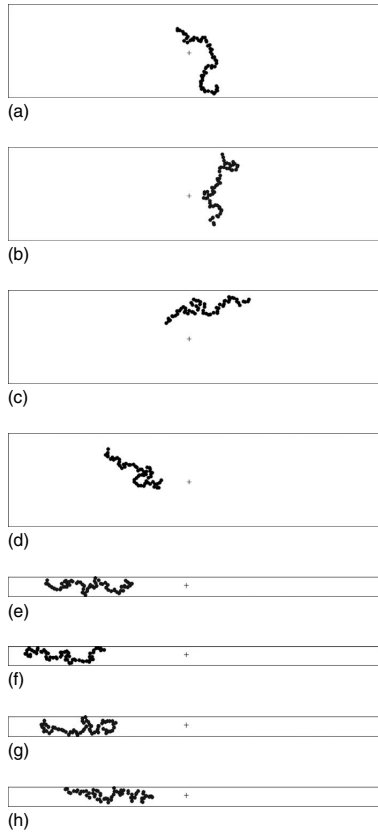


FIG. 10. Polymer conformations taken respectively after 1000, 2000, 4000, and 6000 time steps ($N=60$ beads). The free gyration radius for this chain is $R_G^\infty=1.02 \mu\text{m}$ while the channel gap is $H=5.0$ (four top figures) and $1.0 \mu\text{m}$ (four bottom figures). The corresponding ratio is $H^* \approx 5$ and 1, respectively.

lytical theories predict scaling behavior and give $X^* \propto (H^*)^{-(2/3)}$ in a 3D square channel of width H^* . Recently, these results have been validated numerically by Jendrejack *et al.* using Brownian dynamics techniques [12], showing a good agreement with the de Gennes theory in 3D. Figure 9 shows the analogous scenario in a two-dimensional case for different chain lengths $N=10, 15, 20, 60, 100$. Excellent scaling behavior is obtained. Similarly to what is observed in [12], X^* remains constant up to values of $1/H^*$ approximately equal to 0.2 where confinement effects start to be visible, while for $1/H^* > 0.4$ the scaling regime is fully realized. The slope of the approximate fitted curve prescribes a scaling law $H^{*(-z)}$ where $z=1/3$ in good agreement with the de Gennes theory in two dimensions. Notice that the previous result differs from the 3D case studied by Jendrejack *et al.* [57] where the scaling exponent takes a value equal to $2/3$.

Finally, Fig. 10 shows several time snapshots (after 1000, 2000, 4000, and 6000 time steps) of the polymer configuration for two different channel widths: $H=5.0$ (four snapshots

from the top) and $1.0 \mu\text{m}$ (four snapshots from the bottom). The polymer chain consists of $N=60$ beads and its free gyration radius is $R_G^\infty=1.02 \mu\text{m}$, therefore providing values of the ratio H^* approximately equal to 5 and 1. From the first four snapshots, it is possible to see qualitatively also that a channel gap of $5.0 \mu\text{m}$ will not affect strongly the polymer statistics. The polymer molecule is free to rotate in the channel similarly to the bulk case. This situation is indeed reflected in Figs. 8 and 9 which show quantitatively that the averaged gyration radius and polymer stretch are not affected in this regime and anisotropies in the gyration radius components are small. However, for smaller channel gaps H , the polymer conformations exhibit a totally different behavior (Fig. 10, bottom). For $H=1.0 \mu\text{m}$ it is evident that the polymer maintains its average orientation at any time; therefore confinement has its main effect in inhibiting angular movements of the polymer in the direction perpendicular to the walls. The observed enhanced alignment of the polymer chain for this channel width must necessarily have a big impact on the statistics. This observation is confirmed by inspection of Fig. 8 which shows that $R_{G\parallel}^*$ is more than six times larger than $R_{G\perp}^*$.

V. FINAL REMARKS, OUTLOOK, AND CONCLUSIONS

In this study, a smoothed dissipative particle dynamics method for mesoscopic flows has been formulated for a polymer molecule suspended in a Newtonian liquid. The SDPD model represents a generalization of smoothed particle hydrodynamics to the mesoscale which is thermodynamically consistent, i.e., it respects the first and second laws of thermodynamics and introduces thermal fluctuations according to the fluctuation-dissipation theorem. Although the starting point is represented by a particle discretization of the macroscopic hydrodynamics (SPH), the method can be also interpreted as an improved version of DPD, where the original repulsive and friction forces acting between DPD particles are tightly connected to second-order discretizations of pressure and viscous terms present in the Navier-Stokes equations.

The method is used to study the configurational behavior of the polymer chain in bulk and confined geometries. In the unbounded case, exact static and dynamic scaling relations have been found according to the Zimm theory in two dimensions. In the context of microfluidics, the effect of confined geometries on the conformational properties of the polymer molecules has been analyzed showing results in agreement with previous numerical experiments. The results suggest that the method can be faithfully applied to mesoscopic flow problems at microscales where the effect of hydrodynamic interactions as well as microconfinement play a central role. In the present study, the model is validated for two-dimensional test cases. Extension of the algorithm to the three-dimensional case and its parallel implementation are currently under work. This should allow one to handle in the near future full-scale problems encountered in realistic microfluidics applications such as the micromechanical behavior of DNA molecules under different hydrodynamic flow conditions [5–7].

A final discussion on the Schmidt number is in order. The Schmidt number is defined as $Sc = \nu/D$, where ν is the kinematic viscosity of the solvent and D the molecular diffusivity. Strictly speaking, the applicability of the Zimm theory for the polymer dynamics requires Sc to be much larger than one. For instance, in a real liquid like water $Sc \approx 1000$. This condition implies that mass diffusion is much slower than momentum diffusion, and this is crucial for the validity of the Oseen tensor approximation. In the present work, the Schmidt number evaluated by the input kinematic viscosity and the numerically estimated fluid particle diffusivity is, as in DPD, of order 1. Nevertheless, scaling relations for the polymer dynamics have been recovered in good agreement

with the Zimm theory with full hydrodynamic interactions. These results confirm the fact, already suggested by some authors [18,58], that the Schmidt number is an ill-defined quantity for coarse-graining models. There is therefore no need in principle to increase Sc but numbers of $O(1)$ can still produce the correct hydrodynamic behavior and, at the same time, provide a reasonable choice in terms of CPU time. In order to increase the artificial Schmidt number, a way would be to increase the kinematic viscosity with a numerical bottleneck due to the viscous time step limitation as a consequence. Realistic conditions could, however, be reached by using implicit schemes like those presented in [59,60], which are currently under investigation.

-
- [1] G. E. Karniadakis and A. Beskok, *Micro Flows, Fundamentals and Simulations* (Springer, New York, 2002).
- [2] S. C. Glotzer and W. Paul, *Annu. Rev. Mater. Res.* **32**, 401 (2002).
- [3] A. Uhlherr and D. N. Theodorou, *Curr. Opin. Solid State Mater. Sci.* **3**, 544 (1998).
- [4] H. A. Stone and S. Kim, *AIChE J.* **47**, 1250 (2001).
- [5] M. Mertig, L. Colombi, R. Seidel, W. Pompe, and A. De Vita, *Nano Lett.* **2**, 841 (2002).
- [6] S. Diez, C. Reuther, C. Dinu, R. Seidel, M. Mertig, W. Pompe, and J. Howard, *Nano Lett.* **3**, 1251 (2003).
- [7] M. Mertig, L. Colombi, A. Benke, A. Huhle, J. Opitz, R. Seidel, H. K. Schackert, and W. Pompe, in *Foundations of Nanoscience: Self-Assembled Architectures and Devices*, edited by J. Reif (Science Technica, Snowbird, Utah, 2004), p. 132.
- [8] L. D. Landau and E. M. Lifschitz, *Fluid Mechanics* (Pergamon Press, New York, 1959).
- [9] B. Dünweg and K. Kremer, *J. Chem. Phys.* **99**, 6983 (1993).
- [10] C. Aust, M. Kröger, and S. Hess, *Macromolecules* **32**, 5660 (1999).
- [11] J. M. Polson and J. P. Gallant, *J. Chem. Phys.* **124**, 184905 (2006).
- [12] R. Jendrejack, D. C. Schwartz, M. D. Graham, and J. J. de Pablo, *J. Chem. Phys.* **119**, 1165 (2003).
- [13] K. Mussawisade, M. Ripoll, R. G. Winkler, and G. Gomper, *J. Chem. Phys.* **123**, 144905 (2005).
- [14] P. Ahlrichs and B. Dünweg, *J. Chem. Phys.* **111**, 8225 (1999).
- [15] P. J. Hoogerbrugge and J. Koelman, *Europhys. Lett.* **19**, 155 (1992).
- [16] P. Español and P. Warren, *Europhys. Lett.* **30**, 191 (1995).
- [17] N. A. Spenley, *Europhys. Lett.* **49**, 534 (2000).
- [18] W. Jiang, J. Huang, Y. Wang, and M. Laradji, *J. Chem. Phys.* **126**, 044901 (2007).
- [19] V. Symeonidis, G. E. Karniadakis, and B. Caswell, *Phys. Rev. Lett.* **95**, 076001 (2005).
- [20] Y. Kong, C. W. Manke, W. G. Madden, and A. G. Schlijper, *Tribol. Lett.* **3**, 133 (1997).
- [21] S. Chen, N. Phan-Thien, X.-J. Fan, and B. C. Khoo, *J. Non-Newtonian Fluid Mech.* **118**, 65 (2004).
- [22] X. Fan, N. Phan-Thien, and S. Chen, *Phys. Fluids* **18**, 063102 (2006).
- [23] X. Fan, N. Phan-Thien, and T. Ng, *Phys. Fluids* **15**, 11 (2003).
- [24] The use of soft two-body potentials in DPD may allow for chain crossing (violating topological constraints [18]) as well as particle penetration to the walls in problems involving confined situations.
- [25] P. Español and M. Revenga, *Phys. Rev. E* **67**, 026705 (2003).
- [26] J. J. Monaghan, *Annu. Rev. Astron. Astrophys.* **30**, 543 (1992).
- [27] R. A. Gingold and J. J. Monaghan, *Mon. Not. R. Astron. Soc.* **181**, 375 (1977).
- [28] L. B. Lucy, *Astron. J.* **82**, 1013 (1977).
- [29] J. M. Vianney and A. Koelman, *Phys. Rev. Lett.* **64**, 1915 (1990).
- [30] B. Maier and J. O. Rädler, *Phys. Rev. Lett.* **82**, 1911 (1999).
- [31] R. Azuma and H. Takayama, *J. Chem. Phys.* **111**, 8666 (1999).
- [32] S. R. Shannon and T. C. Choy, *Phys. Rev. Lett.* **79**, 1455 (1997).
- [33] E. Falck, O. Punkkinen, I. Vattulainen, and T. Ala-Nissila, *Phys. Rev. E* **68**, 050102(R) (2003).
- [34] O. Punkkinen, E. Falck, I. Vattulainen, and T. Ala-Nissila, *J. Chem. Phys.* **122**, 094904 (2005).
- [35] A. Milchev and K. Binder, *J. Phys. II* **6**, 21 (1996).
- [36] Y. Kong, C. W. Manke, W. G. Madden, and A. G. Schlijper, *Int. J. Thermophys.* **15**(6), 1093 (1994).
- [37] P. G. de Gennes, *Scaling Concepts in Polymer Physics* (Cornell University Press, Ithaca, NY, 1979).
- [38] J. P. Morris, P. J. Fox, and Y. Zhu, *J. Comput. Phys.* **136**, 214 (1997).
- [39] J. P. Morris, *Int. J. Numer. Methods Fluids* **33**, 333 (2000).
- [40] X. Y. Hu and N. A. Adams, *J. Comput. Phys.* **213**, 844 (2006).
- [41] Note that, unlike DPD, SDPD repulsive interparticle forces have a many-body character due to the dependency of the pressure term P_i on the local value of the particle density $\rho_i = \sum_j m_j W_{ij}$. This is a remarkable property of the method which prevents particle crossing for monomers and confining walls.
- [42] E. G. Flekkøy, P. V. Coveney, and G. de Fabritiis, *Phys. Rev. E* **62**, 2140 (2000).
- [43] J. Bonet and T.-S. L. Lok, *Comput. Methods Appl. Mech. Eng.* **180**, 97 (1999).
- [44] M. Ellero, P. Español, and E. G. Flekkøy, *Phys. Rev. E* **68**, 041504 (2003).
- [45] M. Grmela and H. C. Öttinger, *Phys. Rev. E* **56**, 6620 (1997).

- [46] H. C. Öttinger and M. Grmela, *Phys. Rev. E* **56**, 6633 (1997).
- [47] P. Español, M. Serrano, and H. C. Öttinger, *Phys. Rev. Lett.* **83**, 4542 (1999).
- [48] P. W. Randles and L. D. Libersky, *Mech. Eng.* **139**, 375 (1996).
- [49] H. Takeda, S. M. Miyama, and M. Sekiya, *Prog. Theor. Phys.* **92**, 939 (1994).
- [50] M. Ellero, M. Kröger, and S. Hess, *Multiscale Model. Simul.* **5**, 759 (2006).
- [51] P. Español (private communication).
- [52] Notice that the FENE polymer molecule introduces an additional length in the model. The contour length is an appropriate parameter to estimate this molecular size. According to [23], if L_c denotes one segment of the molecular chain, its average value is of the order of $\sqrt{R_0^2/(b+5)}$, where $b=KR_0^2/(k_B T)$ is a dimensionless parameter approximately equal to 95 in our simulations. This gives $L_c \approx 6.6 \times 10^{-2} \mu\text{m}$. The polymer contour length will be therefore $L=NL_c$ and assumes values ranging from $\approx 1.3 \mu\text{m}$ ($N=20$) to $\approx 7 \mu\text{m}$ ($N=100$) consistent with the contour lengths of λ -DNA molecules.
- [53] M. Ellero, M. Kröger, and S. Hess, *J. Non-Newtonian Fluid Mech.* **105**, 35 (2002).
- [54] M. Ellero and R. I. Tanner, *J. Non-Newtonian Fluid Mech.* **132**, 61 (2005).
- [55] M. Doi and S. F. Edwards, *The Theory of Polymer Dynamics* (Clarendon, Oxford, 1986).
- [56] P. Cifra and T. Bleha, *Macromol. Theory Simul.* **8**, 603 (1999).
- [57] R. Jendrejack, D. C. Schwartz, M. D. Graham, and J. J. de Pablo, *J. Chem. Phys.* **120**, 2513 (2004).
- [58] E. A. J. F. Peters, *Europhys. Lett.* **66**, 311 (2004).
- [59] S. C. Whitehouse, M. R. Bate, and J. J. Monaghan, *Mon. Not. R. Astron. Soc.* **364**, 1367 (2005).
- [60] T. Shardlow, *SIAM J. Sci. Comput.* **24**, 1267 (2003).

8.5 Paper V

Numerical simulation of tethered DNA in shear flow

This article has been downloaded from IOPscience. Please scroll down to see the full text article.

2011 J. Phys.: Condens. Matter 23 184118

(<http://iopscience.iop.org/0953-8984/23/18/184118>)

View [the table of contents for this issue](#), or go to the [journal homepage](#) for more

Download details:

IP Address: 129.187.254.46

The article was downloaded on 03/07/2012 at 11:18

Please note that [terms and conditions apply](#).

Numerical simulation of tethered DNA in shear flow

S Litvinov, X Y Hu and N A Adams

Institute of Aerodynamics, Technische Universität München, D-85747 Garching, Germany

Received 31 May 2010, in final form 11 August 2010

Published 20 April 2011

Online at stacks.iop.org/JPhysCM/23/184118

Abstract

The behavior of tethered DNA in shear flow is investigated numerically by the smoothed dissipative particle dynamics (SDPD) method. Unlike numerical methods used in previous studies, SDPD models the solvent explicitly, takes into account the fully coupled hydrodynamic interactions and is free of the numerical artifact of wall sticking. Based on numerical simulations the static and dynamic properties of a tethered DNA is studied both qualitatively and quantitatively. The observed properties are in general agreement with previous experimental, numerical and theoretical work. Furthermore, the cyclic-motion phenomenon is studied by power spectrum density and cross-correlation function analysis, which suggest that there is only a very weak coherent motion of tethered DNA for a characteristic timescale larger than the relaxation time. Cyclic motion is more likely relevant as an isolated event than a typical mode of DNA motion.

1. Introduction

Deoxyribonucleic acid (DNA)—as the carrier of genetic information—is one of the most widely investigated and understood biomolecules. Although DNA has two negative charges per base pair, the presence of counterions screens the charges. This implies that DNA shares many micro-mechanical properties with polymers. As a model system for the behavior of long, entropic polymer chains in aqueous solution, the static and dynamic mechanical properties of DNA molecules in a stationary solvent or exposed to simple flows have been studied extensively [1–5]. For example, it has been found that static mechanical properties, such as the relation between the end-to-end distance under singular external forces, and dynamic mechanical properties, such as the relaxation time in a static solution, can be well approximated by the worm-like chain (WLC) model [6, 7]. When a single DNA molecule is tethered on a wall surface and exposed to a shear flow it exhibits different mechanical properties due to different hydrodynamic forces and wall–chain interactions [5, 8, 9]. From several experimental and numerical studies [10–13] the static properties of tethered DNA immersed in a flow have been established. For example, it is well known that the mean fractional extension is larger than that of an equivalent free DNA in an unbounded simple shear flow with the same flow strength. However, the dynamic properties are not fully understood.

One important phenomenon resulting from the standard deviation of extension is to exhibit a well-defined maximum

at moderate shear rate, which led to the stipulation of a repetitive recirculating motion, or the so-called cyclic motion. An important question is whether this motion is representative for the behavior of tethered DNA, such as, for example, the tumbling behavior of free DNA in unbounded simple shear flow. Another important question is whether this motion, if representative, is characterized by any, at least loosely, defined timescale which differs from the DNA relaxation timescale. These issues have been studied experimentally, and computationally by different methods [14–18], such as the coarse-grained molecular dynamics (CMD), Brownian dynamics (BD) and lattice Boltzmann (LB) methods. However, no unanimous conclusions have been obtained.

In this work, we perform detailed smoothed dissipative particle dynamics (SDPD) [19, 20] simulations of tethered DNA in shear flow. SDPD can be viewed as a combination of smoothed particle hydrodynamics (SPH), a macroscopic particle method for fluid dynamics, and dissipative particle dynamics (DPD), a popular mesoscopic particle-based method [21]. SDPD has been applied successfully for simulations of free and confined polymers in solution [22] and polymers in free shear flow and Poiseuille flow [23]. Compared to the numerical methods used in previous studies, SDPD has two major advantages. First, other than the BD or LB methods, it models the solvent explicitly and takes into account the fully coupled hydrodynamic interactions. Second, it recovers the polymer–wall interaction without introducing artificial wall-ordering behavior observed in CMD simulations. Note that

SDPD is less efficient than BD or LBM for simulating a single free polymer chain, but it can achieve higher computational efficiency when studying polymer solutions. The SDPD model for solvent and DNA molecules is introduced in section 2. In section 3, the static and dynamic quantities of the DNA chain are compared with theoretical, experimental and previous numerical simulation results. The cyclic motion is discussed in section 4 and finally we give some concluding remarks in section 5.

2. Method

2.1. SDPD modeling of liquid solvent

Within the SDPD formulation a bottom-up mesoscopic modeling approach is used for the liquid solvent. Specifically, the resulting dynamics for the mesoscopic fluid particles is due to the combination of a deterministic and a stochastic part. The deterministic part is modeled by smoothed particle hydrodynamics (SPH), which is a Lagrangian discretization of the Navier–Stokes equations [20, 24]. For the flow of an isothermal, weakly compressible solvent, the SPH formulation is given by

$$\frac{d\mathbf{r}_i}{dt} = \mathbf{v}_i, \quad (1)$$

$$\rho_i = m_i \sum_j W_{ij} = m_i \sigma_i, \quad (2)$$

$$\begin{aligned} \frac{d\mathbf{v}_i}{dt} = & -\frac{1}{m_i} \sum_j \left(\frac{p_i}{\sigma_i^2} + \frac{p_j}{\sigma_j^2} \right) \frac{\partial W_{ij}}{\partial r_{ij}} \mathbf{e}_{ij} \\ & + \frac{\mu}{m_i} \sum_j \left(\frac{1}{\sigma_i^2} + \frac{1}{\sigma_j^2} \right) \frac{\mathbf{v}_{ij}}{r_{ij}} \frac{\partial W_{ij}}{\partial r_{ij}}. \end{aligned} \quad (3)$$

Here, \mathbf{e}_{ij} and r_{ij} are the normalized vector and distance from particle i to particle j , respectively. \mathbf{r}_i , \mathbf{v}_i , m_i , ρ_i and p_i are the position, velocity, mass, density and pressure of a particle i , respectively. σ_i is the inverse of particle volume and $W_{ij} = W(r_{ij}, h)$ is a kernel function with smoothing length h . An isothermal, stiff equation of state is given as

$$p = p_0 \left(\frac{\rho}{\rho_0} \right)^\gamma + b, \quad (4)$$

where p_0 , ρ_0 , b and γ are parameters which may be chosen based on a scale analysis so that the density variation is less than a given value, usually 1% [25]. Using the GENERIC formalism (general equation for non-equilibrium reversible–irreversible coupling) [26] the stochastic dynamics, introducing thermal fluctuations, can be taken into account by postulating the following expressions for mass and momentum fluctuations:

$$d\tilde{m}_i = 0, \quad (5)$$

$$d\tilde{\mathbf{P}}_i = \sum_j B_{ij} d\overline{\overline{W}}_{ij} \mathbf{e}_{ij}, \quad (6)$$

where $d\overline{\overline{W}}_{ij}$ is the traceless symmetric part of a tensor of independent increments of a Wiener process and B_{ij} is defined as

$$B_{ij} = \left[-4k_B T \mu \left(\frac{1}{\sigma_i^2} + \frac{1}{\sigma_j^2} \right) \frac{1}{r_{ij}} \frac{\partial W}{\partial r_{ij}} \right]^{1/2}, \quad (7)$$

where k_B is the Boltzmann constant and T is a prescribed fluid temperature [20]. Note that the SDPD can be written in a generic form of DPD [21] as

$$d\mathbf{v}_i = \frac{1}{m_i} \left(\mathbf{F}_i^C dt + \mathbf{F}_i^D dt + d\tilde{\mathbf{P}}_i \right), \quad (8)$$

$$d\mathbf{r}_i = \mathbf{v}_i dt, \quad (9)$$

where $\mathbf{F}_i^C = \sum_j \left(\frac{p_i}{\sigma_i^2} + \frac{p_j}{\sigma_j^2} \right) \frac{\partial W_{ij}}{\partial r_{ij}} \mathbf{e}_{ij}$ is the conservative force and $\mathbf{F}_i^D = \sum_j \left(\frac{1}{\sigma_i^2} + \frac{1}{\sigma_j^2} \right) \frac{\mathbf{v}_{ij}}{r_{ij}} \frac{\partial W_{ij}}{\partial r_{ij}}$ is the dissipative force, as given by the right-hand side of equation (3). Compared to DPD, with SDPD the transport coefficients can be prescribed as input parameters rather than being an indirect result of other model parameters. Furthermore, thermal fluctuations can be introduced adaptively according to the size of the fluid particles.

2.2. SDPD modeling of polymer chain

As mentioned in section 1, the same coarse-grained models can be used for DNA and polymers. In the following we will therefore use the polymer model synonymous with the DNA model. For the polymer molecule a spring-bead chain model is adopted. The polymer is, in fact, embedded within a number of special SDPD particles (polymer beads) which represent both the segments of the polymer molecule and the surrounding solvent. For a typical size of SDPD particle a polymer bead contains mainly solvent while the volume fraction of the contained polymer segment is small. Therefore, polymer beads interact hydrodynamically, with additional forces due to the chemical bond between the polymer segments contained in neighboring polymer beads. These additional forces are taken into account by a finite extensible nonlinear elastic (FENE) potential:

$$U_{\text{FENE}} = -\frac{1}{2} H R_0^2 \ln \left(1 - \left(\frac{r}{R_0} \right)^2 \right), \quad (10)$$

where r is the spring length between neighboring beads, R_0 is the maximum spring extension and H is the spring constant. The parameter R_0 is chosen as twice the average particle distance in such a way that the crossing of chain segments is avoided. Note that, by using the stiff equation of state, equation (4), the excluded-volume effects between polymer beads are automatically taken into account. We emphasize that in the proposed model hydrodynamic interactions are fully represented due to the fact that fluid particles and polymer beads interact by hydrodynamic forces. The physical basis for this model is discussed in [22].

2.3. SDPD modeling of wall–chain interaction

Since the DNA is tethered on the wall surface, accurate modeling for wall–chain interaction is essential. For a

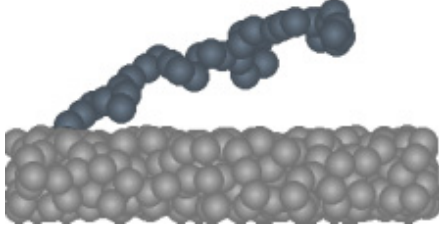


Figure 1. Simulation snapshot: the polymer beads are connected with FENE springs, the solvent particles are not shown and the amorphous wall prevents the polymer from ‘sticking’ to the wall surface.

mesoscopic polymer chain near the wall the dominant wall–chain interaction is the confinement effect. In the original SDPD [20] the wall–solvent interaction is handled by a wall–boundary condition, introducing mirrored or ordered static particles along the wall. While such formulations produce numerical layering of fluid particles near the wall they are free of the depletion problem which is typical for the DPD method, and they predict correct flow and density distributions. However, when these wall–boundary formulations are applied for tethered DNA the numerical layering of fluid particles may result in polymer beads sticking to the wall. Since such a sticking behavior is purely numerical it leads to non-physical near-wall behavior of the polymer.

To cope with this difficulty, a new random wall model is constructed by particles frozen after initial equilibration of the particle distribution with periodic boundary conditions applied at all wall boundaries, which gives an effective wall roughness of about half the average particle distance Δx . Note that the wall–fluid particle interaction formulation for a no-slip boundary condition is unchanged from that with ordered wall particles. Figure 1 gives a typical snapshot of a random wall and a polymer chain in shear flow. Figure 2 shows the typical density of polymer beads across the channel. For a wall with particles on a cubic lattice the effect of wall-induced ordering is very pronounced and persists up to distances of about $2\Delta x$. The random wall strongly reduces the near-wall ordering and inhibits the occurrence of artificial peaks in the polymer bead distribution.

2.4. Computational set-up

The computational domain in non-dimensional units is $D_x \times D_y \times D_z = 1.75 \times 1 \times 1$, containing in total 14 000 particles to model the solvent and a DNA chain with $N = 40$ beads. The average particle distance is $\Delta x = 0.05$ and the DNA contour length is $L = 1.75$. A Couette flow with a shear rate varying from $\dot{\gamma} = 0$ to 250 is applied in the x direction by two parallel walls that are located at $y = 0$ and 1. Periodic boundary conditions are applied in the x and z directions. The material properties of the solvent in non-dimensional units are: density $\rho = 1$, which gives the mass of a particle (both fluid particle and polymer bead) $m = \rho \Delta x^3 = 1.25 \times 10^4$, dynamic viscosity $\mu = 0.1$ and temperature $k_b T = 0.3$. Note that

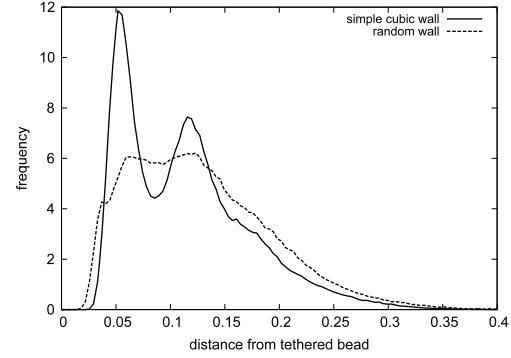


Figure 2. Probability of finding a polymer bead in x coordinates (direction of the flow gradient). The first fixed bead is excluded from the histogram.

the viscosity used here is small compared to that of a typical liquid solvent [27]. The parameters of the FENE chain are $R_0 = 0.1 = 2\Delta x$ and $H = 1500$. The strength of shear flow is characterized by the non-dimensional parameter $Wi = \tau \dot{\gamma}$ ranging from 0 to 136.10, where the relaxation time of the polymer chain $\tau = 0.5444$ was calculated from an exponential fit of the extension history in a stretching relaxation simulation. The DNA is tethered at the center of the lower wall by defining the first DNA bead as a wall particle.

2.5. Validation with a zero-flow case

First, the numerical model is validated by simulating a zero-flow case. Figure 3 gives the distribution of beads along the wall-normal direction. Evidently, the computed distribution is in good agreement with the theoretical prediction:

$$P(z) \propto \left(\frac{y}{R_g}\right)^{-1.611} \exp\left[-0.137\left(\frac{y}{R_g}\right)^{2.427}\right], \quad (11)$$

with R_g a parameter taken as 10% smaller than the gyration radius of a free DNA [28]. Note that, since the sticking effect in this case is insignificant, there is only a slight oscillation in the near-wall region.

Similarly, the distribution of the end bead plotted with the same R_g in figure 4 shows a good agreement with a previously proposed fit of experimental data [29]:

$$P_e(z) \propto \exp\left[-\left(\frac{y}{2R_g}\right)^2\right] - \exp\left[-\left(\frac{y}{R_g}\right)^2\right]. \quad (12)$$

As a test for the effect of hydrodynamic interactions the auto-correlations of the main Rouse modes:

$$\mathbf{R}_p = \frac{1}{N} \sum_{n=1}^N \cos\left[\frac{p\pi\left(n - \frac{1}{2}\right)}{N}\right] \mathbf{r}_n \quad (13)$$

are calculated and used to extract the relaxation time τ_p of these modes. Figure 5 shows that τ_p follows $\tau_p \propto p^{-1.74 \pm 0.05}$, which is different (as it should be) from the theoretical prediction $\tau_p \propto p^{-2.2}$ for the freely draining behavior and is in agreement with $\tau_p \propto p^{-1.8}$ for the presence of hydrodynamic interactions.

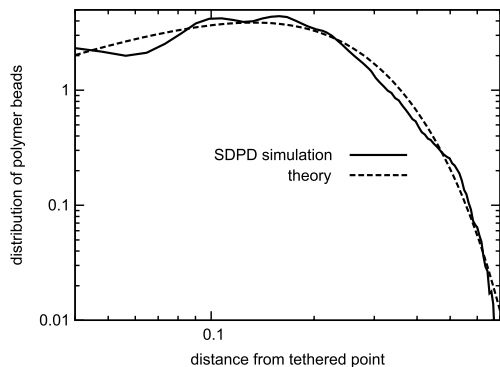


Figure 3. The distribution of all polymer beads at zero-flow condition. The theoretical line is given by equation (11) with R_g in the equation taken as 90% of the gyration radius of the free polymer.

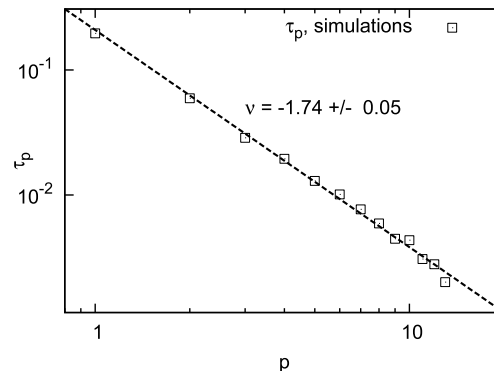


Figure 5. Rouse mode relaxation times versus the number of a Rouse mode: first 13 modes are shown. The slope -1.7 is predicted by the theory with hydrodynamic interactions considered.

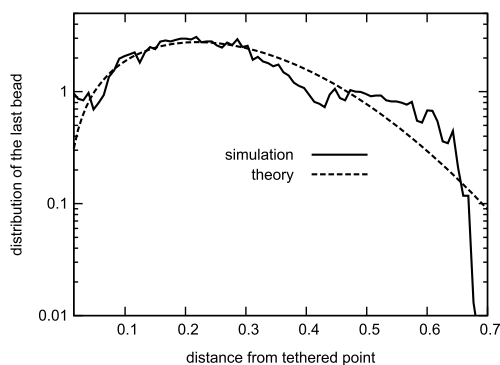


Figure 4. The distribution of the last polymer bead at zero-flow condition. The theoretical line is given by equation (12) with R_g in the equation taken as 90% of the gyration radius of the free polymer.

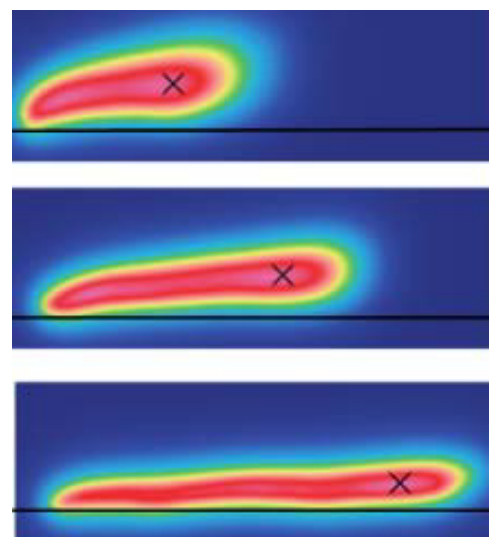


Figure 6. Ensemble averages of the polymer in the flow-gradient plane. From top to bottom $Wi = 5.44, 21.78$ and 136.10 and lengths of the image in the flow direction are 120% of the full extension. A Gaussian filter with a resolution equal to the average inter-particle distance was applied to make images qualitatively comparable to experimental images [18]. Crosses mark the region of the highest bead density (see the discussion in the text).

(This figure is in colour only in the electronic version)

3. Simulation results

3.1. Two-dimensional bead distribution

The average distributions of DNA beads in the flow-gradient plane of three cases with small, moderate and large shear rates are shown in figure 6. A Gaussian filter is used to produce images with comparable resolution to experimental visualizations of the bead distribution [18]. By comparing with experimental data and a previous numerical simulation from a BD method, a qualitative agreement can be found for the relation between the extension, shape of the distribution, fluctuation level at the end of the polymer and flow rate. Note that, at the largest $Wi = 136.10$, the chain collapses to the wall due to the large shear rate. The peak of the distribution (marked by a cross in the images) moves from the center to the end with increasing shear rate. The fact that the average distribution near the end of the chain is widest for the low-shear-rate case shows that there the largest variation of the extension occurs. This phenomenon is an indication of anomalous fluctuations of the chain extension as found by Doyle *et al* [9].

3.2. Measurement of DNA extension

As one of the most important static properties of tethered DNA, the extension can be measured quantitatively by different approaches. First, the extension can be measured by the end-to-end distance $h = \sqrt{(\mathbf{r}_N - \mathbf{r}_1)^2}$. As shown in figure 7, the peak of the distribution of the end-to-end distance $P(h)$ moves to larger extensions with increasing shear rate. This behavior agrees with previous simulations [11, 12], but is different from that of a free polymer chain in shear flow. In

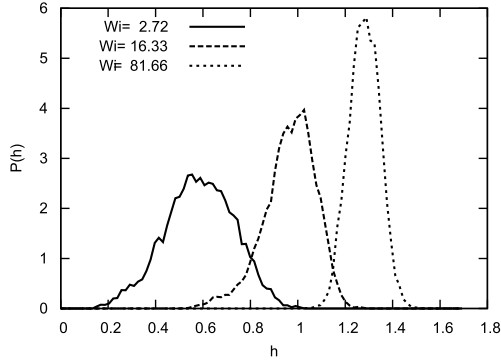


Figure 7. End-to-end distance distribution $P(h)$ for several shear rates. With increasing shear rate the center of the distribution moves to the right and becomes narrow.

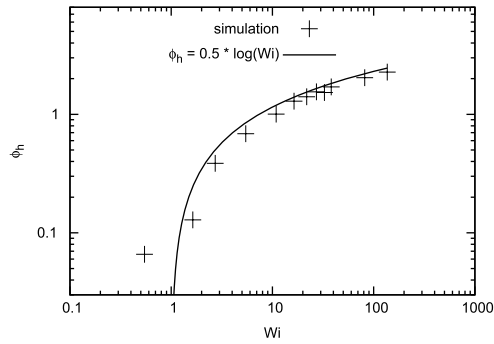


Figure 8. The deformation ϕ_h (defined in the text) as a function of Wi does not follow the simple power law. The empirical formula, equation (14), proposed in [12] offers a good fit of the simulation data.

the latter case, the distribution gradually becomes broader with increasing shear rate and forms a plateau for high shear rates. Second, the extension can be measured by the mean value of the extension distribution $\phi_h = (\langle h^2 \rangle - \langle h^2 \rangle_0) / \langle h^2 \rangle_0$, where $\langle h^2 \rangle_0$ is the mean-squared end-to-end distance at zero-flow condition. Figure 8 shows that, other than following a simple power law, the distributions for moderate and high shear rates can be described by an empirical expression:

$$\phi = 0.5 \log(Wi), \quad (14)$$

which has been proposed as a good fit for experimental data [12]. Third, the extension can be measured by the mean fractional extension $\langle X \rangle / L$ and the extension deficit:

$$\epsilon = 1 - \langle X \rangle / L, \quad (15)$$

where L is the length of the fully stretched DNA, $X = \max_i(x_i) - \min_i(x_i)$, and brackets denote an averaging over time. As shown in figures 9(a) and (b), while the simulations overestimate the extension at very small shear rates a good agreement between experiments and simulations can be found for moderate and high shear rates [9, 18].

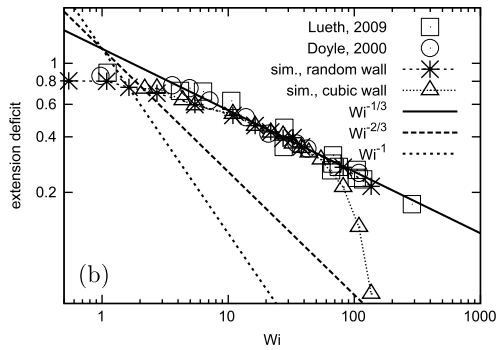
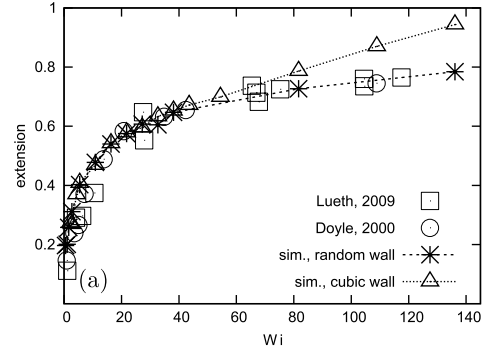


Figure 9. Polymer extension deficit versus non-dimensional shear rate.

Note that it is important to use random wall particles for obtaining a correct chain extension at moderate and high shear rates. For wall particles ordered on a cubic lattice, large over-extension (see figures 9(a) and (b)) occurs as found in [30]. Also note that, compared to the prediction of theoretical models [11], the present result resembles that of the worm-like chain (WLC) model with $\epsilon \propto Wi^{-1/3}$ and not the freely joint chain (FJC) model with $\epsilon \propto Wi^{-2/3}$. This behavior is not unexpected since the FENE potential of equation (10) results in a spring force of $F_{\text{FENE}} \propto (1 - X/R_0/n)^{-1}$, similar to that of FJC when the end-to-end distance X is close to the maximum extension nR_0 , where $n = (N - 1)$. However, in the current simulations, even for $\epsilon \approx 0.2$, $X \approx 0.36nR_0$ is still much smaller than the maximum extension.

3.3. Dynamical properties

To further quantify the behavior of tethered DNA in a shear flow the dynamic properties have to be measured. Obtaining dynamic properties in experiments is significantly more difficult than obtaining static properties. Two important dynamic properties which have been obtained experimentally are the normalized standard deviation of extension and the averaged mean-square distance from the wall.

The normalized standard deviation of extension is defined by

$$\delta = \frac{\langle (X - \langle X \rangle)^2 \rangle}{L^2}. \quad (16)$$

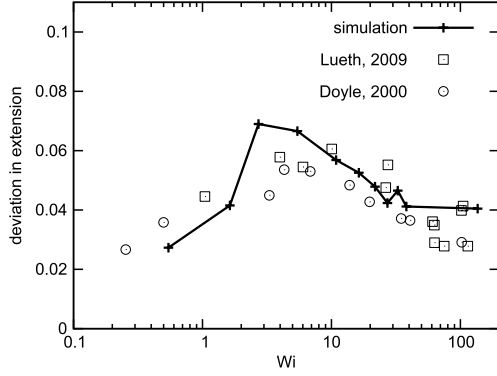


Figure 10. Polymer standard deviation in extension. The simulations reproduce the peak at $2 < Wi < 10$ seen in experiments [9, 18].

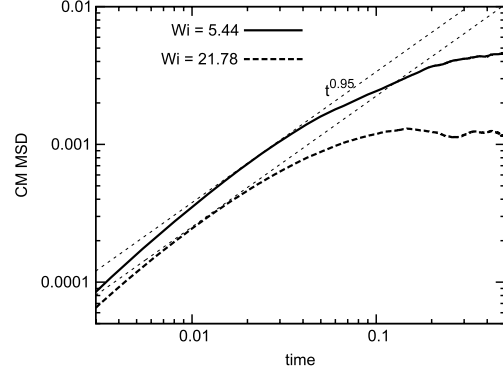


Figure 12. Mean-square displacement (MSD) of the chain center of mass in the direction normal to the wall: for the short-time region the slope of the MSD curve is not constant, while for the long-time MSD reaches a plateau.

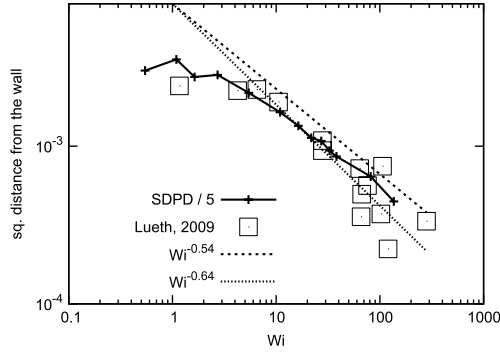


Figure 11. Mean-square distance from the wall. Scales -0.54 and -0.64 correspond to BD and MD simulations of Delgado-Buscalioni [16].

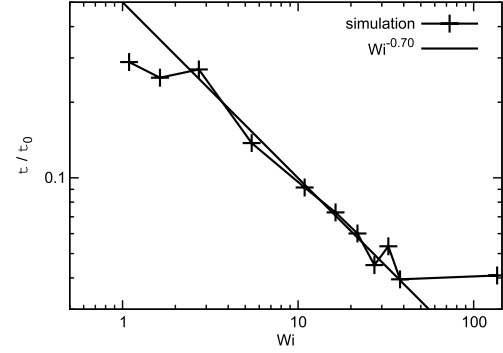


Figure 13. DNA extension relaxation time versus non-dimensional shear rate, where the solid line is a scaling law proposed by Delgado-Buscalioni [16].

As shown in figure 10, the present simulation reproduces the peak within the region $2 < Wi < 10$ as being seen in the experiments. This peak corresponds to the largest transition region near the end of the chain in the above-mentioned two-dimensional distributions. The averaged mean-square distance from the wall is defined as

$$\sigma = \frac{\left\langle \sum_{i=1}^{N_b} y_i^2 \right\rangle}{L^2}. \quad (17)$$

The comparison between the experimental data and rescaled simulation results is given in figure 11, where the lines $W^{-0.54}$ and $Wi^{-0.64}$ correspond to BD and MD simulations of Delgado-Buscalioni [16]. It can be found that, while the present simulations predict the correct scaling, they overestimate this quantity by factor of five compared to the experimental results [18]. This overestimation can be explained by the fact that thermal fluctuations in the simulations are much larger than that in real experiments due to the difference in solvent viscosity.

To study further the dynamics of DNA motion in the flow-gradient direction, the mean-square displacement (MSD)

of the chain center of mass normal to the wall $\langle \Delta Y(t)^2 \rangle = \langle (Y(t) - Y(0))^2 \rangle$, where $Y = \sum_{i=1}^{N_b} y_i^2$, is measured. Typical MSD curves are shown in figure 12 and have three regions: the short-time region where the DNA diffuses similarly to that of a free chain ($\langle \Delta Y(t)^2 \rangle \propto t$), the long-time region where the displacement reaches a plateau and the intermediate region where $\langle \Delta Y(t)^2 \rangle \propto t^\alpha$ with $\alpha < 1$. In contrast to the result from the MD simulations of Delgado-Buscalioni [16, 31] there is no evidence of a clear intermediate scaling regime, that is, α is not constant.

Another relevant dynamic property is the relaxation time of the extended DNA in a flow. This was extracted by fitting the initial part of the DNA extension auto-correlation function. As shown in figure 13, the resulting scaling law in the region $2 < Wi < 40$ is in good agreement with that proposed in [16].

4. Discussion

The peak of the normalized standard deviation of extension at moderate shear rate, figure 10, suggests that both stretched

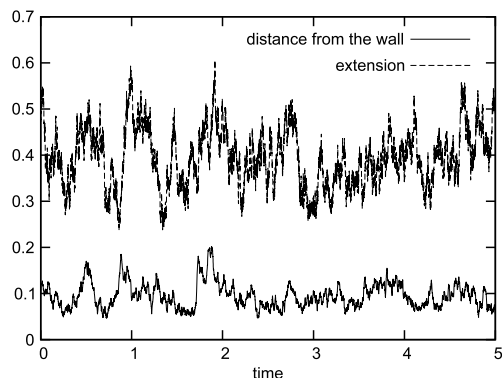


Figure 14. Time history of DNA extension (upper line) and DNA distance from the wall (lower line) for $Wi = 5.44$.

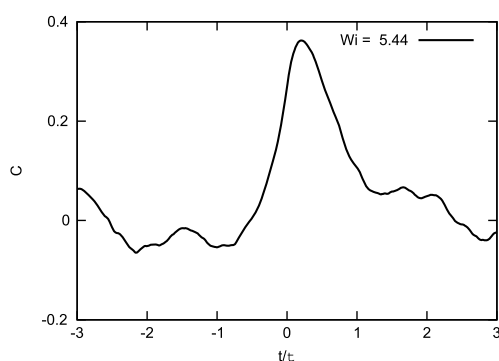


Figure 15. Extension-wall-distance cross-correlation function for $Wi = 5.44$.

and coiled configurations are possible since hydrodynamic forces acting on the DNA have the same order of magnitude compared to the entropic force to recoil the DNA. The DNA is coiled with small fluctuations when shear rate is low, and it is stretched along the wall and only rarely recoils when the shear rate is high. Since the stretched and coiled configurations for a free DNA in unbounded simple shear flow alternate by a transient tumbling motion, and since there is a loosely defined characteristic timescale larger than the relaxation time [32], Doyle *et al* [9] proposed that the tethered DNA changes between stretched and coiled configurations by a repetitive recirculating motion or so-called cyclic motion. This motion can be described as follows. Typically, the chain is coiled and stays close to the wall until thermal fluctuations drive it away from the surface into the region of stronger flow. Subsequently, it stretches and its free end rotates back to the wall and the chain recoils.

As a first step to investigate cyclic motion animated simulation data are visually examined. Although one can find examples of cyclic events similar to those described by [9, 18], these events appear to be much more isolated

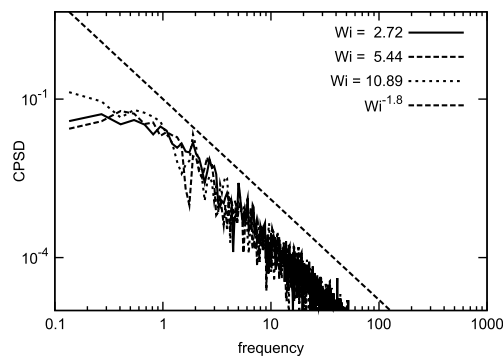


Figure 16. CPSD of DNA extension versus distance from the wall. The straight line indicates the slope observed experimentally [18].

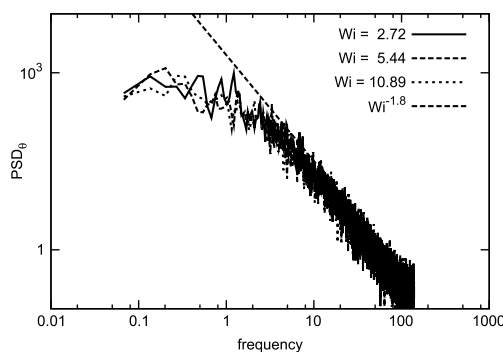


Figure 17. PSD of orientation angle through the tether point. The straight line indicates the slope observed experimentally [18].

and not representative since most of the time the DNA does not exhibit any repeating motion patterns. In order to search for quantitative indicators of periodic motion the histories of mass-center distance from wall, the extension $(X)/L$, and their cross-correlation function (CCF) are calculated. Figures 14 and 15 show the results for $Wi = 5.44$. The CCF profile in the interval from 0 to 2τ is in good agreement with that in [17], which implies a strong correlation of extension and mass-center-wall distance. Since this profile cannot predict the existence of cyclic motion directly, the cross-power spectrum density (CPSD), which is the power density spectrum of the CCF, is calculated to identify the existence of periodically correlated events. Furthermore, the power spectrum density (PSD) of the auto-correlation function (ACF) of the orientation angle, which is the angle of the line connecting the tethered point and DNA mass center in the flow-gradient plane, is also computed. This quantity is similar to the CPSD and can also be used to identify periodically correlated rotation events. As shown in figures 16 and 17, the obtained power spectrum density, for the frequency being scaled with the extension relaxation time, are very similar to those in Lueth *et al* [18], which give a scaling power law at about 1.8 for

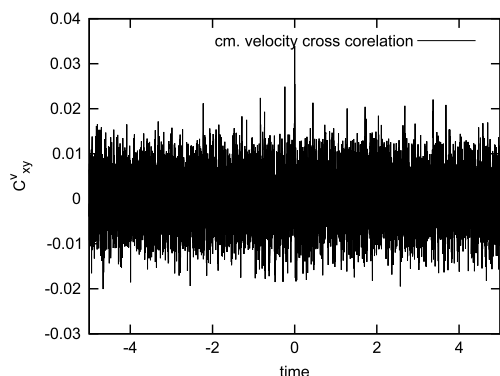


Figure 18. Cross-correlation of the DNA mass-center velocity in flow direction and flow-gradient direction for $Wi = 5.44$.

periods smaller than the relaxation time. Note that, while a very small peak is found in the experimental PSD of Lueth *et al* [18], the present spectrum for periods larger than the relaxation time up to 10τ is very similar to that of white noise, though the PSD of the orientation angle in the low frequency region indicates a slightly oscillatory behavior. These results imply that, at least, there is no clear evidence of cyclic motion. A further verification of this finding is to study the CCF of the y and x components of the mass-center velocity. As shown in figure 18, there is only a very small correlation magnitude. Since a significant non-random motion would exhibit strong correlations we can conclude that cyclic motion of tethered DNA occurs rather as an isolated event and that it is not a representative behavior.

5. Concluding remarks

The behavior of a tethered DNA in shear flow is investigated numerically by SDPD simulations. Based on the simulation data, the static and dynamic mechanical properties of tethered DNA are studied both qualitatively and quantitatively. By comparing previous experiments, numerical simulations and theoretical studies, good agreement has been found for DNA extension, standard deviation of extension, mean-square displacement of the chain center and relaxation time of the extended DNA. For the averaged mean-square distance from the wall we obtain a correct scaling power but an overestimation of the magnitude. This overestimation appears to be related to the difference of the viscosity compared to that of typical liquid solvents. The cyclic motion is discussed by analyzing the CPSD, PSD and CCF data. Except for small discrepancies the obtained results are in good agreement with previous simulations and experiments, and suggest that the cyclic motion is more likely an isolated event and not a representative behavior of tethered DNA in shear flow. However, the possibility of strong cyclic motion cannot be entirely ruled out as it may exist with characteristic times longer than 10τ , which is beyond the timescales that could be considered in this work.

Acknowledgment

Financial support from the Deutsche Forschungsgemeinschaft (DFG) via grant AD186/8 is gratefully acknowledged.

References

- [1] De Gennes P G 1974 Coil-stretch transition of dilute flexible polymers under ultrahigh velocity gradients *J. Chem. Phys.* **60** 5030
- [2] Schroeder C M, Babcock H P, Shaqfeh E S G and Chu S 2003 Observation of polymer conformation hysteresis in extensional flow *Science* **301** 1515–9
- [3] Smith D E, Babcock H P and Chu S 1999 Single-polymer dynamics in steady shear flow *Science* **283** 1724
- [4] LeDuc P, Haber C, Bao G and Wirtz D 1999 Dynamics of individual flexible polymers in a shear flow *Nature* **399** 564–6
- [5] Shaqfeh E S G 2005 The dynamics of single-molecule DNA in flow *J. Non-Newton. Fluid Mech.* **130** 1–28
- [6] Vologodskii A V 1994 DNA extension under the action of an external force *Macromolecules* **27** 5623–5
- [7] Marko J F and Siggia E D 1995 Stretching DNA *Macromolecules* **28** 8759–70
- [8] Perkins T T, Smith D E, Larson R G and Chu S 1995 Stretching of a single tethered polymer in a uniform flow *Science* **268** 83
- [9] Doyle P S, Ladoux B and Viovy J L 2000 Dynamics of a tethered polymer in shear flow *Phys. Rev. Lett.* **84** 4769–72
- [10] Haliloglu T, Bahar I and Erman B 1996 Response of a single grafted polyethylene chain to simple shear flow: a brownian dynamics simulation study *J. Chem. Phys.* **105** 2919–26
- [11] Ladoux B and Doyle P S 2000 Stretching tethered DNA chains in shear flow *Europhys. Lett.* **52** 511–7
- [12] Lemak A S, Balabaev N K, Karnet Y N and Yanovsky Y G 1998 The effect of a solid wall on polymer chain behavior under shear flow *J. Chem. Phys.* **108** 797–806
- [13] Brochard-Wyart F 1993 Deformations of one tethered chain in strong flows *Europhys. Lett.* **23** 105–11
- [14] Gratton Y and Slater G W 2005 Molecular dynamics study of tethered polymers in shear flow *Eur. Phys. J. E* **17** 455–65
- [15] Dubbeldam J and Redig F 2006 Multilayer Markov chains with applications to polymers in shear flow *J. Stat. Phys.* **125** 229–47
- [16] Delgado-Buscacioni R 2006 Cyclic motion of a grafted polymer under shear flow *Phys. Rev. Lett.* **96** 088303
- [17] Zhang Y, Donev A, Weisgraber T, Alder B J, Graham M D and de Pablo J J 2009 Tethered DNA dynamics in shear flow *J. Chem. Phys.* **130** 234902
- [18] Lueth C A and Shaqfeh E S G 2009 Experimental and numerical studies of tethered DNA shear dynamics in the flow-gradient plane *Macromolecules* **42** 9170–82
- [19] Español P and Revenga M 2003 Smoothed dissipative particle dynamics *Phys. Rev. E* **67** 26705
- [20] Hu X Y and Adams N A 2006 A multi-phase SPH method for macroscopic and mesoscopic flows *J. Comput. Phys.* **213** 844–61
- [21] Hoogerbrugge P J and Koelman J M V A 1992 Simulating microscopic hydrodynamic phenomena with dissipative particle dynamics *Europhys. Lett.* **19** 155–60
- [22] Litvinov S, Ellero M, Hu X and Adams N A 2008 Smoothed dissipative particle dynamics model for polymer molecules in suspension *Phys. Rev. E* **77** 66703
- [23] Litvinov S, Ellero M, Hu X and Adams N A 2010 A splitting scheme for highly dissipative smoothed particle dynamics *J. Comput. Phys.* **229** 5457–64
- [24] Monaghan J J 2005 Smoothed particle hydrodynamics *Rep. Prog. Phys.* **68** 1703–59

- [25] Morris J P, Fox P J and Zhu Y 1997 Modeling low Reynolds number incompressible flows using sph *J. Comput. Phys.* **136** 214–26
- [26] Español P, Serrano M and Ottinger H C 1999 Thermodynamically admissible form for discrete hydrodynamics *Phys. Rev. Lett.* **83** 4542–5
- [27] Groot R D and Warren P B 1997 Dissipative particle dynamics: bridging the gap between atomistic and mesoscopic simulation *J. Chem. Phys.* **107** 4423–35
- [28] Kreer T, Metzger S, Muller M, Binder K and Baschnagel J 2004 Static properties of end-tethered polymers in good solution: a comparison between different models *J. Chem. Phys.* **120** 4012–23
- [29] Lehner R, Koota J, Maret G and Gisler T 2006 Segment distributions of end-tethered polymers in a good solvent *Phys. Rev. Lett.* **96** 107801
- [30] Delgado-Buscalioni R and Coveney P V 2006 Structure of a tethered polymer under flow using molecular dynamics and hybrid molecular-continuum simulations *Physica A* **362** 30–5
- [31] Delgado-Buscalioni R 2007 Dynamics of a single tethered polymer under shear flow *AIP Conf. Proc.* **913** 114–20
- [32] Gerashchenko S and Steinberg V 2006 Statistics of tumbling of a single polymer molecule in shear flow *Phys. Rev. Lett.* **96** 38304

Bibliography

- [1] Ahlrichs, P., Dünweg, B.: Simulation of a single polymer chain in solution by combining lattice boltzmann and molecular dynamics. *J Chem Phys* **111**(17), 8225–8239 (1999)
- [2] Altenhoff, A.M., Walther, J.H., Koumoutsakos, P.: A stochastic boundary forcing for dissipative particle dynamics. *J Comput Phys* **225**(1), 1125–1136 (2007)
- [3] Bao, X.Y.R., Lee, H.J., Quake, S.R.: Behavior of complex knots in single DNA molecules. *Phys Rev Lett* **91**(26), 265,506 (2003)
- [4] Bracha, D., Karzbrun, E., Shemer, G., Pincus, P.A., Bar-Ziv, R.H.: Entropy-driven collective interactions in DNA brushes on a biochip. *Proc Natl Acad Sci USA* (2013)
- [5] Brockman, C., Kim, S.J., Schroeder, C.M.: Direct observation of single flexible polymers using single stranded DNA. *Soft Matter* **7**(18), 8005 (2011)
- [6] Bustamante, C., Smith, S.B., Liphardt, J., Smith, D.: Single-molecule studies of DNA mechanics. *Curr Opin Struct Biol* **10**(3), 279–285 (2000)
- [7] Cohen, A.E., Moerner, W.E.: Principal-components analysis of shape fluctuations of single DNA molecules. *Proc Natl Acad Sci USA* **104**(31), 12,622–12,627 (2007)
- [8] Delgado-Buscalioni, R.: Cyclic motion of a grafted polymer under shear flow. *Phys Rev Lett* **96**(8), 088,303 (2006)
- [9] Dittmore, A., McIntosh, D.B., Halliday, S., Saleh, O.A.: Single-molecule elasticity measurements of the onset of excluded volume in poly(ethylene glycol). *Phys Rev Lett* **107**(14), 148,301 (2011)

- [10] Doyle, P.S., Ladoux, B., Viovy, J.L.: Dynamics of a tethered polymer in shear flow. *Phys Rev Lett* **84**(20), 4769–4772 (2000)
- [11] Duong-Hong, D., Phan-Thien, N., Fan, X.J.: An implementation of no-slip boundary conditions in dpd. *Comput Mech* **35**(1), 24–29 (2004)
- [12] Enderlein, J.: Polymer dynamics, fluorescence correlation spectroscopy, and the limits of optical resolution. *Phys Rev Lett* **108**(10), 108,101 (2012)
- [13] Español, P., Revenga, M.: Smoothed dissipative particle dynamics. *Phys Rev E* **67**(2), 026,705 (2003)
- [14] Español, P., Serrano, M., Öttinger, H.C.: Thermodynamically admissible form for discrete hydrodynamics. *Phys Rev Lett* **83**(22), 4542–4545 (1999)
- [15] Español, P., Warren, P.: Statistical-mechanics of dissipative particle dynamics. *Europhys Lett* **30**(4), 191–196 (1995)
- [16] Fan, X., Phan-Thien, N., Yong, N.T., Wu, X., Xu, D.: Microchannel flow of a macromolecular suspension. *Phys Fluids* **15**(1), 11–21 (2003)
- [17] Fan, X.J., Phan-Thien, N., Chen, S., Wu, X.H., Ng, T.Y.: Simulating flow of DNA suspension using dissipative particle dynamics. *Phys Fluids* **18**(6), 63,102 (2006)
- [18] Fedosov, D., Karniadakis, G., Caswell, B.: Dissipative particle dynamics simulation of depletion layer and polymer migration in micro-and nanochannels for dilute polymer solutions. *J Chem Phys* **128**, 144,903 (2008)
- [19] Fedosov, D.A., Karniadakis, G.E., Caswell, B.: Steady shear rheometry of dissipative particle dynamics models of polymer fluids in reverse poiseuille flow. *J Chem Phys* **132**(14), 144,103 (2010)
- [20] de Gennes, P.G.: Molecular individualism. *Science* **276**(5321), 1999–2000 (1997)
- [21] Gingold, R.A., Monaghan, J.J.: Smoothed particle hydrodynamics - theory and application to non-spherical stars. *Monthly Notices of the Royal Astronomical Society* **181**(2), 375–389 (1977)

- [22] Groot, R.D., Warren, P.B.: Dissipative particle dynamics: Bridging the gap between atomistic and mesoscopic simulation. *J Chem Phys* **107**(11), 4423–4435 (1997)
- [23] Henrich, B., Cupelli, C., Moseler, M., Santer, M.: An adhesive DPD wall model for dynamic wetting. *Europhys Lett* **80**(6), 60,004 (2007)
- [24] Hinczewski, M., Schlagberger, X., Rubinstein, M., Krichevsky, O., Netz, R.R.: End-monomer dynamics in semiflexible polymers. *Macromolecules* **42**(3), 860–875 (2009)
- [25] Hoogerbrugge, P.J., Koelman, J.M.V.A.: Simulating microscopic hydrodynamic phenomena with dissipative particle dynamics. *Europhys Lett* **19**(3), 155–160 (1992)
- [26] Howard, M., Milner, S.: Numerical simulation methods for the rouse model in flow. *Phys Rev E* **84**(5), 051,804 (2011)
- [27] Hu, X., Adams, N.: A multi-phase SPH method for macroscopic and mesoscopic flows. *J Comput Phys* **213**(2), 844–861 (2006)
- [28] Hu, X.Y., Adams, N.A.: Angular-momentum conservative smoothed particle dynamics for incompressible viscous flows. *Phys Fluids* **18**(10), 101,702 (2006)
- [29] Hua, C., Schieber, J.: Nonequilibrium brownian dynamics simulations of hookean and FENE dumbbells with internal viscosity. *J Non-Newtonian Fluid Mech* **56**(3), 307–332 (1995)
- [30] Jagodzinski, O., Eisenriegler, E., Kremer, K.: Universal shape properties of open and closed polymer chains: renormalization group analysis and monte carlo experiments. *Journal de Physique I* **2**(12), 2243–2279 (1992)
- [31] Jendrejack, R.M., Dimalanta, E.T., Schwartz, D.C., Graham, M.D., de Pablo, J.J.: DNA dynamics in a microchannel. *Phys Rev Lett* **91**(3), 38,102 (2003)
- [32] Jiang, W.H., Huang, J.H., Wang, Y.M., Laradji, M.: Hydrodynamic interaction in polymer solutions simulated with dissipative particle dynamics. *J Chem Phys* **126**(4), 44,901 (2007)

- [33] Karniadakis, G., Beskok, A., Aluru, N.: *Microflows and Nanoflows: Fundamentals and Simulation*. Springer (2005)
- [34] Kong, Y., Manke, C., Madden, W., Schlijper, A.: Modeling the rheology of polymer solutions by dissipative particle dynamics. *Tribol Lett* **3**(1), 133–138 (1997)
- [35] Koumoutsakos, P.: Multiscale flow simulations using particles. *Annu Rev Fluid Mech* **37**, 457–487 (2005)
- [36] Kuhn, W.: Über die gestalt fadenförmiger moleküle in lösungen. *Kolloid-Zeitschrift* **68**(1), 2–15 (1934)
- [37] Larson, R.G.: The rheology of dilute solutions of flexible polymers: Progress and problems. *Journal of Rheology* **49**(1), 1–70 (2005)
- [38] LeDuc, P., Haber, C., Bao, G., Wirtz, D.: Dynamics of individual flexible polymers in a shear flow. *Nature* **399**(6736), 564–566 (1999)
- [39] Lehner, R., Koota, J., Maret, G., Gisler, T.: Segment distributions of end-tethered polymers in a good solvent. *Phys Rev Lett* **96**(10), 107,801 (2006)
- [40] Lisal, M., Brennan, J., Avalos, J.: Dissipative particle dynamics at isothermal, isobaric, isoenergetic, and isoenthalpic conditions using Shardlow-like splitting algorithms. *J Chem Phys* **135**(20), 204,105 (2011)
- [41] Litvinov, S., Ellero, M., Hu, X., Adams, N.: Smoothed dissipative particle dynamics model for polymer molecules in suspension. *Phys Rev E* **77**(6), 66,703 (2008)
- [42] Litvinov, S., Ellero, M., Hu, X., Adams, N.: Self-diffusion coefficient in smoothed dissipative particle dynamics. *J Chem Phys* **130**, 021,101 (2009)
- [43] Litvinov, S., Ellero, M., Hu, X., Adams, N.: Particle-layering effect in wall-bounded dissipative particle dynamics. *Phys Rev E* **82**(6), 066,704 (2010)
- [44] Litvinov, S., Ellero, M., Hu, X., Adams, N.: A splitting scheme for highly dissipative smoothed particle dynamics. *J. Comp. Phys.* **229**(15), 5457 – 5464 (2010)

- [45] Litvinov, S., Hu, X., Adams, N.: Numerical simulation of tethered DNA in shear flow. *J Phys-Condens Mat* **23**(18), 184,118 (2011)
- [46] Lueth, C.A., Shaqfeh, E.S.G.: Tethered DNA shear dynamics in the flow gradient plane: application to double tethering. *Korea-australia Rheology Journal* **19**(3), 141–146 (2007)
- [47] Lueth, C.A., Shaqfeh, E.S.G.: Experimental and numerical studies of tethered DNA shear dynamics in the flow-gradient plane. *Macromolecules* **42**(22), 9170–9182 (2009)
- [48] Lycy, L.B.: Numerical approach to testing of fission hypothesis. *Astron J* **82**(12), 1013–1024 (1977)
- [49] Mai, D.J., Brockman, C., Schroeder, C.M.: Microfluidic systems for single DNA dynamics. *Soft Matter* **8**(41), 10,560–10,572 (2012)
- [50] Mai-Duy, N., Phan-Thien, N., Khoo, B.: A numerical study of strongly overdamped dissipative particle dynamics (DPD) systems. *J Comput Phys* **245**, 150–159 (2013)
- [51] Marciel, A.B., Schroeder, C.M.: New directions in single polymer dynamics. *J Polym Sci Pol Phys* **51**(7), 556–566 (2013)
- [52] Marsh, C.A., Backx, G., Ernst, M.H.: Static and dynamic properties of dissipative particle dynamics. *Phys Rev E* **56**(2), 1676–1691 (1997)
- [53] McHale, K., Mabuchi, H.: Precise characterization of the conformation fluctuations of freely diffusing DNA: Beyond Rouse and Zimm. *J Am Chem Soc* **131**(49), 17,901–17,907 (2009)
- [54] Metzler, R., Reisner, W., Riehn, R., Austin, R., Tegenfeldt, J.O., Sokolov, I.M.: Diffusion mechanisms of localised knots along a polymer. *Europhys Lett* **76**(4), 696–702 (2006)
- [55] Monaghan, J.J.: Smoothed particle hydrodynamics. *Annu Rev Astron Astroph* **30**, 543–574 (1992)
- [56] Monaghan, J.J.: SPH and Riemann solvers. *J Comput Phys* **136**(2), 298–307 (1997)

- [57] Nepal, M., Yaniv, A., Shafran, E., Krichevsky, O.: Structure of DNA coils in dilute and semidilute solutions. *Phys Rev Lett* **110**(5), 058,102 (2013)
- [58] Nikunen, P., Karttunen, M., Vattulainen, I.: How would you integrate the equations of motion in dissipative particle dynamics simulations? *Comput Phys Comm* **153**(3), 407–423 (2003)
- [59] Noguchi, H., Gompper, G.: Transport coefficients of off-lattice mesoscale-hydrodynamics simulation techniques. *Phys Rev E* **78**(1), 016,706 (2008)
- [60] Öttinger, H.C.: *Stochastic Processes in Polymeric Fluids: Tools and Examples for Developing Simulation Algorithms*, softcover reprint of the original 1st ed. 1996 edn. Springer (1995)
- [61] Pagonabarraga, I., Hagen, M., Frenkel, D.: Self-consistent dissipative particle dynamics algorithm. *Europhys Lett* **42**(4), 377–382 (1998)
- [62] Pecora, R.: DNA: a model compound for solution studies of macromolecules. *Science* **251**(4996), 893–898 (1991)
- [63] Perkins, T.T., Quake, S.R., Smith, D.E., Chu, S.: Relaxation of a single DNA molecule observed by optical microscopy. *Science* **264**(5160), 822–826 (1994)
- [64] Perkins, T.T., Smith, D.E., Chu, S.: Single polymer dynamics in an elongational flow. *Science* **276**(5321), 2016–2021 (1997)
- [65] Perkins, T.T., Smith, D.E., Larson, R.G., Chu, S.: Stretching of a single tethered polymer in a uniform-flow. *Science* **268**(5207), 83–87 (1995)
- [66] Peters, E.A.J.F.: Elimination of time step effects in dpd. *Europhys Lett* **66**(3), 311–317 (2004)
- [67] Petrov, E.P., Ohrt, T., Winkler, R.G., Schwille, P.: Diffusion and segmental dynamics of double-stranded DNA. *Phys Rev Lett* **97**(25), 258,101 (2006)
- [68] Pivkin, I.V., Karniadakis, G.E.: Controlling density fluctuations in wall-bounded dissipative particle dynamics systems. *Phys Rev Lett* **96**(20), 206,001 (2006)

- [69] Prentis, J.J.: Spatial correlations in a self-repelling ring polymer. *J Chem Phys* **76**(3), 1574–1583 (1982)
- [70] Quake, S.R., Babcock, H., Chu, S.: The dynamics of partially extended single molecules of DNA. *Nature* **388**(6638), 151–154 (1997)
- [71] Randall, G.C., Schultz, K.M., Doyle, P.S.: Methods to electrophoretically stretch DNA: microcontractions, gels, and hybrid gel-microcontraction devices. *Lab Chip* **6**(4), 516 (2006)
- [72] Ripoll, M., Mussawisade, K., Winkler, R.G., Gompper, G.: Dynamic regimes of fluids simulated by multiparticle-collision dynamics. *Arxiv preprint cond-mat/0506484* (2005)
- [73] Ripoll, M., Mussawisade, K., Winkler, R.G., Gompper, G.: Dynamic regimes of fluids simulated by multiparticle-collision dynamics. *Phys Rev E* **72**(1), 016,701 (2005)
- [74] Robertson, R.M., Laib, S., Smith, D.E.: Diffusion of isolated DNA molecules: Dependence on length and topology. *Proc Natl Acad Sci USA* **103**(19), 7310–7314 (2006)
- [75] Schroeder, C.M., Teixeira, R.E., Shaqfeh, E.S.G., Chu, S.: Dynamics of DNA in the flow-gradient plane of steady shear flow: Observations and simulations. *Macromolecules* **38**(5), 1967–1978 (2005)
- [76] Shaqfeh, E.S.G.: The dynamics of single-molecule DNA in flow. *J Non-Newtonian Fluid Mech* **130**(1), 1–28 (2005)
- [77] Shardlow, T.: Splitting for dissipative particle dynamics. *SIAM J Sci Comput* **24**(4), 1267–1282 (2003)
- [78] Shusterman, R., Alon, S., Gavrinyov, T., Krichevsky, O.: Monomer dynamics in double- and single-stranded DNA polymers. *Phys Rev Lett* **92**(4), 048,303 (2004)
- [79] Smith, D.E., Babcock, H.P., Chu, S.: Single-polymer dynamics in steady shear flow. *Science* **283**(5408), 1724–1727 (1999)
- [80] Smith, D.E., Babcock, H.P., Chu, S.: Single-polymer dynamics in steady shear flow. *Science* **283**(5408), 1724–1727 (1999)

- [81] Smith, D.E., Chu, S.: Response of flexible polymers to a sudden elongational flow. *Science* **281**(5381), 1335–1340 (1998)
- [82] Smith, D.E., Perkins, T.T., Chu, S.: Dynamical scaling of DNA diffusion coefficients. *Macromolecules* **29**(4), 1372–1373 (1996)
- [83] Soranno, A., Buchli, B., Nettels, D., Cheng, R.R., Müller-Späh, S., Pfeil, S.H., Hoffmann, A., Lipman, E.A., Makarov, D.E., Schuler, B.: Quantifying internal friction in unfolded and intrinsically disordered proteins with single-molecule spectroscopy. *Proc Natl Acad Sci USA* **109**(44), 17,800–17,806 (2012)
- [84] Spenley, N.A.: Scaling laws for polymers in dissipative particle dynamics. *Europhys Lett* **49**(4), 534–540 (2000)
- [85] Steiner, T., Cupelli, C., Zengerle, R., Santer, M.: Simulation of advanced microfluidic systems with dissipative particle dynamics. *Microfluidics and Nanofluidics* **7**(3), 307–323 (2009)
- [86] Symeonidis, V., Karniadakis, G., Caswell, B.: Schmidt number effects in dissipative particle dynamics simulation of polymers. *J Chem Phys* **125**, 184,902 (2006)
- [87] Symeonidis, V., Karniadakis, G.E.: A family of time-staggered schemes for integrating hybrid dpd models for polymers: Algorithms and applications. *J Comput Phys* **218**(1), 82–101 (2006)
- [88] Symeonidis, V., Karniadakis, G.E., Caswell, B.: Dissipative particle dynamics simulations of polymer chains: Scaling laws and shearing response compared to dna experiments. *Phys Rev Lett* **95**(7), 076,001 (2005)
- [89] Tang, J., Du, N., Doyle, P.S.: Compression and self-entanglement of single DNA molecules under uniform electric field. *Proc Natl Acad Sci USA* **108**(39), 16,153–16,158 (2011)
- [90] Teixeira, R.E., Babcock, H.P., Shaqfeh, E.S.G., Chu, S.: Shear thinning and tumbling dynamics of single polymers in the flow-gradient plane. *Macromolecules* **38**(2), 581–592 (2005)

- [91] Teixeira, R.E., Babcock, H.P., Shaqfeh, E.S.G., Chu, S.: Shear thinning and tumbling dynamics of single polymers in the flow-gradient plane. *Macromolecules* **38**(2), 581–592 (2005)
- [92] Thomen, P., Bockelmann, U., Heslot, R.: Rotational drag on DNA: a single molecule experiment. *Phys Rev Lett* **88**(24), 248,102 (2002)
- [93] Thompson, P.A., Robbins, M.O.: Shear-flow near solids - epitaxial order and flow boundary-conditions. *Phys Rev A* **41**(12), 6830–6837 (1990)
- [94] Tüzel, E., Ihle, T., Kroll, D.: Dynamic correlations in stochastic rotation dynamics. *Phys Rev E* **74**(5), 056,702 (2006)
- [95] Valle, F., Favre, M., De Los Rios, P., Rosa, A., Dietler, G.: Scaling exponents and probability distributions of DNA end-to-end distance. *Phys Rev Lett* **95**(15), 158,105 (2005)
- [96] Viovy, J.L., Miomandre, F., Miquel, M.C., Caron, F., Sor, F.: Irreversible trapping of DNA during crossed-field gel electrophoresis. *Electrophoresis* **13**(1-2), 1–6 (1992)
- [97] Wijmans, C.M., Smit, B.: Simulating tethered polymer layers in shear flow with the dissipative particle dynamics technique. *Macromolecules* **35**(18), 7138–7148 (2002)
- [98] Willemsen, S.M., Hoefsloot, H.C.J., Iedema, P.D.: No-slip boundary condition in dissipative particle dynamics. *Internat J Modern Phys C* **11**(5), 881–890 (2000)
- [99] Wirtz, D.: Direct measurement of the transport properties of a single DNA molecule. *Phys Rev Lett* **75**(12), 2436–2439 (1995)
- [100] Xu, Z.J., Meakin, P.: A phase-field approach to no-slip boundary conditions in dissipative particle dynamics and other particle models for fluid flow in geometrically complex confined systems. *J Chem Phys* **130**(23), 234,103 (2009)
- [101] Yang, X.D., Melnik, R.V.: Effect of internal viscosity on brownian dynamics of DNA molecules in shear flow. *Comput Biol Chem* **31**(2), 110–114 (2007)

- [102] Zhang, Y., Donev, A., Weisgraber, T., Alder, B.J., Graham, M.D., de Pablo, J.J.: Tethered DNA dynamics in shear flow. *J Chem Phys* **130**(23), 234,902–234,902–13 (2009)
- [103] Zimm, B.H.: Dynamics of polymer molecules in dilute solution: Viscoelasticity, flow birefringence and dielectric loss. *J Chem Phys* **24**(2), 269–278 (1956)